Biotransformation, physico-chemical properties and environmental fate of bisphenol A bis(diphenyl phosphate): *in silico*, *in vitro* and non-target metabolites using a Wistar-Han rat liver microsomal model

by

Sofia Mercedes Herczegh

A thesis submitted to the Faculty of Graduate and Postdoctoral Affairs in partial fulfillment of the requirements for the degree of

Master of Science

in

Chemistry with Specialization in Chemical and Environmental Toxicology

Carleton University
Ottawa, Ontario

ABSTRACT

Organophosphate ester (OPE) flame retardants and plasticizers have replaced several legacy, banned brominated flame retardants. Bisphenol A bis(diphenyl phosphate) (BPADP) exemplifies a growing industry trend towards production of complex, high molecular weight, 'novel' OPEs. An assay method was optimized for quantification of BPADP biotransformation to target metabolites bisphenol-A (BPA) and diphenyl phosphate (DPHP) in an *in vitro* Wistar-Han rat liver microsomal assay. *In silico* modelling via OECD Toolbox v4.4.1 and Non-Target Analysis (NTA) via Q-E-Orbitrap HRMS/MS were applied to predict physico-chemical properties and identify additional non-targeted metabolites of BPADP. DPHP and BPA were predicted *in silico* and confirmed *in vitro*, with BPADP demonstrating slow *in vitro* microsomal metabolism. Additional Phase I oxidation metabolites & one Phase II GSH adduct were identified via NTA. These findings add to the understanding of BPADP stability and biotransformation, factors highly applicable to hazard assessment of the compound as an alternative to legacy flame retardants.

LIST OF WORKS ASSOCIATED WITH THESIS

Refereed Journal Publications:

Herczegh, S.M., Chu, S. & Letcher, R.J. 2022. Biotransformation and Environmental Fate of bisphenol-A bis(diphenyl phosphate) in a Wistar-Han rat liver microsomal model: a lines of evidence approach. *Chemosphere*, in prep.

Refereed Conference and Workshop Presentations and Proceedings:

Poster: Herczegh, S.M., Chu, S. & Letcher, R.J. Understanding Biotransformation of the 'Novel' Organophosphate Ester, Bisphenol-A bis(diphenyl phosphate); *In Silico, In vitro* and Non-Target Analysis Approaches (in prep). SETAC Europe 2022; May 15-19, 2022, Copenhagen, Denmark.

Platform: Herczegh, S.M., Chu, S. & Letcher, R.J. *In Silico* Prediction of the Biotransformation of 'Novel' Organophosphate Ester (OPEs): Understanding Metabolic Pathways and Influence on Biological Fate. SETAC North America; November 14-18, 2021, virtual.

Platform: Herczegh, S.M. & Letcher, R.J. Predicting the metabolism and biotransformation of 'novel' organophosphate esters (OPEs): *in silico* modelling to prioritize OPEs of potential environmental concern. SETAC Laurentian & Prairie Northern Annual General Meeting & Conference, June 14-18, 2021, virtual.

Platform: Herczegh, S.M. & Letcher, R.J. Fate and Stability of 'Novel' Organophosphate Esters in the Environment: A Review of Current Knowledge. SETAC SciCon2, November 15-19, 2020, virtual.

Dissemination of Thesis Results:

Herczegh, S.M., Chu, S. & Letcher, R.J. Biotransformation and Environmental Fate of bisphenol-A bis(diphenyl phosphate): *In silico* predictions, *in vitro* microsomal metabolism assays and Non-Target Analysis applied in a lines of evidence approach. (in prep.) BizNGO Working Group Meeting, June 21, 2022, virtual.

Herczegh, S.M., Chu, S. & Letcher, R.J. Metabolism & biotransformation of bisphenol-A bis(diphenyl phosphate) (BPADP): *In silico* predictions & *in vitro* microsomal metabolism assays. BizNGO Working Group Meeting, November 23, 2020, virtual.

Herczegh, S.M. & Letcher, R.J. Predicting the Biotransformation of BPADP using *in silico* modelling: Understanding Metabolic Products and Influence on Biological Fate of 'Novel' Organophosphate Esters (OPEs). BizNGO Working Group Meeting, June 15, 2021, virtual.

Herczegh, S.M. & Letcher, R.J. Environmental Fate and Stability of 'Novel' Organophosphate Esters (OPEs): A Review of Current Knowledge. BizNGO Working Group Meeting, November 10, 2020, virtual.

ACKNOWLEDGEMENTS

I greatly appreciate the opportunity to have studied under the supervision of Dr. Rob Letcher and conduct this research project. In the midst of altered timelines and uncertainty the excellent support throughout from Rob has been much appreciated and I am proud of how we managed to pivot when faced with closed facilities and achieve the completion of this project. This was supported by everyone at the OCRL, including Shaogang Chu who was instrumental (pun intended) in my conducting not only UHPLC analysis but also applying the Q-E-Orbitrap to this project. Thank you to David Blair and Luke Periard for welcoming my questions particularly as I started in the laboratory, and to Tristan Smythe for the crucial support in showing me around the lab, learning the *in vitro* assay procedure and working with the instrument software.

Many mentors were instrumental in my decision to continue with research post-undergrad. Thank you to Dr. Robert Burk for providing much needed confidence when I was doubting whether I should go for a research M.Sc. (CHEM 1001&1002 led me to a minor in chemistry and my specialization of environmental chemistry!), and to Dr. David Miller for instilling the fundamentals of toxicology and suggesting I apply to the OCRL. To the personal mentors who generously offered their time and shared insight regarding different programs and schools, and to my parents who are always in my corner cheering me on, thank you. While working from home for extended periods of time the bright aspects were being with hometown friends, pets and in nature.

Funding for this project was provided by the National Science and Engineering Research Council (NSERC) CREATE-REACT Program (to S.M.H), by BizNGO of Clean Production Action through Carleton University (to S.M.H), and the Environment & Climate Change Canada Chemical Management Plan (CMP) (to R.J.L.).

TABLE OF CONTENTS

LIST OF TABLES

Table 3-2. *In silico* predicted *in vivo* rat liver & *in vitro* rat S9 metabolites of additional novel organophosphate esters resorcinol diphenyl phosphate (RDP), tetrakis(2,6-dimethylphenyl)-m-phenylene biphosphate (RDX) and tetrakis(2-chloroethyl)dichloroisopentyldiphosphate (V6) presented by probability of occurrence as predicted via the OECD Toolbox v4.4.1, including chemical formula, structure, molecular weight (MW) and chemical abstract service registry number (CAS RN).

Table 3-3. EPI Suite™ predicted physico-chemical properties of bisphenol A bis(diphenyl phosphate) (BPADP), resorcinol diphenyl phosphate (RDP), tetrakis(2,6-dimethylphenyl)-m-phenylene biphosphate (RDX) and tetrakis(2-chloroethyl)dichloroisopentyldiphosphate (V6).

Table 3-4. EPI Suite™ environmental fate predictions of bisphenol A bis(diphenyl phosphate) (BPADP), resorcinol diphenyl phosphate (RDP), tetrakis(2,6-dimethylphenyl)-m-phenylene biphosphate (RDX) and tetrakis(2-chloroethyl)dichloroisopentyldiphosphate (V6). Fate predictions of RDP and RDX are based on EPI Suite v4.1.1 predicted properties (**Table 3-3**), while V6 experimental solubility and logK_{OW} were inputted into the model. Inputs to the model for BPADP were a water solubility of 0.212 mg/L and a logK_{OW} of 8.

Table 3-5. Octanol-water coefficient (logK_{OW}), molecular weight, bioconcentration and bioaccumulation factor values of bisphenol A bis(diphenyl phosphate) (BPADP) (based on a saturated water concentration of 0.212 ppm and logK_{ow} of 8) in comparison to PCB-153, tetraBDE and pentaBDE. Estimated values as predicted by EPI Suite™ are denoted via an asterisk (*).

Table 3-6. Additional novel metabolites of bisphenol A bis(diphenyl phosphate) (BPADP) analyzed via UHPLC-MS/MS, including abbreviation, chemical formula and molecular weight.

Table 3-7. Chemical formula, parent compound, transformations, composition change (from parent compound), Δ mass shift, molecular weight, retention time (RT) and replicated group areas of identified GSH adduct. A potential structure is posited.

Table 3.8. Detailed list of all confirmed and tentatively confirmed metabolites of BPADP identified via Q-E-Orbitrap NTA, including chemical formula, abbreviation, retention time (RT), molecular weight and confirmation status.

Table 3-9. Summary of all identified bisphenol A bis(diphenyl phosphate) (BPADP) metabolites and agreement between lines of evidence. Metabolites predicted only *in vivo* via the OECD Toolbox are denoted with an asterisk (*). The predicted unidentifiable metabolite (*in vivo*: 6; **Table 3.1**) is excluded as it is an isomer of M5. The tentatively confirmed metabolite MM5 (BPADP+2O+2H) is italicized and empty boxes indicate a metabolite not studied using the particular line of evidence.

LIST OF FIGURES

LIST OF ABBREVIATIONS

ACN	acetonitrile
AGC	Automatic Gain Control
ANOVA	analysis of variance
BAF	bioaccumulation Factor
BCF	bioconcentration Factor
BFR	brominated flame retardant
BPADP	bisphenol A bis(diphenyl phosphate)
BPA	bisphenol A
CAS RN	chemical abstract service registry number
CEPA	Canadian Environmental Protection Act
CYP450	cytochrome P450 enzyme
decaBDE	decabromodiphenyl ether
DMSO	dimethyl sulfoxide
DPHP	diphenyl phosphate
EC_{50}	half maximal effect concentration
EHDPHP	2-ethylhexyl diphenyl phosphate
ESI	electrospray ionization
FR	flame retardant
GSH	glutathione
HBCDD	hexabromocyclododecane
HLM	human liver microsomal
HRMS/MS	high resolution tandem mass spectrometry
IDDPP	isodecyl diphenyl phosphate
ILOQ	instrument limit of quantification
IS	internal standard
IUPAC	International Union of Pure and Applied Chemistry

m/z	mass-to-charge ratio
K_{AW}	air-water partition coefficient
K_m	Michaelis rate constant
K_{OA}	octanol-air partition coefficient
K_{OC}	soil adsorption coefficient
K_{OW}	octanol-water partition coefficient
kV	kilovolt
LC_{50}	lethal concentration 50
logP	partition coefficient, [organic]/[aqueous]
LRT	long-range transport
mg/L	milligram per litre
mM	millimolar
MS/MS	tandem mass spectrometry
MW	molecular weight
NADPH	nicotinamide adenine dinucleotide phosphate
NTA	non-target analysis
OECD	Organisation for Economic Co-operation and Development
OPEs	organophosphate ester flame retardants
PBDEs	polybrominated diphenyl ethers
PBT	persistent, bioaccumulative, toxic
PCB	polychlorinated biphenyl
pH	power of hydrogen
$PM_{2.5}$	fine particulate matter
PON	paraoxonase enzyme
ppb	parts per billion
ppm	parts per million
PTFE	polytetrafluorethylene
QSAR	quantitative structure-activity relationship

rCYP	recombinant cytochrome P450 enzyme
RDP	resorcinol bis (diphenylphosphate)
RDX	tetrakis(2,6-dimethylphenyl)-m-phenylene biphosphate
RLM	rat liver microsomal
rpm	revolutions per minute
RT	retention time
SMILES	simplified molecular-input line-entry system
SPM	suspended particulate matter
S9	cellular fraction containing Phase I and Phase II enzymes
TBOEP	tris(2-butoxyethyl) phosphate
TCEP	tris(2-chloroethyl) phosphate
TCHBDP	trans-1,4-cyclohexanediol bis(diphenyl phosphate)
TCIPP	tris (1-chloro-2-propyl) phosphate
TDCIPP	tris(1,3-dichloro-2-propyl) phosphate
TDCP	tris(1,3-dichloro-2-propyl) phosphate
TEP	triethyl phosphate
TEHP	tris(2-ethylhexyl) phosphate
TMP	trimethyl phosphate
TMPP	tricresyl phosphate
TNBP	tri-n-butyl phosphate
ToCP	tri(o-cresyl) phosphate
TPHP	triphenyl phosphate
TPPO	triphenyl-phosphine oxide
TPRP	tripropyl phosphate
t-SIM	targeted selected ion monitoring
TTBPP	tris(p-tert-butylphenyl) phosphate
t_0	initial time zero
UHPLC	ultra-high performance liquid chromatography

µg	microgram
µL	microlitre
µm	micrometre
µM	micromolar
V6	tetrakis(2-chloroethyl)dichloroisopentyldiphosphate
v_0	initial reaction rate
V_{max}	maximum rate of biotransformation in a saturated enzyme system
WWTP	wastewater treatment plant

LIST OF APPENDICES

Chapter 1: Introduction

1.1 Production and Use of Flame Retardant Chemicals, Evolution of OPEs

Flame retardant (FR) chemicals are commonly used in a variety of consumer products as both plasticizers and FRs, and produced industrially for use in textiles, electronics, upholstery, transportation products and construction materials (Government of Canada, 2019). FRs include a large variety of compounds categorized by chemical properties and structure (van der Veen & de Boer, 2012; NIEHS, 2018; Yao et al., 2021). Inorganic examples of FRs include compounds containing metals and nitrogen, with the two main categories of defined as halogenated (brominated or chlorinated) and phosphorous-containing (NIEHS, 2018).

Brominated FRs (BFRs) include a subset of congeners defined as polybrominated diphenyl ethers (PBDEs) which were used abundantly before largely being replaced by Organophosphate Ester FRs (OPEs) (van der Veen & de Boer, 2012; Blum et al., 2019). Commercial applications of PBDEs included in consumer electronics, plastics and furniture (US EPA, 2017), however following strong evidence of the persistent, bioaccumulative and toxic (PBT) nature of PBDEs, select congeners in chemical formulations were added to the Stockholm Convention in 2009 and 2017 (UNEP, 2019). Usage of PBDEs, once widespread, began declining when concerns of cancer, endocrine disruption and neurological impairment became apparent (NIEHS, 2018). The resulting restrictions and phase outs were followed by replacement compounds such as OPEs, which were thought to be less persistent (Blum et al., 2019).

As a class of compounds OPEs are structurally centered around a phosphate molecule and of the general structure $O=P(OR)_3$ with surrounding aromatic or alkyl

moieties (van der Veen & de Boer, 2012). Inorganic, halogen-containing and organic OPEs are considered to be the three main groups of OPE FRs (van der Veen & de Boer, 2012). Similar to previous iterations of FR compounds, OPEs are used in both industrial and consumer products for a variety of applications as both plasticizers and FRs (Andresen et al., 2004; van der Veen & de Boer, 2012). **Table 1-1** summarizes several typical OPEs that have been produced and used in recent decades.

The phasing out of FRs such as PBDEs (including decabromodiphenyl ether (DecaBDE) or BDE-209) and isomers of hexabromocyclododecane (HBCDD) created a need for replacement compounds (van der Veen & de Boer, 2012) such as triphenyl phosphate (TPHP) and other alkyl-substituted TPHP OPEs (USTPO, 2009) therefore OPE production and consumption has increased accordingly. Globally, OPE consumption in 2011 was 500,000 tons (Ma et al., 2016) and in 2015, 498,000 metric tons of FRs were consumed in Europe alone, of which OPEs accounted for 18%, equivalent to 89,640 metric tons (Chupeau et al., 2020). While production of tris(1-chloro-2-propyl)phosphate (TCIPP) is expected to remain constant, tris(1,3-dichloro-2-propyl)phosphate (TDCIPP) and tris(2-chloroethyl)phosphate (TCEP) were expected to decline rapidly towards elimination by 2020 (Schreder et al., 2016).

Table 1-1. Examples of typical 'legacy' organophosphate esters (OPEs) including compound name, molecular weight, chemical abstract service registry number (CAS RN) and chemical structure.

Chemical Structure	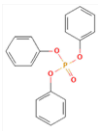	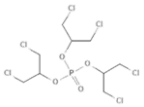	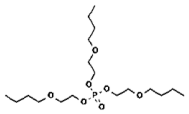	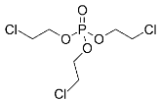	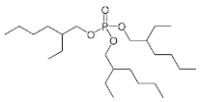
Compound Name	triphenyl phosphate (TPHP)	tris(1,3-dichloro-2-propyl) phosphate (TDCIPP)	tris(2-butoxyethyl) phosphate (TBOEP)	tris(2-chloroethyl) phosphate (TCEP)	tris(2-ethylhexyl) phosphate (TEHP)
Molecular Weight (amu)	326.3	430.9	398.5	285.5	434.6
CAS RN	115-86-6	13674-87-8	78-51-3	115-96-8	78-42-2
Chemical Structure	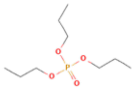	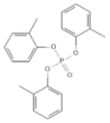		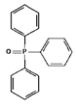	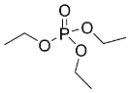
Compound Name	tripropyl phosphate (TPRP)	tri(o-cresyl) phosphate (ToCP)	trimethyl phosphate (TMP)	triphenyl-phosphine oxide (TPPO)	triethyl phosphate (TEP)
Molecular Weight (amu)	224.23	368.4	140.07	278.3	182.15
CAS RN	513-08-6	78-30-8	512-56-1	791-28-6	78-40-0
Chemical Structure	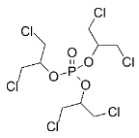	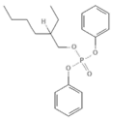	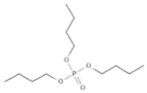	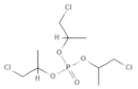	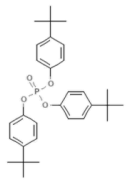
Compound Name	tris(1,3-dichloro-2-propyl) phosphate (TDCP)	2-ethylhexyl diphenyl phosphate (EHDPHP)	tri-n-butyl phosphate (TNBP)	tris (1-chloro-2-propyl) phosphate (TCIPP)	tris(p-tert-butylphenyl) phosphate (TTBPP)
Molecular Weight (amu)	430.9	362.4	266.31	327.6	494.6
CAS RN	13674-87-8	1241-94-7	126-73-8	13674-84-5	78-33-1

In 2006, the production volume of bisphenol A bis(diphenyl phosphate) (BPADP) in the United States alone was estimated to be within the range of 454-4500 tonnes (van der Veen & de Boer, 2012). Similar to many legacy/phased out FRs, OPEs are often added to a product in the manufacturing stage rather than chemically bonded to said product and are therefore more prone to leaching as a result of their additive nature (Reemstma et al., 2008). This increases the likelihood of discharge to the environment via volatilization to air, physical abrasion (Reemstma et al., 2008; Chupeau et al., 2020) and release to aquatic environments (Rodriguez et al., 2020).

1.1.1 OPEs of Environmental Concern

In response to increased production and usage, studies have investigated OPE levels in the environment, commonly focusing on legacy compounds. OPEs have been measured in air (Bergh et al., 2011), wastewater effluent (Meyer & Bester, 2004; Yao et al., 2021), sediment (Cao et al., 2017), wildlife (Greaves & Letcher, 2014; Strobel et al., 2018a,b) and human samples (Ding et al., 2016). Screening of OPEs in several countries has demonstrated concentrations in food including cereals, oils, rice and starches (Li et al., 2019b). Numerous study examples are available of OPEs in the environment, both in abiotic and biotic compartments. Of the OPEs defined in **Table 1-1**, TNBP, TBOEP, TCEP, TCIPP and TPHP are frequently quantified in wastewater influent, sludge and effluent with TBOEP at the highest concentrations (up to 38,700 ng/L) in effluent (Yao et al., 2021). TBOEP, TCEP and TCIPP have demonstrated biomagnification potential (Brandsma et al., 2015).

Aquatic toxicity of diphenyl phosphate (DPHP) (the diester of TPHP) is known (Choi et al., 2020; Chen et al., 2021). Long-range transport (LRT) as well as persistence

were suggested for TBOEP and TEHP in a study of arctic fox from Svalbard, Norway (Hallanger et al., 2015). Glacial melt has been identified as a source of OPEs in the high arctic (Sun et al., 2020), and OPEs have been sampled in ocean sediments (Ma et al., 2017) and the marine atmosphere (Möller et al., 2011), further underscoring the relevance of LRT to the Arctic where persistent OPEs have been sampled in the tissues of polar bears and ringed seals (Strobel et al., 2018a). Ecologically-relevant behavioural effects have been demonstrated in quail post-TPHP exposure (Hanas et al., 2020), and TCEP was found to demonstrate persistence in both water and air (Reemstma et al., 2008).

1.1.2 The Evolution of Produced and Used OPEs and New/Novel OPEs

Wide variation exists within OPEs as a chemical class, with compounds increasing in molecular weight (MW) and structural complexity due to innovation of industrial synthesis. OPEs could be categorized as 'legacy' and 'novel'; the former consisting of well-studied compounds with known exposure and toxicity data; the latter being recently developed, highly complex OPEs for which human and environmental health data is scarce. Production of novel OPEs is trending towards larger, more complex and/or oligomeric structures with higher MW than legacy compounds (Velencoso et al., 2018), often with physico-chemical properties consisting only of estimations rather than experimentally measured values.

The novel OPE BPADP (CASRN 5945-33-5) is among the alkyl-substituted TPHP OPEs, and is a proposed replacement for the phased-out DecaBDE (Rossi & Heine, 2007). BPADP possesses high flame retardancy, for example when combined with polytetrafluorethylene (PTFE) via a reduction in both flame spread and fire load

(Pawlowski & Schartel, 2007). Resorcinol bis (diphenyl phosphate) (RDP) is another alkyl-substituted TPHP OPE and proposed replacement for DecaBDE (Ye et al., 2021), a further example of novel oligomeric OPEs being increasingly produced and used. In environmental studies where several novel OPEs have been analysed, many are below instrument limits of detection or quantification (ILOD/ILOQ), suggesting the need for further improvement and development of analytical methods for such OPEs. BPADP and three other novel OPEs are presented in **Table 1-2**.

Table 1-2. Comparison of chemical structure and molecular weight between BPADP and three additional novel organophosphate esters (OPEs): resorcinol diphenyl phosphate (RDP), tetrakis(2,6-dimethylphenyl)-m-phenylene biphosphate (RDX) and tetrakis(2-chloroethyl)dichloroisopentyldiphosphate (V6).

Chemical Name	Abbreviation	Chemical Structure	CAS RN	Molecular Weight (amu)
Bisphenol A bis (diphenyl phosphate)	BPADP	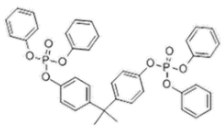	5945-33-5	692.64
Resorcinol bis (diphenylphosphate)	RDP, PBDPP	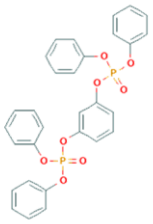	57583-54-7	574.4
Tetrakis(2,6-dimethylphenyl)-m-phenylene biphosphate	RDX, PBDMPP	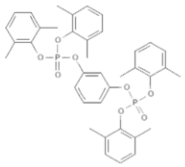	139189-30-3	686
Tetrakis(2-chloroethyl) dichloroisopentyl diphosphate	V6, BCMP-BCEP		38051-10-4	583

Current environmental studies of BPADP focus on occurrence and fate while there is a severe lack of data concerning persistence and bioaccumulation, hindering

risk/hazard assessments of suitability as a potential replacement compound. The current understanding of physico-chemical properties of BPADP consists of modelled estimates and few experimental values. Additionally, study of its metabolism has at present yielded proposed, unconfirmed metabolites (Alves et al., 2018). This lack of information is the case for many, if not all, novel OPEs: occurrence in the environment and exposure to humans and biota is somewhat understood, however data regarding stability and metabolism is lacking. Identifying the properties, stability and metabolic products of novel OPEs is vital to an understanding of persistence, toxicity and bioaccumulation.

1.1.3 Physico-chemical Properties of OPEs including BPADP

As a class of compounds, OPEs exhibit a wide range of physico-chemical properties dependent on their structure (Chokwe et al., 2020). While some OPEs are quite soluble, others are immiscible and solubility was found to decrease with increasing MW (van der Veen & de Boer, 2012). Octanol-water coefficient (LogK_{OW}) values represent the affinity of a compound for organic fractions (e.g. lipids) versus aqueous media and generally increase with increasing MW. LogK_{OW} values often reach a plateau between 400 and 500 amu, with a similar trend being seen for bioconcentration factor (BCF) (van der Veen & de Boer, 2012). In a similar fashion, soil adsorption coefficients (logK_{OC}) typically increase with increasing MW, indicating high sorption to soil with limited mobility for the highest MW OPEs. Several novel OPEs, including BPADP, RDP, RDX and V6, lack experimentally derived values for many common physico-chemical properties such as water solubility, logK_{OC} and logK_{OW}. Rather, values are often limited to modelled estimates with a considerable margin of error. When compared to PBDEs, OPEs as a chemical class are often more soluble and have higher vapour

pressures (Blum et al., 2019), though much variation is seen amongst different compounds within the chemical class.

The physico-chemical properties of novel OPEs, particularly oligomeric compounds, often differ from those of legacy OPEs due to the higher MW and degree of molecular complexity leading to lipophilicity. For example, at 692.63 amu (US EPA, 2014) the MW of BPADP is high compared to legacy OPEs and many other novel OPEs, increasing its lipophilicity. Solubility in water has been both estimated and investigated experimentally, with reported solubility values ranging from $1.92E^{-7}$ ppm to 0.4151ppm (Waaijers et al., 2013b; van der Veen & de Boer, 2012). An aryl phosphate, the volatility of BPADP (vapour pressure 9.0E-6 mmHg; van der Veen & de Boer, 2012) is lower than some legacy OPEs (e.g. TEP; 0.29 mmHg; van der Veen & de Boer, 2012), which contributed to the assumption that limited leaching would occur and that unlike PBDEs, BPADP would be less likely to enter the environment. Various estimates and measured values are reported for the different properties of BPADP, for example two experimentally derived logK_{OW} values are available, reported as 4.5 (Pakalin et al., 2007) and '≥ 6' (ECHA, 2011) while modelled values vary widely from 8.29 to >10 (Bergman et al., 2012; US EPA, 2014). The estimated logK_{OC} of BPADP is ~10.52 (US EPA, 2012), and a BCF of 3.16 was calculated (Pakalin et al., 2007), though variation in reported solubility values adds uncertainty to any calculation of a BCF for BPADP.

1.2 Environmental Fate of Legacy and Novel OPEs

Screening of the contaminant load of OPEs in the environment remains minimal, and as such understanding of environmental fate, distribution and human exposure sources are limited (Chokwe et al., 2020). An assessment of 16 different OPEs within

herring gull populations of the North American Great Lakes showed highest contaminant concentrations in the fat compartments, followed by egg yolk, albumen, muscle and red blood cells (Greaves & Letcher, 2014). Non-detectable concentrations of OPEs were found in all other compartments including liver, brain and blood plasma which supports the current understanding of the high lipophilicity and large molecular size of these compounds. *In ovo* transfer to egg yolk is substantial in herring gulls (Greaves & Letcher, 2014), for which exposure has likely persisted more than two decades due to biomagnification from a diet based on fish predation leading to transfer of the chemicals to herring gull eggs (Greaves et al., 2016).

OPEs have been sampled in all environmental media and display ubiquitous distribution, often at environmental concentrations higher than the BFRs they replaced (van der Veen & de Boer, 2012; Blum et al., 2018). The wide variation in structure and physico-chemical properties (particularly varying logK_{OW} values) of OPEs results in differences in their environmental fate, though preliminary data suggests many of the more novel OPEs may reside in soil 'sinks' due to deposition of airborne OPEs to soil (Li et al., 2019a). Some novel OPEs have been found to be bioavailable in tadpoles (Liu et al., 2020), as well as identified in invertebrates, plankton and multiple fish species (Santin et al., 2016; Wang et al., 2019; Zhao et al., 2019). Many legacy and novel OPEs are detected at high frequencies in surface water, rain, boreal rivers, sediment, and the atmosphere (Allan et al., 2018; Gustavsson et al., 2018; Li et al., 2019a; Zhang et al., 2016). Recently, TPHP and its OPE diester DPHP were identified in flowback water from hydraulic fracturing, with DPHP found to have low sorption in a pH range of 5-9

suggesting potential for migration in groundwater (Funk et al., 2019). Several OPEs are predicted to have a high potential for LRT in the atmosphere (Suhring et al., 2020).

Like the majority of OPEs, BPADP is an additive FR compound and therefore poses a higher risk of entering the environment compared to reactive FRs (Velencoso et al., 2018). BPADP tends to be sampled at high frequencies in sediment when compared to other OPEs, likely in part due to its MW, suggesting hydrophobicity as well as stability in terrestrial environments. In a study of one electronic waste (e-waste) disposal site, BPADP concentrations in river sediments (4-20 ng/g dry weight) were up to three orders of magnitude higher than urban control sites, with concentrations also reported for RDP (1.7-78 ng/g dry weight) and TPHP (4.1-38 ng/g dry weight) (Matsukami et al., 2015b). Matsukami *et al*. also sampled several legacy OPEs including TCIPP, TDCIPP, TCEP and TMP (**Table 1-1**) all of which were below ILOQ in the majority of samples both at control urban and e-waste disposal sites, with no samples exceeding FR concentrations of 4.5 ng/g dry weight. High sorption to soil is estimated from its high calculated logK_{OC} value, which may be a limiting factor in the bioavailability of BPADP in terrestrial ecosystems. Further, the estimated low water solubility of BPADP may also limit bioavailability of the compound in aquatic ecosystems.

BPADP has been found to biodegrade in sewage (Jurgens et al., 2014) with an approximate removal rate of 72% in wastewater treatment at one treatment plant (WWTP) (Liang et al., 2018). Detection in WWTP is indicative of BPADP being well dispersed through the environment, however preliminary data on its removal during the treatment process suggests a reduced burden on receiving waters near treatment plants. Other OPEs studied in WWTPs include tricresyl phosphate (TMPP), found to have a

high removal efficiency due to the ability of the compound to sorb to suspended particulate matter (SPM), while negative removal efficiency was found for RDP and DPHP (Kim et al., 2017). This contrasts with experimental data from a sewage treatment plant in Beijing, China, where a removal rate of 83.3% was reported for RDP (Liang et al., 2018), suggesting variation in removal efficiency globally and/or between different treatment systems. The same study noted a low removal efficiency of 24.4% for the novel OPE, V6 (Liang et al., 2018).

BPADP has been detected in several biological species including fish, amphibians, plankton and invertebrates (Zhao et al., 2019; Liu et al., 2020). The findings of one research study indicate bioavailability of BPADP and other OPEs in two frog species, including maternal transfer to tadpole eggs (Liu et al., 2020). Given its nature as a novel OPE, there is almost a complete dearth of literature reports concerning this particular compound in the environment (Ballesteros-Gomez et al., 2014, Zhang et al., 2016). As industry trends move towards polymerization and longer-chain replacement FRs such as BPADP, there is a need for experimental data concerning the fate and effects of polymers and other long-chain replacement FRs compared to monomers.

The above chemical properties are evidence that BPADP likely partitions into sediment and soil. Bisphenol A (BPA) is a listed physical breakdown product of BPADP in-laboratory (Maine Department of Environmental Protection and Maine Center for Disease Control & Prevention 2007), however the toxicity, metabolism and breakdown of BPADP with respect to biota is currently unknown, with data pertaining to environmental fate highly limited.

1.2.1 OPE Bioaccumulation

Multiple legacy OPEs have been sampled across taxa in all food web levels, with some compounds found to accumulate moving upwards in trophic level at concentrations between 0.85 and 17 ng/g wet weight (Brandsma et al., 2015). Of the nine OPEs studied, Brandsma et al. did not find correlation between OPE concentration and lipid content. Bioaccumulation data concerning novel OPEs is at most preliminary, and non-existent for several novel compounds. Singular studies have suggested potential exposure risk through fish consumption due to bioaccumulation of BPADP and another novel OPE, 2-ethylhexyl diphenyl phosphate (EHDPHP) (Zhao et al., 2019; Wang et al., 2019). Long-chain molecules and polymers are often found to pose higher bioaccumulation potential than their shorter chain counterparts as compounds of higher MW can be less easily excreted from some organisms due to high lipophilicity (Chmiel et al., 2019; Bekele et al., 2021). Further study is required to describe the bioaccumulation factor (BAF) and BCF values for novel, polymeric OPEs, since at very high logK_{OW} values high sorption may minimize bioaccumulation and biomagnification potential.

In particular, BPADP may pose high potential for persistence and bioaccumulation due to its properties, specifically high MW, logP, log*K*ow and log*K*oc. An example of industrial production of plasticizers trending towards long-chain polymers, BPADP may bioaccumulate and persist in nature due to its longer polymeric backbone. This has been suggested for several fish species, though an *in vitro* crucian carp liver microsomal assay at a 10 μM BPADP incubation concentration demonstrated clearance of the compound (Zhao et al., 2019). The same study determined the highest

BAF for BPADP to be between water and plankton/fish, suggesting further study of novel OPE bioaccumulation is warranted.

1.2.2 Toxicological Implication of OPEs

Evidence has suggested OPEs and their metabolites to have potential deleterious effects including cytotoxicity and transcriptomic effects (Pagé-Larivière et al., 2018; Shen et al., 2019), and potent neurotoxicity to zebrafish (Glazer et al., 2018; Poopal et al., 2021). Several OPEs have been detected in multiple fish species (Santin et al., 2016; Zhao et al., 2019) and one study quantified multiple OPEs in the muscle, blubber and brain tissue of dolphins including isodecyl diphenyl phosphate (IDDPP) which was found to cross the blubber-brain barrier and accumulate in brain tissue (Sala et al., 2019). Chlorine-containing OPEs have been demonstrated as carcinogens (van der Veen & de Boer, 2012) suggesting the potential of a carcinogenicity endpoint post V6 exposure.

Aquatic toxicity of novel OPEs is widely reported, partly because most publications concerning these compounds to date focus on aquatic taxa. Most toxicity studies of novel OPEs use zebrafish as the model species, and a range of toxic effects have been reported including developmental changes and acute embryonic and larval toxicity (Zhang et al., 2020; Chen et al., 2021). Screening of groups of OPEs has been conducted in avian embryonic hepatocytes, mostly chicken and double crested cormorant, identifying multiple novel OPEs to pose potent cytotoxicity and transcriptomic effects (Pagé-Larivière et al., 2018). The detection of several novel OPEs across taxa underscores the need to further study environmentally relevant exposures of these compounds to determine the relative risk of the toxicological implications demonstrated above.

1.2.3 OPE Exposure in Humans

The use of a Wistar-Han rat microsomal model in the present study is a relevant mammalian model often applied as a proxy to understanding biotransformation in humans as well as in other mammals. Currently, screening of multiple OPEs indicates the potential for absorption from household dust and subsequent ingestion (de Boer et al., 2016; Brits et al., 2019), which could also be a primary exposure route for BPADP. Dermal absorption of OPEs has been identified as an important exposure pathway in humans (Frederiksen et al., 2018), however the high molecular mass of BPADP renders this pathway less likely. Inhalation of OPEs from household dust, indoor air and fine particulate matter ($PM_{2.5}$) are additional exposure pathways of importance, with recorded occurrences recently noted in humans (Cao et al., 2019). In one study of household dust, BPADP was measured at concentrations up to 1300 µg/g, with the highest concentrations sampled around household electronics (Brandsma et al., 2013b). Ingestion of OPEs through drinking water has occurred mainly from surface water sources contaminated by WWTP effluent, at exposure levels comparable to inhalation of indoor air (Ding et al., 2015). Though lipophilicity of OPEs is lower than that of the BFRs they replaced, OPEs still possess a high affinity for lipids, and have been found in human placenta (Ding et al., 2016).

1.3 Known OPE Stability and Degradation

1.3.1 Degradation

Due to the wide variety of physico-chemical properties of OPEs, chemical or abiotic degradation potential differs between compounds. While not a degradation pathway for some OPEs, chemical hydrolysis has been reported for others, and found to

be pH-dependent with aryl-OPEs found to be the least stable in alkaline media (Su et al., 2016). Chemical hydrolysis has been found to rapidly degrade RDP (US EPA, 2014), though hydrolysis of V6 and tripropyl phosphate (TPRP) required a pH at or above 13 (Su et al., 2016). Hydrolysis of TMPP was found to occur at all studied pH levels (pH of 7, 9, 11 and 13), though hydrolysis was fastest in alkaline media (pH 13) (Su et al., 2016). Overall, Su et al. demonstrated evidence indicating some aryl-substituted OPEs hydrolyze at all studied pH levels, with much faster rates of hydrolysis observed at a pH of 13. In contrast, the studied non-halogenated or halogenated alkyl-substituted OPEs were only observed to degrade via hydrolysis at pH 13. As an aryl-OPE, abiotic hydrolysis may be a degradation pathway of BPADP, though a hydrolysis rate constant would be dependent on water solubility. Such a pathway could also be pH-dependent, though hydrolysis has not been studied experimentally.

1.3.2 Metabolism and Biotransformation in Biota and Humans

Two examples of enzyme classes involved in the catalysis of OPE mammalian metabolism are cytochrome P450 (CYP450) enzymes and paraoxonases (PONs) (Van den Eede et al., 2013). CYP450 mediated metabolism is dependent on nicotinamide adenine dinucleotide phosphate (NADPH) while PON-mediated metabolism occurs independent of NADPH (Van den Eede et al., 2013). Involvement of PON1 has been demonstrated in the enzymatic hydrolysis of OPE insecticides as an important factor in the toxicity of these compounds (Costa et al., 2013). Due to the high prevalence of CYP450 enzymes in the liver, microsomal assays have been conducted to quantify metabolism of several OPEs.

Metabolism of many OPEs has been demonstrated, with the most prevalent pathway of excretion being through urine (Alves et al., 2014). In human liver microsomal (HLM) assays, multiple common metabolism pathways have been identified such as enzymatic hydrolysis (by PONs) and enzyme-mediated hydroxylation, oxidative dehalogenation and dealkylation by CYP450s (Van den Eede, 2013). Both *in vivo* and *in vitro* studies of fish have identified major products of metabolism to be OPE diesters, produced via dealkylation of a parent triester (Li et al., 2020). Specifically, *in vivo* studies of fish have determined that for some legacy OPEs liver metabolism in the form of hydroxylation via CYP450 is of high importance (Hou et al., 2018). The importance of CYP450s is also supported by *in vitro* study of human liver metabolites following exposure to TPHP (Zhang et al., 2018). Biotransformation and metabolism of TPHP into DPHP via dealkylation was reported within embryonated quail eggs and chick carcasses (Marteinson et al., 2020). *In vitro* metabolism of TPHP has been studied in chicken embryonic hepatocytes, where phase I metabolites and phase II conjugates were quantified, and hydroxylation was identified as a biotransformation pathway of particular importance (Su et al., 2015a). Recently, rapid TPHP metabolism and formation of glutathione (GSH) conjugates was reported in an *in vitro* Wistar-Han rat liver microsomal (RLM) assay (Chu & Letcher, 2019).

Some recent studies have focused on the metabolism of OPEs in wildlife, with results from analyses of herring gulls displaying links between chemical structure and metabolism rate, as halogenated OPEs tend to be metabolized with higher efficiency (Greaves et al., 2016). Structurally dependent changes in metabolism were demonstrated in the *in vitro* microsomal assays of polar bears and ringed seals, including alkyl-

substituted TPHP hindering metabolism and species-specific variations in depletion rate (Strobel et al., 2018b). Preliminary data identified metabolism products for TBOEP in an *in vivo* zebrafish liver study (Wang et al., 2017). The phase I and II transformations produced metabolites via hydrolysis, including oxidative O-cleavage/ether bond cleavage and dephosphorylation, dechlorination, oxidative hydroxylation and glucuronic acid conjugation (Wang et al., 2017).

Experimental evidence of novel OPE metabolism is preliminary, with the current understanding of BPADP, RDP, RDX and V6 metabolism summarized in **Table 1-3**.

Table 1-3. Preliminary understanding of the metabolism of bisphenol A bis(diphenyl phosphate) (BPADP) and additional novel organophosphate esters (OPEs) resorcinol diphenyl phosphate (RDP), tetrakis(2,6-dimethylphenyl)-m-phenylene biphosphate (RDX) and tetrakis(2-chloroethyl)dichloroisopentyldiphosphate (V6). Human liver microsomal is abbreviated as 'HLM'.

Novel OPE	Experimental metabolism	Relevant biotransformation reactions	Enzyme mediation
BPADP	Identified *in vitro:* • Liver clearance in crucian carp • HLM & S9 (Phase I & II)	• Phase I: O-dealkylation, hydrolysis • Phase II: glucuronidation, sulphation	• Several metabolites via non-CYP450 mediation • DPHP via CYP450
RDP	Identified *in vitro:* • HLM & S9 (Phase I & II)	• Phase I: abiotic hydrolysis, • Phase II: glucuronidation, sulphation	• CYP450 mediated • DPHP produced with or without NADPH
RDX	No experimental data	No experimental data	No experimental data
V6	Identified *in vitro:* • HLM & S9 (Phase I & II)	Phase I: O-cleavage, O-dealkylation, oxidation, oxidative dichlorination, chemical hydrolysis, enzymatic hydrolysis Phase II: sulphation	May be primarily CYP450 mediated

Ballesteros-Gomez et al., 2015; Alves et al., 2018; Zhao et al., 2019

In a 2019 study of BPADP, metabolites nor metabolism kinetics were determined during the *in vitro* crucian carp incubations but clearance of BPADP was reported via an *in vitro* liver microsomal assay (Zhao et al., 2019). While *in vitro m*etabolism and biotransformation in rat models currently remains unknown, a study of BPADP metabolism with *in vitro* HLM, S9 fraction and serum proposed BPA and DPHP as probable, but unconfirmed, metabolites (Alves et al., 2018). This study also identified phase I metabolites via O-dealkylation and hydrolysis, suggesting abiotic hydrolysis as well as PON enzyme-mediated hydrolysis to be degradation pathways of BPADP. Alves *et al.* indicate PONs to be predominant in the *in vitro* formation of BPA, while DPHP was the only metabolite determined to be produced via CYP450-mediated metabolism. Metabolite concentrations were not quantified, nor were Phase I metabolism kinetics determined, but Phase II glucuronidated and sulfated conjugation products of BPADP were identified (Alves et al., 2018).

1.3.3 Hazard Assessment of BPADP

Based on its structure, DPHP and BPA are potential metabolites of interest for BPADP, however BPA has also been identified as a ~0.01% impurity of some technical BPADP mixtures (Pakalin et al., 2007). TPHP should be quantified throughout all experiments of BPADP metabolism to monitor background contamination and impurity of the standard which may inflate DPHP formation (Matsukami et al., 2015a). DPHP has been found to pose a risk of aquatic toxicity, though studies of acute effects do not often consider environmentally relevant concentrations. Chronic, more environmentally relevant doses (1-100 μg/L) of DPHP have recently been studied and found to inhibit zebrafish growth and metabolism (Chen et al., 2021).

Of prime concern is the high potential for BPADP to degrade into BPA, where the latter is a well-known plastic additive listed as a toxic substance by the Canadian government in 2010 (CBC News, 2010). A recent government notice by Environment and Climate Change Canada (ECCC) in the Canada Gazette considers BPA, its structural analogues and functional alternatives to be toxic or capable of becoming toxic in relation to the Canadian Environmental Protection Act (CEPA, 1999) (Canada Gazette, 2021).

Estrogenic and endocrine disrupting effects of BPA (Rubin, 2011) have been linked to infertility and cancer, gaining attention in the media and with the general public. Recent research suggests common 'BPA-free' bisphenol analogs may lead to similar endocrine disruption as BPA (Mesnage et al., 2017; Rosenmai et al., 2014). As newer industry alternative polymers such as BPADP emerge, the toxicities of which are largely unknown, determining degradation pathways and kinetics are likely to be of critical importance, particularly with the potential of BPA formation. Potent toxicity has been recorded in both rat and human stem cells post-exposure to doses of BPA ranging between one and 10 μM (Harnett et al., 2021). At doses of 50, 150 and 250 μg of BPA per egg, slower embryonic development was observed in chicken, specifically the bursa of fabricius (Cetin & Ozaydin, 2021).

Deleterious effects of BPA exposure have been reported in several aquatic species with early-life stages displaying the highest sensitivity, possibly leading to population level effects (Wu & Seebacher, 2020). This meta-analysis displayed an overall significant ($p=0.002$) negative effect on biota, including on the growth, development and survival rate of many taxa. An acute hazardous concentration was estimated at 1.18 mg/L for marine and estuarine species, a value higher than environmental concentrations but

suggested to indicate sub-lethal adverse effects following BPA exposure (Naveira et al., 2021). Applying Species Sensitivity Distribution Analysis, Naveira *et al.* reported the lowest trophic level, microalga, to have the highest tolerance to BPA with tolerance decreasing up the trophic web.

Proposed to be a suitable alternative to DecaBDE (van der Veen & de Boer, 2012; Brandsma et al., 2013b) despite a lack of environmental fate and toxicity data (Waaijers et al., 2013a), adverse effects of BPADP are thought to be minimal, however a high potential for bioaccumulation and environmental persistence was reported (US EPA, 2014). Preliminary conclusions drawn through analogy from compounds of similar chemical structure indicate that BPADP likely remains immobile in soil and is not believed to leach into groundwater nor vaporize from surface water (US EPA, 2014). Similar initial conclusions determined low biodegradation potential of BPADP in environmental media (US EPA, 2014).

1.4 Applicability of *in silico* Modelling Tools and Non-Target Analysis (NTA) in Understanding OPE Metabolism

One line of evidence used in the present thesis project to approach the study of BPADP is the use of *in silico* modelling tools, which consist of computer software for desktop analyses outside of the laboratory. In recent years, *in silico* methods are increasingly employed in scientific research, due to reduced costs, shorter timeframes and the fact that the field is shifting away from animal testing. The US EPA has announced a phase out of all mammal testing by 2035 (US EPA, 2020) and a 2021 vote saw the European Parliament approve a resolution for the European Commission to phase out animal testing (Naujokaitytė, 2021). Alternatives to animal testing, including *in*

silico tools, are being developed and optimized for meeting these goals, increasing their validity in the prediction of chemical metabolism and toxicity.

With a large chemical class such as OPEs, *in silico* tools allow for screening of several chemicals for preliminary hazard assessment and prioritization of future research goals. Given the nature of novel OPEs being developed as replacements for legacy FRs and plasticizers, this screening is particularly useful when production levels are low and/or experimental data is scarce. To this end, *in silico* computer modelling was conducted to generate predictions of biotransformation and environmental fate for BPADP as well as multiple novel OPEs. By comparing *in silico* predicted and empirical *in vitro* metabolism results, predictive power of modelling tools can be assessed in the specific context of novel OPEs. Further, NTA can be applied to identify non-targeted metabolites and determine the feasibility of such additional *in vitro* metabolites. A non-target approach was therefore applied to screen BPADP incubations for all potential metabolites and identify compounds not yet known or predicted as biotransformation products. NTA is highly applicable to the study of novel OPEs given the lack of data surrounding these compounds and in some cases a lack of relevant internal standards (IS). Recently, several novel OPEs were identified via NTA with some sampled for the first time in the study area (Ye et al., 2021).

1.5 Objectives and Hypotheses of Thesis

To better understand the behaviour of this novel OPE in the environment, the major objective of this thesis research is to detail the fate and biotransformation of BPADP. An analytical method was developed for quantification of BPADP, target metabolites DPHP and BPA, and TPHP impurities. Analysis will determine whether

BPADP is metabolized to target compounds, whether this is mediated by enzymes, and will evaluate the degradation kinetics. A lines of evidence approach is applied, using *in silico, in vitro* and NTA to address the dearth of information concerning the biotransformation, stability and toxicity of BPADP (**Figure 1-1**).

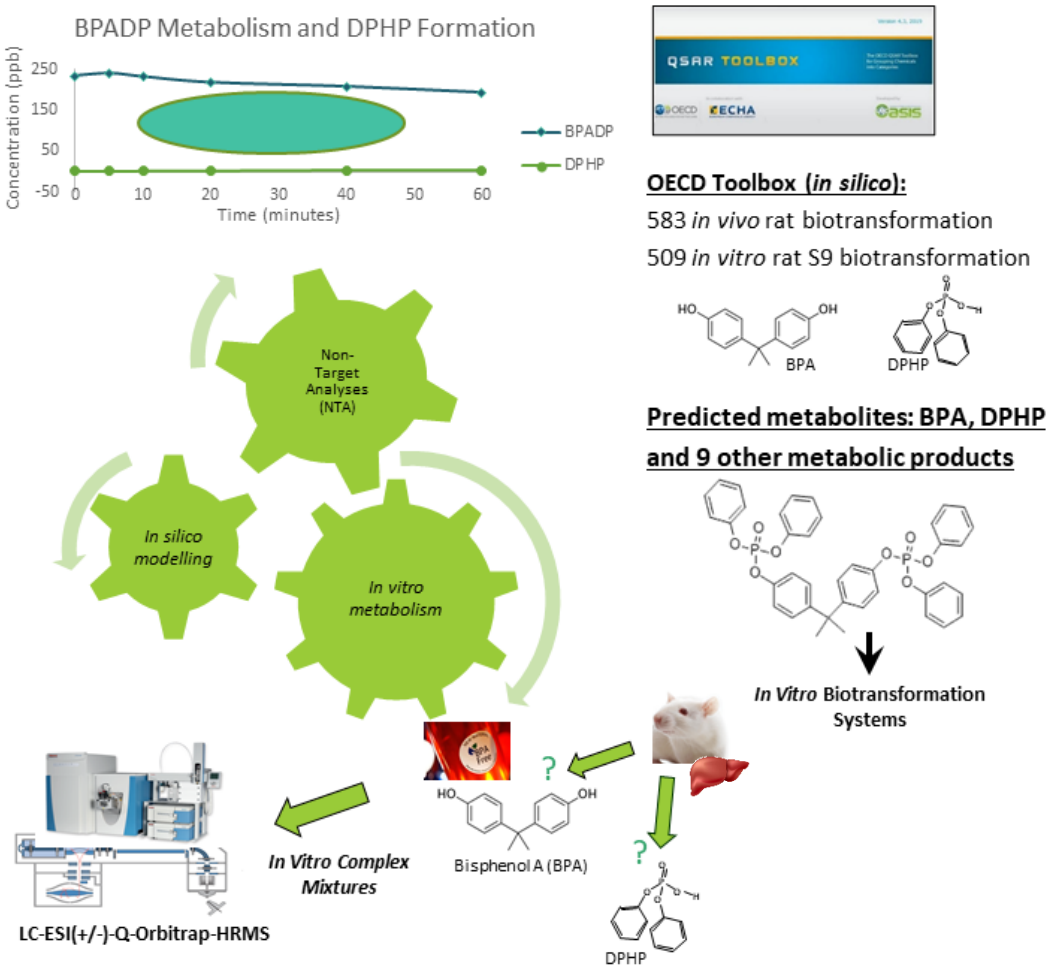

Figure 1-1. Application of a lines of evidence approach towards understanding the array of feasible biotransformation products of bisphenol A bis(diphenyl phosphate) (BPADP), and assess stability and toxicity of the compound and identified products.

The specific objectives of the present thesis project are as follows:

Objective 1: Use *in silico* tools to predict *in vitro* (S9 fraction) and *in vivo* mammalian metabolism of BPADP in rat models via the Organisation for Economic Co-operation and Development (OECD) Quantitative structure-activity relationship (QSAR) Toolbox v4.4.1 and identify the uncertainties and/or limitations of the model with respect to this application. Further, to predict the physico-chemical properties and environmental fate of BPADP and its predicted metabolites using EPI Suite™, including biodegradation, aquatic toxicity, fugacity modelling, logK_{OC}, logK_{OW} and octanol-air coefficient (logK_{OA}). The same method is applied to evaluate the metabolism and physico-chemical properties of the following novel, high MW OPEs: V6, RDX and RDP; comparing the results with those of BPADP. RDP, in particular, will be a focus for comparison due to its high structural similarity to BPADP. OECD Toolbox v4.4.1 was selected as it is a free, publicly available software commonly used in the prediction of metabolites- increasing the reproducibility of the results. Similarly, high reproducibility can be achieved with the application of EPI Suite™, with the capabilities of the software including prediction of stability, aquatic toxicity and physico-chemical properties. EPI Suite™ allows an investigation into the environmental fate and persistence of BPADP, complementary to the prediction of rat metabolites.

> **Hypothesis***:* QSAR software results demonstrate DPHP as a metabolite of BPADP based on known mammalian metabolism reactions. The model identifies that BPA is also a metabolite. *In silico* modelling shows that BPADP is predicted to persist in the environment, demonstrating high BAF and limited biodegradation.

Objective 2: To investigate the degradation and *in vitro* biotransformation of BPADP using enzymatically viable, commercial suspensions of liver microsomes, and compare the findings to that of *in silico* model outcomes. *In vitro* metabolite formation and clearance rate resulting from enzyme-mediated degradation of BPADP will be characterized via ultra-high performance liquid chromatography tandem mass spectrometry (UHPLC-MS/MS), including determination of biotransformation kinetics and confirmation of target metabolites BPA and DPHP. The following animal model will be used: mammalian (Wistar-Han rat liver microsomes).

> **Hypothesis:** BPADP is metabolized, forming both target metabolites BPA and DPHP via sequential dephosphorylation in the Wistar-Han RLM *in vitro* assays. However, the rate of BPADP *in vitro* depletion is slow. The *in vitro* results validate the metabolites predicted by the *in silico* modelling.

Objective 3: To conduct NTA screening of BPADP using a Q-E-Orbitrap UHPLC-HRMS/MS system to generate an understanding of the breadth of *in vitro* biotransformation products in the Wistar-Han RLM model, comparing findings to *in silico* predicted metabolites.

> **Hypothesis:** Several metabolites are identified, demonstrating oxidation and sequential dephosphorylation as major metabolic/biotransformation pathways. Additional *in silico* predicted metabolites are validated via NTA screening of the BPADP *in vitro* metabolism incubate.

Chapter 2: Materials & Methods

2.1 Chemical Compounds and Reagents

BPA and TPHP, each 99+ % purity, as well as $^{13}C_{12}$-BPA (> 98 % purity), DPHP, 99 % purity and trans-1,4-cyclohexanediol bis(diphenyl phosphate) (TCHBDP; > 97 % purity) were obtained from Sigma-Aldrich (St. Louis, MI). Solid BPADP, 98 % purity, was obtained from Toronto Research Chemicals (Toronto, ON, CA) and was prepared in dimethyl sulfoxide (DMSO). All other standards were prepared in HPLC-grade methanol. d_{15}-TPHP (> 98 % purity), in toluene, was obtained from Wellington Laboratories (Guelph, ON, CA) and solid d_{10}-DPHP (95 % purity) obtained from Toronto Research Chemicals (Toronto, ON, CA). Chemical names, abbreviations, structures, and CAS RN of BPADP, BPA and DPHP are provided in **Table 2-1**.

Table 2-1. Chemical name, abbreviation, chemical abstract service registry number (CAS RN), molecular weight and chemical structure of bisphenol A bis(diphenyl phosphate) (BPADP) and its hypothesized metabolites bisphenol A (BPA) and diphenyl phosphate (DPHP).

Abbreviation	**BPADP**	**BPA**	**DPHP**
Chemical Name	Bisphenol A bis (diphenyl phosphate)	Bisphenol A	Diphenyl phosphate
CAS RN	5945-33-5	80-05-7	838-85-7
Molecular Weight	692.64	228.29	250.19
Chemical Structure	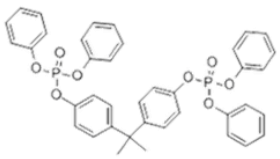	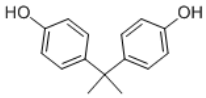	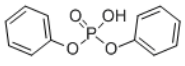

Gentest Male Wistar-Han rat liver microsomes, 20 mg/mL in 250 mM sucrose, and NADPH regenerating system solutions A (NADP+ and Glc-6-PO_4) and B (G6PDH) were obtained from Corning Inc. (Corning, New York, United States). Potassium

phosphate buffer (0.5M; pH 7.4) was purchased from Alfa Aesar (Ward Hill, MA). L-Glutathione reduced (≥ 98 % purity) was obtained from Sigma-Aldrich in powdered form (CAS RN 70-18-8; Lot # SLBS9950). **Appendix I** consists of a complete list of chemicals and reagents, including CAS RN, purities and suppliers.

2.2 *In silico* Metabolite Prediction

Prior to *in vitro* microsomal assays (see section 2.3), rat liver S9 and microsomal metabolites were predicted using the publicly available OECD Toolbox v4.4.1 (OECD, Paris, France). The additional novel OPEs RDP, RDX and V6 (chapter 1, subsection 1.1.2) were also selected for *in silico* profiling. Other software programs were considered including ADMET Predictor (Simulations Plus, Lancaster, California) and MetaPC (MultiCASE Inc., Cleveland, OH), with the OECD Toolbox ultimately selected given the >1000 simulated metabolic transformation reactions available in the database, comparable to other programs and including Phase I and II transformations both *in vivo* and *in vitro.* There is an additional advantage of high reproducibility offered by a free, publicly available program, and the ability to draw comparisons between predicted metabolites (*in vivo* rat metabolites and *in vitro rat liver* S9 and microsomal) with experimental *in vitro* data. Chemical structures were entered via CAS RN as well as unique simplified molecular-input line-entry system (SMILES) code. Predicted metabolites were presented by the toolbox via SMILES code and in ranked order from highest to lowest estimated probability of occurrence. A complete list of SMILES codes for each predicted metabolite, from which compounds were identified and CAS RN assigned, is provided in **Appendix II**. A test of the OECD Toolbox v4.4.1 was performed using the model OPE TPHP, for which *in vitro* rat metabolites have been identified (Chu

& Letcher, 2019) to verify the capacity of the model for identification of both Phase I and II metabolism reactions relevant to OPEs.

Parent compounds BPADP, RDP, RDX and V6 as well as predicted metabolites were screened through EPI Suite™ v4.1.1, publicly available through the United States Environmental Protection Agency (US EPA, 2012). Given the lack of data concerning the physico-chemical properties and environmental fate of novel, high molecular weight OPEs, this screening tool was applied to fill knowledge gaps in the literature, with literature values used where available. Widely used, free and accessible, the program encourages reproducibility and transparency in addition to offering several options for modelling physico-chemical properties and environmental fate. The following models within EPI Suite™ v4.1.1 were used in the prediction of the environmental fate of BPADP and the selected additional novel OPEs: KOWWIN™, WSKOWWIN™, KOAWIN™, KOCWIN™, HENRYWIN™, WATERNT™, BCFBAF™, MPBPVP™, STPWIN™ and LEV3EPI™. The training and validation sets of these models were evaluated to verify whether flame retardant compounds as well as high molecular weight and high logK_{ow} compounds were used to calibrate and test the models during their development. Some EPI Suite™ models have been made available for use within the OECD Toolbox v4.4.1, creating overlap in some toxicological and environmental fate predictions therefore such predictions were reported only once.

Multiple individual models within EPI Suite™ were identified as unsatisfactory for application to OPEs due to model limitations, high molecular weight and low solubility of these compounds and/or lack of sufficient data for reliable estimation. The following individual models were excluded: BioHCwin, ECOSAR™ Version 1.11,

AOPWIN™, HYDROWIN™, AEROWIN™, WVOLWIN™, and DERMWIN™. Where overlap occurred between predicted values from each modelling tool, models were evaluated and one identified as the more accurate estimation based on formulas used and model limitations.

2.3 *In vitro* Microsomal Assays

2.3.1 Concentration Range Finding, Determination of Kinetic Parameters

Michaelis-Menten zero-order enzyme kinetics refers to saturation of the enzyme system such that the maximum biotransformation rate (V_{max}) is independent of the substrate concentration. The substrate concentration corresponding to half of the V_{max} is denoted as the Michaelis rate constant (K_m). BPADP metabolism kinetics were investigated to determine the concentration of BPADP that is >> 2x $K_{m,}$ thereby saturating the enzyme system. A kinetics assay was designed based on previous findings that enzyme system saturation is achieved when herring gull, polar bear and ringed seal liver microsomal incubations are carried out with a final OPE dosing concentration of 2 µM (Greaves et al., 2016; Strobel et al., 2018a). To determine V_{max} and K_m, five dosing concentrations of BPADP were selected, with resulting incubation concentrations ranging from 356 ppb (0.514 µM) to 1.78 ppm (2.57 µM) to exceed 2 µM and include lower concentrations similar to experimentally derived solubility values (chapter 1, section 1.1.3). Analysis of a suite of phosphorous flame retardants found decreasing solubility with increasing molecular weight (van der Veen & de Boer, 2012), including for OPE FRs with phenyl groups similar to BPADP. In the context of aqueous assays, this further underscores the suitability of a 2 µM (1.44 ppm) incubation concentration as being >>2x the K_m and ensuring zero-order metabolism kinetics. At each of the five

concentrations, the initial depletion of BPADP and formation of target metabolite DPHP, were quantified in a 10 minute incubation with aliquots taken at zero, two, five and 10-minute time points.

2.3.2 *In vitro* Assay Method Optimization

The liver microsomal assay procedure followed previously published methods for assays conducted with rat, ringed seal, polar bear and herring gull liver microsomes (Chu et al., 2011; Greaves et al., 2016b; Strobel et al., 2018a,b) with minor modifications for optimization based on the low solubility and high adsorption of BPADP, as well as mitigation of background BPA contamination.

BPADP standard in toluene was replaced by solid BPADP prepared in DMSO due to low % recovery of BPADP at initial *in vitro* assay time points (t_0). Glass test tubes were replaced by Teflon test tubes with the goal of reducing adsorption of BPADP to glass surfaces, with ice bath assays conducted to increase t_0 concentrations to within 15-20 % of the known dosed incubation concentration. Considering the low BPADP water solubility, dosing solutions were prepared in amber bottles, covered in aluminum foil then sonicated 24 hours immediately prior to each assay to minimize any potential chemical hydrolysis. Thus, a 60 mL BPADP buffer solution was prepared prior to each experiment, consisting of: 120 µL 1000 ppm BPADP standard (in DMSO) and 59.88 mL 0.5 M pH 7.4 buffer diluted to 0.1 M in deionized water. To reduce background contamination, the vacuum filtration step was removed during preparation of the mobile phases prior to UHPLC analysis.

2.3.3 Time-Dependent Biotransformation Assay Procedure

Wistar-Han rat liver microsomes, NADPH Regenerating System Solutions A and B were stored at -80ºC, with aliquots thawed on ice prior to each assay. All chemicals, internal standards and reagents were stored in the fridge between assays. Glass was cleaned at 450ºC for eight hours prior to each assay to avoid contamination, with one test tube cleaned for each microsomal incubation, as well as for each time point at which the metabolism reaction was stopped. To each time point test tube, 300 µL of acetonitrile (ACN) was added, as well as 100 µL of 40 ppb combined internal standard for a total volume of 400 µL. Each reaction tube was covered with aluminum foil to prevent evaporation while avoiding the use of plastic caps due to potential BPA contamination.

To each sample 890 µL of either 400 ppb or 2 ppm freshly sonicated BPADP buffer solution was added, as well as 50 µL microsomes, 50 µL NADPH system solution A and 10 µL NADPH system solution B. The resulting incubation concentrations of BPADP were therefore 356 ppb and 1780 ppb, selected after completion of the kinetics assays detailed in sub-section 2.4.1 above. In agreement with available experimental data regarding BPADP water solubility (Waaijers et al., 2013b), assays were initially conducted at 356 ppb (0.514 µM), followed by assays at a concentration of 1780 ppb (2.57 µM) to achieve the 2 µM dosing concentration previously demonstrated to achieve zero-order enzyme kinetics for several OPEs. **Figure 2-1** illustrates the *in vitro* assay design following method optimization. Triplicate assays were conducted which included three active replicates (active microsomes, NADPH System Solution and BPADP solution) in addition to a method blank, positive control and two negative controls as detailed in 2.4.3.

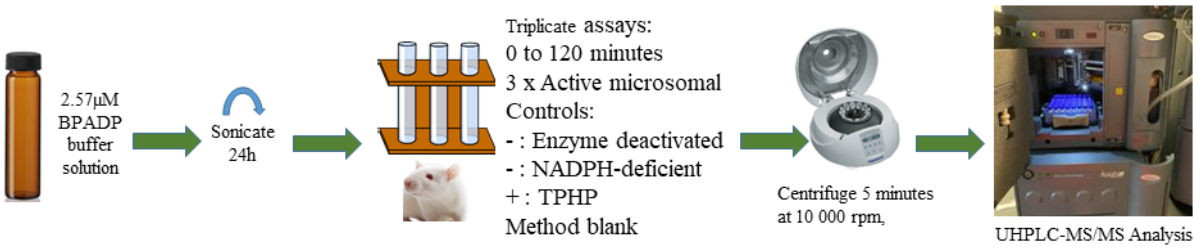

Figure 2-1. Optimized *in vitro* assay method design for quantifying time-dependent biotransformation of bisphenol A bis(diphenyl phosphate) (BPADP).

Enzymatically deactivated negative control incubations were prepared using an equal volume of deactivated microsomes (method of deactivation is described in subsection 2.4.3). In place of NADPH A & B, 60 µL deionized water was added to the second (NADPH-deficient) negative control while method blanks contained 50 µL active microsomes, 50 µL NADPH A, 10 µL NADPH B, 790 µL deionized water and 100 µL pH 7.4 buffer. The positive control consisted of: 2 µL of 60 ppm TPHP, 788 µL deionized water, 100 µL pH 7.4 buffer, 50 µL active microsomes, 50 µL NADPH A and 10 µL NADPH B.

The incubation test tubes, each at total volumes of 950 µL were placed in a water bath at 37°C and shaken at 80 rpm for at least two minutes. The timer was started immediately after addition of 50 µL Wistar-Han rat liver microsomes to the first incubation test tube (total volume 1 mL), indicating time zero. Each incubation test tube was vortexed for twenty seconds to allow for homogenization of the incubate and a 100 µL aliquot taken within 30 seconds of the addition of microsomes. The TPHP positive controls were vortexed for only five seconds due to known rapid metabolism, with the aliquot taken within 10 to 15 seconds after addition of microsomes. Aliquots were dispensed into appropriate t_0 test tubes, covered with tin foil and vortexed, with the incubation test tube returned to the water bath. At five, 10, 20, 40, 60, 90 and 120 minute

time points, 100 µL samples were then taken and added to the appropriate test tube, covered and vortexed. The assays were completed in this way for all incubation test tubes, with the exception of the TPHP positive control incubations, during which an additional two minute aliquot was taken to account for rapid metabolism. All samples from each time point were filtered through VWR Modified Nylon 0.2 µm, 500 µL centrifugal filters, which had been pre-rinsed with 500 µL of HPLC-grade methanol. The samples were centrifuged at 10 000 rpm for five minutes through the cleaned filters and transferred to labelled HPLC 700 µL glass vials for analysis.

2.3.3.1 Optimized Assay for Possible Paraoxonase (PON) Enzyme Mediation

The exact procedure detailed in 2.3.3 was followed for this experiment, with the following exceptions: each of the three replicates were deficient of NADPH system solutions A and B, one set of active replicate controls was conducted and the positive control quantified depletion of BPA (rather than TPHP) in the presence of both NADPH and active microsomes to assess the rate of BPA depletion over the course of an optimized assay. The main purpose was to increase the number of negative control replicates and further investigate the role of non-CYP450 enzymes (which do not require NADPH) in BPADP metabolism and subsequent formation of DPHP and BPA, particularly a potential role of PON enzymes. Additionally, adjusting the positive control to BPA confirmed both that the assay was functional and *in vitro* depletion of BPA was occurring under optimized assay conditions as described in section 2.3.3 above.

2.3.4 *In vitro* RLM Assay for Q-E-Orbitrap Non-Target Analysis (NTA)

The procedure was replicated as in section 2.3.3 with modifications such that samples were made suitable for Q-E-Orbitrap identification of target *in vitro* metabolites

as well as NTA for unknown metabolites. A 2 ppm BPADP solution was prepared in deionized water and pH 7.4 buffer the day prior and sonicated for 24 hours as per the methodology in section 2.4.2. Samples consisted of a method blank, four replicates at the zero minute time point and four replicates at the 120- minute time point. The blank sample incubation contained 1748 µL 0.1 M Biotage Potassium Phosphate (pH 7.4) buffer while all replicates (t=0 and t=120) contained 1748 µL of the 2 ppm BPADP solution. All samples contained 32 µL deionized water, 100 µL Wistar-Han rat liver microsomes, 100 µL NADPH A and 20 µL NADPH B.

Reactions were initiated for the method blank and zero minute replicates via addition of the microsomes, with the reaction stopped by addition of 4 mL diethyl ether within 30 seconds of initiation. Reactions of the four 120- minute replicates were initiated, incubated for 120 minutes in a water bath at 37ºC and shaken at 80 revolutions per minute (rpm), then terminated by addition of 4 mL diethyl ether. All samples were covered with tin foil, parafilmed, and vortexed for one minute immediately after addition of diethyl ether, then centrifuged at 3500 rpm for five minutes. Frozen for a minimum of one hour, the ether phase of each sample was retained and volatilized with the ice discarded. To the dried samples 100 µL HPLC-grade methanol was added before each sample was sonicated for 10 minutes and filtered through pre-rinsed PALL Life Sciences Nanosep 0.2 µm wwPTFE centrifuge filters for five minutes at 3500 rpm. Lastly, samples were transferred to vials for Q-E-Orbitrap analysis.

2.3.5 *In vitro* Glutathione Adduct Assay

Though Phase I metabolism was the focus of this research, the *in vitro* microsomal assay procedure in 2.3.4 was adapted for identification of glutathione (GSH)

adducts with BPADP Phase I metabolites. Formation of GSH adducts was recently reported in an *in vitro* rat microsomal assay with TPHP (Chu & Letcher, 2019) and following a similar method, 0.15 g/mL GSH solution was prepared in deionized water immediately prior to the experiment. A 2 ppm BPADP solution prepared in deionized water and buffer the day prior and sonicated for 24 hours as per the methodology in section 2.3.2. Assays consisted of a method blank, four replicates at the zero minute time point and four replicates at the 120- minute time point. The blank sample incubation contained 1748 µL 0.1 M Biotage Potassium Phosphate (pH 7.4) buffer while all replicates (t_0 and t_{120}) contained 1748 µL of the 2ppm BPADP solution. All sample incubations contained 20 µL GSH (for an incubation GSH concentration of 0.5 M), 100 µL Wistar-Han rat liver microsomes, 100 µL NADPH A, 20 µL NADPH B and 12 µL of 1 M magnesium chloride. From this point the procedure was identical to 2.3.4.

2.4 *In vitro* Assay Quality Assurance & Quality Control

2.4.1 Internal Standards

The internal standards for BPADP, BPA, DPHP and TPHP were TCHBDP, $^{13}C_{12}$-BPA), d_{10}-DPHP and d_{15}-TPHP, respectively. In the absence of an isotopically enriched internal standard for BPADP, TCHBDP was selected given the similar structures and molecular weights of the two compounds. Combined 40 ppb internal standard solution, consisting of the four aforementioned internal standards each at a concentration of 40 ppb, was added to all samples in the kinetics and time-dependent biotransformation assays.

2.4.2 Method Blanks

Method blanks contained all reagents present in the assay incubation mixture samples except for BPADP, and the same procedure was followed for method blanks as for samples. Contamination was minimized wherever possible following the recommendations of a worldwide inter-laboratory study of OPE flame retardant and plasticizer analysis (Brandsma et al., 2013a). While the purity of BPADP was 98 %, TPHP is a known impurity in technical mixtures of BPADP and therefore its concentration was monitored in all blanks, controls and replicates. Analysis of a commercially available BPADP standard found the composition to be 82% monomer, 7% TPHP and 11% dimer (Riddell et al., 2017). Thus, any TPHP formation could be attributed to slight impurity of the BPADP standard and DPHP formation can be reliably attributed mostly to BPADP depletion rather than depletion of TPHP impurities.

2.4.3 Positive & Negative Controls

The positive control assays were based on the time-dependent biotransformation of TPHP, which was added to assay samples (as described in subsection 2.3.3) in place of BPADP, with all other reagents kept consistent with the samples. The same assay method was conducted for the positive control as the samples, which demonstrated depletion of TPHP via Wistar-Han rat liver microsomes during the assays. TPHP depletion and subsequent metabolite formation has previously been demonstrated with *in vitro* microsomal assays (Strobel et al., 2018b; Chu & Letcher, 2019).

Two types of negative controls were included in the time-dependent biotransformation *in vitro* assays. The first negative control was based on enzymatically deactivated microsomes, to account for non-enzymatic activity. The second type of

negative control was based on the exclusion of NADPH system solutions A and B to account for mediation by non-CYP450 enzymes. All other reagents and the procedure were kept consistent with the samples, deactivated microsomes having been denatured for five minutes at 100°C and an equal volume of deionized water used in place of NADPH A and B.

2.5 UHPLC Analysis

2.5.1 Quantification of BPADP and Target Metabolites DPHP and BPA

Analysis of all time-dependent *in vitro* assay samples was conducted utilizing Waters Acquity Ultra High Performance Liquid Chromatography coupled to a Waters Xevo TQ-S Triple Quadrupole Mass Spectrometer (UHPLC-MS/MS) operated with an electrospray ionization (ESI) source. Similar, robust methods for UHPLC-MS/MS analysis of organophosphate triesters and diesters have previously been published (Chu & Letcher, 2015; Su et al., 2015b; Chu & Letcher, 2018). The stationary phase being non-polar, a Kinetex EVO C18 column (50 x 2.1 mm, 1.7 µm particle size) separated analytes by polarity from most to least polar (DPHP, BPA, TPHP and lastly BPADP), with a column and sample temperature of 45 °C and 20 °C, respectively. Water and methanol mobile phases (A and B, respectively) were each prepared to contain 2 mM ammonium acetate, and each sample injection consists of a 10 µL aliquot. The initial flow rate was set to 0.5mL/min, mobile phase B starting at 5 % and the gradient increasing over the first five minutes until mobile phase B is at 95 %, which is held for five minutes. The column equilibrates for five minutes while the initial composition of the mobile phase is restored, concluding at a total run time of 15 minutes.

A calibration curve, sample replicates, method blank, positive control and negative control were quantified, with a methanol blank run before and after each set of replicates to ensure accuracy and minimize carry-over. The calibration standards were re-analyzed after every two sets of sample replicates (before and after every 16 samples). The MS/MS was operated in both ESI+ and ESI- modes, with the chromatogram function of multiple reaction monitoring (MRM-Channel 4-ES+/-). From one to 4.2 minutes the elution of DPHP, BPA and their corresponding internal standards (d_{10}-DPHP, $^{13}C_{12}$-BPA) are monitored using ESI-, while TPHP, BPADP and their internal standards (d_{15}-TPHP and T-CH-BDP) are monitored in ESI+ from elution times of 4.2 to 10 minutes. Analysis of BPADP consisted of two functions: function 3 (BPADP) capable of high sensitivity at low concentrations, while function 4 (BPADP(2v)) is suitable for analysis of higher concentrations. The nebulizing gas being nitrogen and argon used as the collision gas, the capillary voltage is 2.5 kV with respective source and desolvation temperatures of 150 ℃ and 500 ℃. The desolvation gas flow rate is 1000 L/hr and the cone gas flow rate 150 L/hr. **Table 2-2** provides the ILODs and ILOQs for all target compounds.

Table 2-2. Instrument limit of detection (ILOD) and limit of quantification (ILOQ) values for target compounds: bisphenol A bis(diphenyl phosphate) (BPADP), diphenyl phosphate (DPHP), triphenyl phosphate (TPHP) and bisphenol A (BPA).

#	Name	ILOD (ng/mL)	ILOQ (ng/mL)	Linearity-H (ng/mL)	Linearity-L (ng/mL)	r
1	TPHP	0.001	0.004		0-10	>0.99
3	BPADP	0.0008	0.003		0-10	>0.99
4	BPADP(2v)	0.05	0.15	0-500		>0.99
5	BPA	0.09	0.29	0-500	0-500	>0.99
6	DPHP	0.01	0.04	0-500	0-500	>0.99

Using MassLynx v4.1 (Waters, 2014), depletion of BPADP and formation of target metabolites were quantified. Using the optimized methodology of the present

thesis work, **Table 2-3** contains the complete list of monitored transitions, and further details regarding instrument analysis. For quantification and linearity of response, a calibration curve of eight standards was prepared for each analysis and quantified at the beginning and end of each analysis as well as after every 16 samples. Observation via multiple reaction monitoring allowed for identification of compounds using characteristic mass transitions and the comparison of retention times (RT) between samples and authentic standards. Following quantification, 'TargetLynx' software was utilized to integrate peaks for calculation of the area under the curve and translate the chromatogram response to concentration, considering the internal standard response.

Table 2-3. UHPLC-MS/MS analysis for determination of bisphenol A bis(diphenyl phosphate) (BPADP), diphenyl phosphate (DPHP), triphenyl phosphate (TPHP) and bisphenol A (BPA) and corresponding internal standards: functions, transitions (including molecular and fragment ions) and compound-dependent operation parameters.

Function	Compound	Precursor ion (m/z)	Product ion (m/z)	Cone(v)	Coll.(v)	ESI	RT(min)	Internal Standard
1	**TPHP**	**327.1**	**152.1**	**48**	**32**	**(+)**	**4.41**	**d_{15}-TPHP**
		327.1	*77*	*48*	*36*			
	d_{15}-TPHP	**342.2**	**160**	**48**	**32**			
		342.2	*82*	*48*	*36*			
2	**T-CH-BDP**	**581**	**251**	**42**	**18**	**(+)**	**4.95**	
		581	*331.1*	*42*	*6*			
3	**BPADP**	**693.2**	**367.1**	**80**	**38**	**(+)**	**5.45**	**T-CH-BDP**
		693.2	*327.1*	*80*	*34*			
4	**BPADP(2v)**	**693.2**	**327.1**	**2**	**38**	(+)	5.45	T-CH-BDP
		693.2	*367.1*	*2*	*34*			
5	**BPA**	**227**	**133.1**	**52**	**26**	**(-)**	**3.45**	**$^{13}C_{12}$-BPA**
		227	*212.1*	*52*	*12*			
	$^{13}C_{12}$-BPA	**239**	**139.1**	***52***	***26***	**(-)**	**3.45**	
		239	*224.1*	*52*	*12*			
6	**DPHP**	**249**	**93.2**	**65**	**25**	**(-)**	**2.3**	**d_{10}-DPHP**
		249	*155.1*	*65*	*20*			
	d_{10}-DPHP	**259.1**	**98.2**	**65**	**25**	**(-)**	**2.26**	
		259.1	*159.1*	*65*	*20*			

All peaks were reviewed, tails corrected where necessary and RT verified. Concentration values (in units of ppm) were back calculated to represent the incubation solution concentration consistent with the assay. Concentrations of each compound were graphed as well with intercepts set to include a zero value.

Table 2-4 displays internal standard recovery efficiencies for all replicates in each of the three triplicate time-dependent assays (n = 9), including all compounds analyzed. Recovery efficiency varied between compounds and assays, with consistently high efficiencies of BPADP and TPHP recovered in assays one and three. Recovery efficiencies of DPHP and BPA varied between each inter-day assay and between some replicates in the first and second assays, while consistent and acceptable recoveries of BPADP and TPHP were recorded in all assays except the first, where higher recovery efficiencies were recorded. With few exceptions, recovery efficiencies of all four compounds were consistent across replicates and time points in the second and third assays. Consistent, high recovery efficiencies were recorded in assay one, particularly for BPADP and TPHP as well as certain replicates of BPA and DPHP time points.

Low recovery efficiencies may be attributed in part to air bubbles present in a sample vial, interfering with an accurate acquisition and the sample volume. Total analysis durations were typically 20 to 30 hours and while each sample vial was shaken immediately prior to the start of each analysis run, air bubble formation may have occurred at a later point during an analysis due to temperature changes within samples over the course of the analysis. Further, adsorption to glass vials may account for recovery loss of DPHP and BPA in the second assay as well as BPADP in certain samples of the third assay. Increased likelihood of adsorptive loss over time during an

analysis may account for the lower recovery efficiencies of DPHP and BPA in the second and third replicates of the second assay (2021-11-30). Greater than 100% recovery efficiencies may be due in part to evaporation of the solvent, resulting in a higher analyte concentration quantified during analysis. Highest recovery efficiencies were calculated for the first assay, while values were typically within the acceptable 80 – 120% range for the second and third assays. Particularly for BPADP and TPHP, loss of solvent due to evaporation during analysis may have occurred in the first assay samples and leading to recovery efficiencies greater than 100%. This may have also resulted from a pipetting error when dispensing the combined internal standard solution into sample incubations, resulting in higher concentrations of internal standard across replicates when compared to the calibration curve. This would account for the high recovery efficiencies found predominantly in the first assay samples and variation of recovery efficiencies across assays.

Table 2-4. Internal standard recovery efficiencies (%) for UHPLC-MS/MS analysis of bisphenol A bis(diphenyl phosphate) (BPADP), diphenyl phosphate (DPHP), triphenyl phosphate (TPHP) and bisphenol A (BPA), reported for each inter-day triplicate assay (1, 2, 3) conducted at a 1.78 ppm BPADP incubation concentration.

	Internal Standard Recovery Efficiency, %				
Date	**Time point**	**BPADP**	**DPHP**	**BPA**	**TPHP**
1: **2021-11-22**		139.470;	122.653;	129.100;	156.590;
Replicates:	t_0	139.530;	95.255;	104.429;	157.782;
1; 2; 3		129.179	110.736	122.944	150.260
	t_5	135.490;	70.392;	117.816;	154.649;
		141.339;	93.197;	97.216;	163.494;
		132.762	106.79	110.145	155.811
	t_{10}	140.273;	118.248;	114.612;	159.919;
		143.100;	91.814;	103.081;	165.118;
		132.461	100.542	124.574	156.303
	t_{20}	139.724;	107.798;	120.595;	158.039;
		142.840;	52.871;	105.622;	165.095;

		131.584	102.27	110.089	156.896
	t_{40}	147.792; 148.550; 135.347	107.272; 54.014; 105.192	108.640; 114.088; 120.514	168.491; 169.908; 159.966
	t_{60}	144.559; 143.715; 138.309	106.792; 85.025; 100.721	113.416; 102.755; 131.955	164.269; 164.139; 163.192
	t_{90}	137.376; 132.350; 119.227	101.327; 76.891; 56.209	120.872; 86.303; 119.312	158.033; 152.554; 139.558
	t_{120}	137.959; 141.296; 121.649	93.949; 81.428; 86.588	119.040; 95.249; 108.597	157.207; 163.116; 144.350
Date	**Time point**	**BPADP**	**DPHP**	**BPA**	**TPHP**
2: **2021-11-30 Replicates: 1; 2; 3**		96.019;	102.459;	137.092;	103.566;
	t_0	96.426; 89.671	46.301; 43.099	45.331; 35.659	103.195; 101.918
	t_5	101.261; 100.246; 91.066	48.487; 41.759; 44.175	52.659; 44.886; 31.302	111.465; 108.979; 103.524
	t_{10}	99.784; 98.600; 91.151	44.186; 103.814; 43.781	52.034; 118.439; 38.815	110.321; 107.239; 104.860
	t_{20}	96.149; 91.731; 95.610	92.146; 38.935; 45.767	129.864; 38.592; 46.891	106.534; 99.755; 108.997
	t_{40}	97.916; 90.973; 89.931	42.931; 39.681; 37.642	48.232; 43.098; 39.025	108.245; 98.955; 102.356
	t_{60}	97.290; 93.635; 87.879	103.231; 39.793; 101.413	133.937; 40.252; 144.854	108.265; 102.538; 99.999
	t_{90}	94.736; 103.518; 93.794	45.054; 44.349; 42.511	57.168; 39.047; 47.650	107.844; 113.495; 107.278
	t_{120}	94.274; 96.38; 91.919	99.803; 40.161; 40.237	155.183; 44.363; 57.557	105.363; 106.748; 106.028
Date	**Time point**	**BPADP**	**DPHP**	**BPA**	**TPHP**
3: **2021-12-10 Replicates: 1; 2; 3**	t_0	85.587; 92.085; 78.212	86.212; 83.633; 89.523	90.668; 86.706; 73.7054	92.325; 94.117; 89.703

t_5	86.097;	85.809;	89.017;	88.372;
	94.531;	84.926;	89.665;	96.714;
	67.454	72.955	70.159	76.252
t_{10}	90.484;	85.629;	76.709;	87.372;
	95.011;	85.079;	75.255;	89.214;
	79.782	90.192	91.080	88.878
t_{20}	66.809;	63.542;	69.097;	61.864;
	92.904;	80.155;	77.461;	82.355;
	76.243	83.168	69.255	82.642
t_{40}	89.206;	83.759;	91.560;	80.880;
	86.453;	70.755;	80.922;	76.740;
	89.019	98.318	90.006	96.009
t_{60}	87.905;	81.655;	87.072;	80.207;
	94.695;	73.897;	87.837;	84.195;
	88.797	90.201	76.913	95.830
t_{90}	92.148;	85.512;	85.118;	85.167;
	96.251;	79.742;	85.218;	84.989;
	90.431	90.319	95.738	96.223
t_{120}	94.239;	84.085;	95.073;	85.493;
	97.436;	74.758;	82.497;	88.506;
	90.142	95.713	85.625	94.842

2.5.2 Analysis of Additional Metabolites

Trends in the response of five additional *in vitro* metabolites (**Table 2-5**) were measured and monitored over time to further understand the mass balance of BPADP metabolism and metabolite formation. Following biotransformation assays, *in vitro* samples were sealed and refrigerated before triplicate samples of replicates, method blanks, enzymatically deactivated and NADPH-deficient controls were re-analyzed via UHPLC-MS/MS using an analytical method developed for identification of select novel metabolites. The method is the same as that used to quantify biotransformation samples with the following differences: 5 uL sample injection, 5 uL/min flow rate, ESI+ operation only, and elution times of between two and 10 min. While internal standards were not available, the response over time was identified using TargetLynx software and plotted.

Table 2-5. UHPLC-MS/MS analysis for determination of non-targeted metabolites: channels, transitions (including molecular and fragment ions) and compound-dependent parameters.

Channel	Compound	Precursor ion (m/z)	Product ion (m/z)	Cone(v)	Coll.(v)	ESI	RT(min)
1	**BPA-DPHP**	461.20	135.00	80	40	**(+)**	4.68
2	**BPA-DPHP**	461.20	327.10	80	40		
3	**T-CH-BDP**	581	251	42	18	**(+)**	4.79
4	**BPADP-BZ**	617.1	327.1	80	40	**(+)**	4.27
5	**BPADP -BZ**	617.1	367.1				4.28
6	**BPADP**	693.2	327.1	80	40	**(+)**	5.29
7	**BPADP**	693.2	367.1				5.29
8	**BPADP +O**	709.2	327.1	80	40	**(+)**	5.10
9	**BPADP +O**	709.2	367.1				5.08
10	**BPADP +2O**	725.2	367.1	80	40	**(+)**	4.86
11	**BPADP +2O**	725.2	465.2				4.81
12	**BPADP +2O+2H**	727.2	327.0	80	40	**(+)**	4.52
13	**BPADP +2O+2H**	727.2	367.1				

2.6 UPLC Q-Exactive Orbitrap HRMS Analysis

2.6.1 BPADP Metabolites Non-Target Analysis (NTA) Analytical Parameters

The QE-Vanquish ultra-high performance liquid chromatography (UHPLC) method consisted of a 26 minute total run time, beginning at 95 % A with a 0.3 mL/min flow rate and ramping up to 5 % A in 10 minutes, held for 10 minutes before returning to 95 % A over one minute and holding until the end of the run. A Kinetex xB-C18100A column (100 x 2.1 mm, 1.7 µm particle size) was used, with mobile phases identical to those used in UHPLC analysis (see section 2.5.1). The Q-Exactive Orbitrap HRMS (Thermo Scientific, Waltham, MA, United States) system method was operated in both Full Scan mode and fragment analysis (ddMS) mode, positive polarity, ESI (+) and with

70 000 resolution, scanning in a range of 70 to 1050 mass-to-charge ratio (*m/z*). Lock masses were: 445.12003 *m/z* $(Si(CH3)2O))_6$, with a six second chromatograph peak width and 20 minute duration. Set to a target of 10^6 ions, Automatic Gain Control (AGC) determined when ions captured in the quadrupole C-trap reached the Orbitrap. Ion source parameters consisted of: 2.5 K spray voltage, S-lens RF level of 55, 45 sheath gas flow rate, 10 auxiliary gas flow rate and zero sweep gas flow rate, 350 °C desolvation capillary temperature, 450 °C aux gas heater temperature.

2.6.2 GSH Adduct Identification: Analytical Parameters

Three specific GSH adducts (**Table 2-6**) were of particular interest, and analyses used the final samples from section 2.3.4 as non-GSH controls given that they were prepared to contain the same total incubation volume. The LC targeted selected ion monitoring (t-SIM) method used a Zorbax eclipse Plus C18 Rapid Resolution HT column (2.1x100mm 1.8-Micron 600Bar), suitable for basic groups, at a column temperature of 40 °C with a 0.4 mL/min flow rate for each mobile phase (0.1 % formic acid in deionized water (A) and acetonitrile (B)). The gradient consisted of a 0.3 mL/min flow throughout, beginning at 5 % B and holding for 30 seconds to concentrate compounds before ramping up to reach 95 % B at 10 minutes, holding for five minutes, decreasing to 5 % B at minute 16, and this was held for five minutes until the end of the run at 21 minutes.

The MS t-SIM method was operated in positive polarity, at a resolution of 70 000 and with a six second peak width, scanning mass spectra in a range of 150 to 1200 *m/z* with a 4.5 *m/z* isolation window. Ion source parameters consisted of: 1.00 kV spray voltage, AGC of $5e^4$, S-lens RF level of 40.0, 80 sheath gas flow rate, 20 auxiliary gas

flow rate and zero sweep gas (N_2) flow rate, 300 °C desolvation capillary temperature, 500 °C aux gas heater temperature. Lock masses were 445.12003 *m/z* ($(Si(CH3)_2O)_6$), with a six second chromatograph peak width.

Table 2-6. Selected glutathione (GSH) adducts analyzed via Q-E-Orbitrap, including molecular formula, molecular mass and transformations of the parent compound.

Molecular Formula	**Ions monitored *(m/z)***	**Transformations**
$C_{49}H_{49}N_3O_{14}SP_2$	998.24832	BPADP + GSH -2H
$C_{49}H_{51}N_3O_{15}SP_2$	1016.25884	BPADP + GSH +O
$C_{49}H_{49}N_3O_{16}SP_2$	1030.23815	BPADP + GSH +2O – 2H

2.6.3 Identification of Feasible Metabolites

Metabolite identification was conducted using the automatic search capabilities of Compound Discoverer version 3.2 (Thermo Fisher Scientific, Waltham, MA, U.S.A.) with results confirmed via the manual search function of FreeStyle version 1.6 (Thermo Fisher Scientific, Waltham, MA, U.S.A.). Expected compounds were generated in Compound Discoverer v3.2 following the criteria in the workflow tree (**Figure 2-2**). The method included automatic blank subtraction, with the following transformations searched: dearylation, dehydration, demethylation, desaturation, hydration, oxidation, reduction, ionization and loss of a diphenyl phosphate group. Results were filtered to minimize interference and background levels, specifically filtering for the following criteria: 'RT [min] is greater than 3.00'; 'Parent Compound is equal to Bisphenol A bis(diphenyl phosphate)'. Further, generated compounds were evaluated for a mass shift of < 5 ppm and a t_{120}/t_0 response ratio > 2 as generated compounds present at t_0 were considered background rather than metabolites. Of the remaining 80 expected compounds generated, first comparisons were made between NTA results and the

compounds predicted *in silico* to prioritize feasibility determination. Due to time constraints, the 80 generated compounds were then screened for products of applicable oxidation reactions as well as loss of DPHP and loss of a benzene ring.

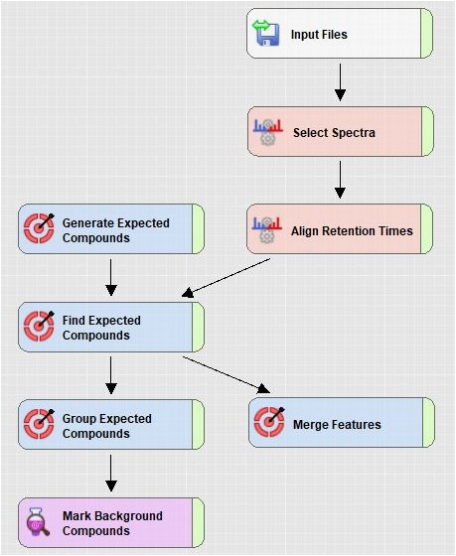

Figure 2-2: Compound Discoverer v3.2 workflow tree developed for bisphenol A bis(diphenyl phosphate (BPADP) metabolite Non-Target Analysis (NTA).

Verified in FreeStyle v1.6, the mass spectra and chromatographs of each aforementioned potential metabolite were searched manually and evaluated. Due to the presence of buffer in the *in vitro* assay procedure, chromatograph peaks of $[M + H]^+$, $[M + NH_4]^+$ and $[M + Na]^+$ were monitored with a metabolite confirmed if the *m/z* and RT matched for at least two of three ions. Metabolites were deemed 'probable' if only one ion was in agreement, though agreement of $[M + H]^+$ consisted of confirmation given the basic (low $[H]^+$) nature of the buffer solution. Peaks were averaged, background subtracted and the Gaussian 3 smoothing operator was applied. In the event a mass spectra did not exactly correspond to the *m/z* of each ion, an isotopic simulation was processed for each ion considering relevant abundances of all isotopes applicable to the potential metabolite. The metabolite was considered confirmed if the mass spectra matched the results of the isotopic simulation.

2.7 Data Analysis

With respect to the *in vitro* kinetics assays, the difference in concentration of BPADP between t=0 and t=2, divided by two minutes, represented the initial rate of reaction (V_0). This was calculated for each dosing concentration, and further for the difference in BPADP concentration between t=0 and additional time points (t=5, t=10). A Hanes-Woolf plot was used to investigate V_{max} and K_m, with further use of both Lineweaver-Burk and Eadie-Hofstee plots for confirmation.

Time-dependent *in vitro* BPADP depletion was plotted separately from metabolite formation due to low % conversion. All statistical analyses were conducted using GraphPad Prism v9.3.1 (GraphPad Software, San Diego, California, USA). Using a D'Agostino-Pearson normality test, the distribution of the data was assessed compared to a Gaussian distribution. Where the sample size of n=6 was too small for the D'Agostino-Pearson and Anderson-Darling tests, the Kolmogorov-Smirnov test of normality was used. Non-linear one-phase decay/association least squares fit functions were then used to plot time-dependent BPADP depletion and formation of target metabolites DPHP and BPA. The Brown-Forsythe test was applied to determine the equality of means, and significance was set to a p-value of < 0.05. Depletion of BPADP and target metabolite formation at each time point tested for level of significance when compared to t_0 using a one-way analysis of variance (ANOVA) and post-hoc Dunnet's multiple comparisons test. NADPH-deficient data from both the active triplicate assays and the investigation of NADPH-deficient metabolism (section 2.3.3 and subsection 2.3.3.1, respectively) were combined for a total n=6 sample size to allow for statistical analyses.

Chapter 3: Results & Discussion

3.1 *In silico* Predicted Metabolism, Physico-chemical Properties, Fate

3.1.1 *In Silico* Predicted Metabolites of BPADP, RDP, RDX and V6

Predicted metabolites of BPADP are presented in **Table 3-1** in order of probability of occurrence, with all metabolite chemical structures presented in **Figure 3-1**. Highest probability of occurrence is indicated by a rank of 1, and rank is specified for both simulated *in vivo* and S9 rat liver metabolites. Compound names include supplier synonyms where applicable and are listed as 'Unidentifiable' if no CAS RN, International Union of Pure and Applied Chemistry (IUPAC) nomenclature or record could be identified. Properties were determined via unique SMILES code and the full list of SMILES codes generated by the OECD Toolbox v4.4.1 is presented in **Appendix II**.

DPHP (M7) was predicted as a metabolite both *in vivo* and *in vitro* in the rat models, whereas BPA (M1) was only predicted as an *in vivo* metabolite, though at the highest estimated probability. Despite the two most probable BPADP metabolites being products of the loss of DPHP (BPA (M1) from the loss of two DPHP moieties and SCHEMBL811002 (M2) from the loss of one DPHP moiety), DPHP was predicted as the seventh metabolite suggesting lower probability of occurrence. This indicates that interpretations of *in silico* predictions should be made with caution, particularly for novel OPEs, and that empirical corroboration may still be necessary for the purposes of decision making. Less probable predicted *in vivo* metabolites included monophenyl phosphate (M8), hydroquinone (or diphenol) (M9), phenol (M10) and catechol (M11), with phenol also predicted *in vitro*.

Table 3-1. Simulated *in vivo* rat liver & simulated *in vitro* rat liver S9 metabolites of bisphenol A bis(diphenyl phosphate) (BPADP) predicted via the OECD Toolbox v4.4.1: chemical formula, molecular weight (MW) and chemical abstract service registry number (CAS RN).

Metabolite Name	Identifier label (see Fig. 3-1)	Chemical Formula	CAS RN	MW (amu)	Ranked Probability
bisphenol A	M1	$C_{15}H_{16}O_2$	80-05-7	228.29	*in vivo:* 1
Phosphoric acid diphenyl=[4-[1-(4-hydroxyphenyl)-1-methylethyl]phenyl] ester; 'SCHEMBL811002'	M2	$C_{27}H_{25}O_5P$	n/a	460.5	*in vivo:* 2 *in vitro:* 1
[4-[2-(4-Hydroxyphenyl)propan-2-yl]phenyl] phenyl hydrogen phosphate; 'SCHEMBL2290182'	M3	$C_{21}H_{21}O_5P$	n/a	384.4	*in vivo:* 3
[4-[2-[4-[hydroxy(phenoxy)phosphoryl]oxyphenyl]propan-2-yl]phenyl] diphenyl phosphate; 'SCHEMBL12670502'	M4	$C_{33}H_{30}O_8P_2$	n/a	616.5	*in vivo:* 4 *in vitro:* 2
[4-[2-[4-[Hydroxy(phenoxy)phosphoryl]oxyphenyl]propan-2-yl]phenyl] phenyl hydrogen phosphate; 'SCHEMBL3693240'	M5	$C_{27}H_{26}O_8P_2$	n/a	540.45	*in vivo:* 5
Unidentifiable (isomer of the above)	M6	$C_{27}H_{26}O_8P_2$	n/a	540.45	*in vivo:* 6
diphenyl phosphate	M7	$C_{12}H_{11}O_4P$	838-85-7	250.19	*in vivo:* 7 *in vitro:* 3
monophenyl phosphate	M8	$C_6H_7O_4P$	701-64-4	174.09	*in vivo:* 8
hydroquinone	M9	$C_6H_6O_2$	123-31-9	110.11	*in vivo:* 9
phenol	M10	C_6H_6O	108-95-2	94.11	*in vivo:* 10 *in vitro:* 4
catechol	M11	$C_6H_6O_2$	120-80-9	110.11	*in vivo:* 11

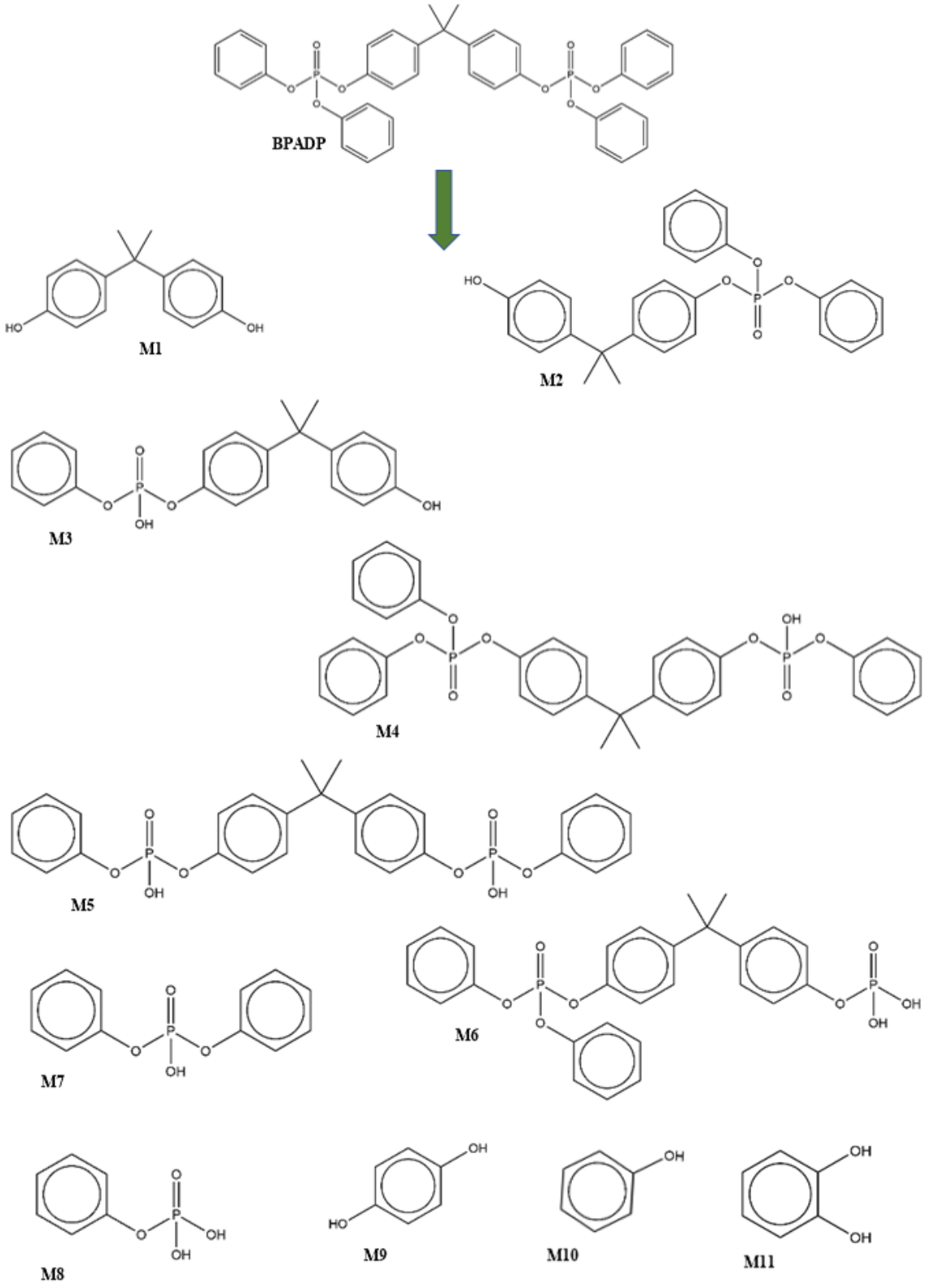

Figure 3-1. 2D chemical structures of *in silico* predicted bisphenol A bis(diphenyl phosphate) (BPADP) metabolites including both *in vivo* rat liver and *in vitro* rat liver S9 fraction simulated metabolites. (See **Table 3-1** for identifier labels).

Four of the *in vivo* metabolites (M2-M6) were identified via supplier name, all of which have several listed patents for use as polymers, resins and FRs (USPTO, 2022), and with M2 and M4 additionally predicted *in vitro*. Of the eleven total predicted metabolites, several are large molecules MW > 500 such as M4, M5 and M6. Several metabolites of BPADP (**Table 3-1, Figure 3-1**) could be considered 'novel' as per the criteria defined in Chapter 1, section 1.1.2. Given that M6 is unidentifiable and M2-M5 are primarily identified by supplier nomenclature rather than IUPAC name or CAS RN, further study of the composition and properties of BPADP metabolites is warranted. Based on the predicted metabolites in **Figure 3-1**, several transformation reactions can be posited including hydrolysis, oxidation, dephosphorylation, O-cleavage/ether bond cleavage and loss of a benzene ring.

Table 2-2 in Chapter 2 details the chemical structures of RDP, RDX and V6. Chemical structures and identifiers of each predicted metabolite are presented in **Appendix III**. Predicted RDP metabolites are primarily of lower MW, though M_a3, approaches the threshold at 498.4 amu (**Table 3-2**). Hundreds of listed patents were identified for RDP metabolites with the majority of registered usages listed as an FR (USPTO, 2022). DPHP (M_a3) has been demonstrated experimentally as an *in vitro* human liver microsomal (HLM) metabolite of RDP, while M_a1 and M_a9 were demonstrated as products of RDP chemical hydrolysis (Ballesteros-Gomez et al., 2015).

In the context of *in silico* prediction, all *in vitro* simulated metabolites of RDX were also predicted *in vivo*, and include five predicted metabolites (M_b6, M_b7, M_b8,

M_b12, M_b17) of high MW >500 amu. Though RDX and RDP have similar molecular structures, their predicted metabolites were quite different, with only resorcinol in common. No common metabolites were predicted between RDX and BPADP, or RDX and V6 (**Figure 3-1**).

Table 3-2. *In silico* predicted *in vivo* rat liver & *in vitro* rat S9 metabolites of additional novel organophosphate esters resorcinol diphenyl phosphate (RDP), tetrakis(2,6-dimethylphenyl)-m-phenylene biphosphate (RDX) and tetrakis(2-chloroethyl)dichloroisopentyldiphosphate (V6) presented by probability of occurrence as predicted via the OECD Toolbox v4.4.1, including chemical formula, structure, molecular weight (MW) and chemical abstract service registry number (CAS RN).

Parent Compound	**Metabolite Name**	**Identifier label** (see Appendix III)	**Chemical Formula**	**CAS RN**	**MW (amu)**	**Ranked Probability**
RDP	[3-[hydroxy(phenoxy)phosphoryl] oxyphenyl] diphenyl phosphate	M_a1	$C_{24}H_{20}O_8P_2$	n/a	498.4	*in vivo:* 1 *in vitro:* 1
	[3-[hydroxy(phenoxy)phosphoryl] oxyphenyl] phenyl hydrogen phosphate; SCHEMBL15910518	M_a2	$C_{18}H_{16}O_8P_2$	n/a	422.27	*in vivo:* 2
	diphenyl phosphate	M_a3	$C_{12}H_{11}O_4P$	838-85-7	250.19	*in vivo:* 3 *in vitro: 2*
	Unidentifiable (isomer of *in vivo 2*)	M_a4	$C_{18}H_{16}O_8P_2$	n/a	422.27	*in vivo:* 4
	phenyl phosphate	M_a5	$C_6H_7O_4P$	701-64-4	174.09	*in vivo:* 5
	(2,5-dihydroxyphenyl) diphenyl phosphate; SCHEMBL3158378	M_a6	$C_{18}H_{15}O_6P$	n/a	358.29	*in vivo:* 6
	hydroquinone	M_a7	$C_6H_6O_2$	123-31-9	110.11	*in vivo:* 7
	resorcinol	M_a8	$C_6H_6O_2$	108-46-3	110.11	*in vivo:* 8

	resorcinol diphenyl phosphate; SCHEMBL1025837	M_a9	$C_{18}H_{15}O_5P$	105937-68-6	342.3	*in vivo:* 9 *in vitro:* 3
	(3-hydroxyphenyl) phenyl hydrogen phosphate; SCHEMBL5222942	M_a10	$C_{12}H_{11}O_5P$	n/a	266.19	*in vivo:* 10
	phenol	M_a11	C_6H_6O	108-95-2	94.11	*in vivo:* 11 *in vitro:* 4
	catechol	M_a12	$C_6H_6O_2$	120-80-9	110.11	*in vivo:* 12
RDX	**Metabolite Name**	**Identifier label** (see Appendix III)	**Chemical Formula**	**CAS RN**	**MW (amu)**	**Ranked Probability**
	2,6-dimethyl hydroquinone	M_b1	$C_8H_{10}O_2$	654-42-2	138.16	*in vivo:* 1
	2,6-dimethylphenol	M_b2	$C_8H_{10}O$	576-26-1	122.16	*in vivo:* 2 *in vitro:*1
	(2,5-dihydroxyphenyl) bis(2,6-dimethylphenyl) phosphate	M_b3	$C_{22}H_{23}O_6P$	n/a	414.4	*in vivo:* 3
	resorcinol bis(2,6-dimethylphenyl) phosphate; SCHEMBL1013059	M_b4	$C_{22}H_{23}O_5P$	154162-69-3	398.4	*in vivo:* 4 *in vitro:* 2
	Unidentifiable (isomer of *in vivo* 3)	M_b5	$C_{22}H_{23}O_6P$	n/a	414.39	*in vivo:* 5
	Unidentifiable	M_b6	$C_{38}H_{38}O_{10}P_2$	n/a	716.66	*in vivo:* 6
	Unidentifiable	M_b7	$C_{38}H_{38}O_9P_2$	n/a	700.66	*in vivo:* 7
	Unidentifiable	M_b8	$C_{38}H_{40}O_9P_2$	n/a	702.68	*in vivo:* 8 *in vitro:* 4
	Unidentifiable	M_b9	$C_{22}H_{24}O_8P_2$	n/a	478.37	*in vivo:* 9
	Bis(2,6-dimethylphenyl)phosphate; 'SCHEMBL272850'	M_b10	$C_{16}H_{19}O_4P$	18350-99-7	306.29	*in vivo:* 10 *in vitro:* 5
	(2,6-dimethylphenyl) (3-hydroxyphenyl)	M_b11	$C_{14}H_{15}O_5P$	n/a	294.24	*in vivo:* 11

	hydrogen phosphate 'SCHEMBL1609938'					
	Unidentifiable	M_b12	$C_{30}H_{32}O_8P_2$	n/a	582.53	*in vivo:* 12 *in vitro:* 6
	[3-[(2,6-dimethylphenoxy)-hydroxyphosphoryl]oxyphenyl] (2,6-dimethylphenyl) hydrogen phosphate 'SCHEMBL76820'	M_b13	$C_{22}H_{24}O_8P_2$	n/a	478.37	*in vivo:* 13
	(2,6-dimethylphenyl) dihydrogen phosphate; 'SCHEMBL2220467'	M_b14	$C_8H_{11}O_4P$	n/a	202.14	*in vivo:* 14
	2-(hydroxymethyl)-6-methylphenol; 'SCHEMBL1901144'	M_b15	$C_8H_{10}O_2$	n/a	138.17	*in vivo:* 15
	resorcinol	M_b16	C_6H_6O2	108-46-3	110.11	*in vivo:* 16
	Unidentifiable (isomer of *in vivo* 8)	M_b17	$C_{38}H_{40}O_9P_2$	n/a	702.68	*in vitro:* 3
V6	**Metabolite Name**	**Identifier label** (see Appendix III)	**Chemical Formula**	**CAS RN**	**MW (amu)**	**Ranked Probability**
	2-chloroacetaldehyde	M_c1	C_2H_3ClO	107-20-0	78.5	*in vivo:* 1 *in vitro:* 1
	Unidentifiable	M_c2	$C_9H_{17}Cl_4O_5P$	n/a	378.00	*in vivo:* 2 *in vitro:* 2
	Unidentifiable	M_c3	$C_{13}H_{23}Cl_5O_9P_2$	n/a	562.52	*in vivo:* 3
	Unidentifiable	M_c4	$C_9H_{15}Cl_4O_6P$	n/a	391.99	*in vivo:* 4 *in vitro:* 3
	2-chloracetic acid	M_c5	$C_2H_3ClO_2$	79-11-8	94.5	*in vivo:* 5 *in vitro:* 4
	Unidentifiable	M_c6	$C_9H_{23}Cl_5O_{10}P_2$	n/a	578.51	*in vivo:* 6
	Unidentifiable	M_c7	$C_9H_{17}Cl_4O_5P$	n/a	378.00	*in vivo:* 7 *in vitro:* 5
	Unidentifiable	M_c8	$C_7H_{14}Cl_3O_5P$	n/a	315.51	*in vivo:* 8 *in vitro:* 6
	2-chloroethanol	M_c9	C_2H_5ClO	107-07-3	80.51	*in vivo:* 9 *in vitro:* 7
	Unidentifiable	M_c10	$C_{13}H_{25}Cl_5O_9P_2$	n/a	564.53	*in vivo:* 10

Unidentifiable	M_c11	$C_{11}H_{21}Cl_5O_8P_2$	n/a	520.48	*in vivo:* 11 *in vitro:* 8
Unidentifiable	M_c12	$C_9H_{18}Cl_4O_8P_2$	n/a	457.98	*in vivo:* 12 *in vitro:* 9
bis(2-chloroethyl) phosphate	M_c13	$C_4H_9Cl_2O_4P$	3040-56-0	222.99	*in vivo:* 13 *in vitro:*10
Unidentifiable (isomer of *in vivo* 12	M_c14	$C_9H_{18}Cl_4O_8P_2$	n/a	457.98	*in vivo:* 14
2-chloroethyl dihydrogen phosphate; 'SCHEMBL991756'	M_c15	$C_2H_6ClO_4P$	n/a	160.49	*in vivo:* 15

The six supplier-named predicted metabolites, M_b4, M_b10, M_b11, M_b13, M_b14 and M_b15, are each patented for uses including but not limited to: polyamide resins, thermoplastic elastomers, heat conduction, and transparent flame retardants (USPTO, 2022).

The majority of *in silico* predicted metabolites of V6 were unidentifiable (**Table 3-2**), and M_c3, M_c6, M_c10 & M_c11 were of MW >500. This further underscores that for BPADP, RDP, RDX and V6 several predicted metabolites can be considered novel OPEs. For these parent compounds (**Figure 3-1, Table 3-2**) the complex structures, including oligomeric compounds, give rise to a wider array of potential degradation and transformation products which can themselves be transformed (Ballesteros-Gomez et al., 2015; Alves et al., 2018). The lack of information concerning oligomeric OPEs, including occurrence, toxicity and toxicokinetics (Liang et al., 2018; Zhao et al., 2019), differentiates these and similar novel compounds from well-studied legacy chemicals.

While available data is limited, the array of transformation products of novel OPEs may differ from the products of legacy OPEs and warrants further investigation.

Four predicted *in vitro* metabolites of V6 (M_c7, M_c10, M_c11, M_c13) agree with literature results of HLM *in vitro* metabolism (Alves et al., 2018), despite the Toolbox predicting only rat metabolites not simulations of HLM metabolites. Overall there is little similarity between the predicted metabolites of these four novel OPEs despite high structural similarity between BPADP and RDP, as well as RDP and RDX. Structurally complex, novel OPEs can produce a vast array of degradation products and the *in silico* predicted metabolites of one novel OPE cannot be assumed to occur from another parent compound even where structural similarity is high. It should also be noted that several predicted metabolites of RDP, RDX and V6 (**Table 3-2**) have not been empirically confirmed and caution is required when interpreting results. No Phase II metabolites were predicted for any of the novel OPEs studied, likely due to the smaller number of Phase II transformation reactions built into the OECD Toolbox training set, which is trained on (479 and 450 enzymatic *in vivo* and *in vitro* Phase I reactions, respectively vs 104 and 15 enzymatic *in vivo* and *in vitro* Phase II reactions, respectively). Combined with the novel nature of these compounds and the lack of available experimental data upon which the toolbox can be trained, feasible Phase II metabolites of novel OPEs should not be ruled out based on the present results.

3.1.2 *In Silico* Predicted Physico-chemical Properties

In silico predictions concerning BPADP and many other novel OPEs are inherently uncertain due to the high MWs of these compounds and particularly the lack of experimentally derived physico-chemical properties (logK_{OW}, logK_{OA}, logK_{OC}, etc.) of environmental importance (Zhang et al., 2016). All physico-chemical properties presented in **Table 3-3** were predicted using EPI Suite^{TM} v4.1.1 except for available experimental values denoted with an asterisk (*). Predictions of vapour pressure via the MPBPVP model contain uncertainty given that the training model was based on a set of 6000 organic chemicals for which the list is not available. The training set of compounds used in the development of the KOCWIN, WSKOWWIN and KOAWIN models for prediction of logK_{OC}, water solubility and logK_{OA}, respectively, included compounds with MWs up to 650 amu but predominantly included lower MW compounds. Predictions generated from these models are therefore considered to have more uncertainty and variability than predictions of logK_{OW} from the KOWWIN model, for which the training and validation sets included compounds of MWs in the 700s and 900s (amu). Given the uncertainty surrounding a precise, experimentally derived, logK_{OW} for BPADP, only the logK_{OC} estimate derived via first order Molecular Connectivity Index (MCI) was considered and presented in **Table 3-3**, rather than the logK_{OC} calculated from predicted logK_{OW}. A second water solubility estimation tool (WATERNT), while still based on logK_{OW} values, applied a 'fragment constant' method which for BPADP analyzed aromatic vs. aliphatic carbons as well as single and double bonds between oxygen and phosphorous to estimate solubility.

Predictions of water solubility via both WSKOWWIN and WATERNT yielded estimated low water solubility for BPADP, RDP and RDX, while the water solubility of V6 is estimated to be several orders of magnitude higher. Predicted water solubility of BPADP is far lower than experimentally reported water solubility and saturated water concentrations of 0.4 ppm of 0.212 ppm, respectively (van der Veen & de Boer, 2012; Waaijers et al., 2013b). At values greater than 4.5, the predicted logK_{OC} values for all four compounds suggest very high adsorption to and low mobility in sediment (US EPA, 2012) and possible deleterious effects to terrestrial ecosystems. One experimentally-derived logK_{OC} value of BPADP has been reported as 4.76 ± 0.252, and for water - SPM as 4.00 ± 0.473 (Zhong et al., 2021). These values are far below the modelled estimate (**Table 3-3**) yet the water-sediment logK_{OC} remains above 4.5, still suggesting high adsorption.

Table 3-3. EPI Suite™ predicted physico-chemical properties of bisphenol A bis(diphenyl phosphate) (BPADP), resorcinol diphenyl phosphate (RDP), tetrakis(2,6-dimethylphenyl)-m-phenylene biphosphate (RDX) and tetrakis(2-chloroethyl)dichloroisopentyldiphosphate (V6).

	BPADP	RDP	RDX	V6
Water Solubility (mg/L)				
WSKOWWIN™	1.09e-7	$1.11e^{-4}$	$3.70e^{-9}$	0.80
WATERNT™	*$1.88e^{-6}$*	*$6.88e^{-3}$*	*$6.87e^{-7}$*	*33.4*
Experimental	0.212* to 0.4*	0.015*	n/a	2.1*
Soil Adsorption Coefficient (logK_{OC}) (KOCWIN™)	10.52	8.32	10.03	6.29
Octanol-Water Coefficient (logK_{OW}) (KOWWIN™)	10.02	7.41	11.79	2.83*
Octanol-Air Coefficient (logK_{OA}) (KOAWIN™)	21.74	18.33	22.37	15.03
Air-Water Coefficient (logK_{AW}) (HENRYWIN™)	-11.72	-10.92	-10.58	-12.20
Vapour Pressure (MPBPVP™)	$5.99e^{-10}$ to $5.61e^{-6}$	$5.99e^{-10}$ to $5.61e^{-6}$	$5.99e^{-10}$ to $5.61e^{-6}$	$5.99e^{-10}$ to $5.61e^{-6}$

*Measured experimentally in a commercial product.

Predicted logK_{OW} values are very high for BPADP, RDP and RDX, suggesting lipophilicity and supporting the estimates of low water solubility. Conversely, the experimentally measured logK_{OW} value of V6 is lower than the other OPEs, which corresponds to its comparatively higher predicted water solubility. The modelled logK_{OW} value of BPADP was calculated given the indefinite nature of the available experimental values (4.5, Pakalin et al., 2007; ≥ 6, ECHA, 2011). The predicted logK_{OW} values of BPADP and RDX being very high (>10) suggest uncertainties in the prediction of such properties with respect to these novel OPEs and highlight the need for experimentally derived values. Of note is the combination of predicted high lipophilicity (or superhydrophobicity) and soil adsorption, which may indicate persistence and bioaccumulation in sediment or terrestrial environments, however this may also limit

contaminant availability in aquatic environments (Gobas et al., 2003). In both phytoplankton and zooplankton the OPEs TMPP, EHDPP, TPHP, TEHP and TDCIPP were quantified and bioavailability between sediment and biota increased with hydrophobicity (Wang et al., 2019). Bioavailability was also found to plateau at logK_{OW} values >5.73 and was affected by biotransformation rates of individual organisms at various trophic levels. High sediment concentrations of OPEs can contribute to aquatic species ingesting OPEs on a continuous basis, potentially leading to magnification up a trophic system depending on the properties of individual compounds (Yao et al., 2021).

Similarly, predicted logK_{OA} values are very high for each novel OPE and suggest greater affinity to organic fractions, though such high values indicate a need for corroboration via experimentally-derived values. Negative predicted logK_{AW} values suggest low affinity to atmospheric compartments, further supported by the estimated vapour pressures which suggest limited transport into the vapour phase.

3.1.3 *In Silico* Predicted Environmental Fate and Aquatic Toxicity

All *in silico* fate predictions were estimated using EPI Suite™ v4.1.1 and are presented in **Table 3-4**. STPWIN model predictions of fugacity with respect to wastewater treatment carry similar uncertainty as they are based on results from predicted physico-chemical properties, specifically MPBPVP described in subsection 3.1.2. The BCFBAF model predicts bioconcentration and bioaccumulation factors, which carry uncertainty as they are generated using only the predicted logK_{OW} and would benefit from experimentally-derived input values. ECOSAR toxicity estimations were not considered due to the low water solubility of BPADP, RDP, RDX and V6. Fugacity modelling relates experimental or estimated rate constants pertaining to different

environmental compartments (logK_{OW}, logK_{OC}, logK_{OA}) to persistence of a compound in various media.

Table 3-4. EPI Suite™ environmental fate predictions of bisphenol A bis(diphenyl phosphate) (BPADP), resorcinol diphenyl phosphate (RDP), tetrakis(2,6-dimethylphenyl)-m-phenylene biphosphate (RDX) and tetrakis(2-chloroethyl)dichloroisopentyldiphosphate (V6). Fate predictions of RDP and RDX are based on EPI Suite v4.1.1 predicted properties (**Table 3-3**), while V6 experimental solubility and logK_{OW} were inputted into the model. Inputs to the model for BPADP were a water solubility of 0.212 mg/L and a logK_{OW} of 8.

	BPADP	**RDP**	**RDX**	**V6**
Estimated Fugacity $t_{1/2}$ (hr) (LEV3EPI™)	10.94	12.13	5.48	3.32
Air	1440	900	4320	4320
Water	2880	1800	8640	8640
Soil	1.30e^4	8100	3.89e^4	3.88e^4
Sediment	94.02	93.96	94.04	4.48
Modelled Removal in Wastewater Treatment (%) (STPWIN™)	4.08	0.80	93.09	0.06
Biological Half-life Normalized to 10g fish at 15°C (days) (BCFBAF™)	2.81	3.10	0.95	0.71
Bioconcentration Factor (logBCF)	3.25	1.91	2.74	1.26
Bioaccumulation Factor (logBAF) (upper trophic) (BCFBAF™)				

Waaijers *et al.,* 2013b; van der Veen & de Boer, 2012

Highest affinity was estimated for sediment across all four novel OPEs, which is in agreement with the high estimated logK_{OC} values between 6.24 and 10.52 (**Table 3-3**). BPADP is also predicted to partition to soil and water, and with the shortest estimated half-life in the atmosphere (**Table 3-4**).Compared to BPADP and RDP, RDX and V6 have longer half-lives in soil and water, though these estimates remain an order of magnitude shorter than the estimates in sediment. Similarly, V6 was the only compound

not estimated to be efficiently removed via an average wastewater treatment system. A 72.2% removal of BPADP was reported in a treatment plant in Beijing, China (Liang et al., 2018), a lower though comparable removal rate to the *in silico* prediction (**Table 3-4**). In the same study, removal of RDP was determined experimentally to be 83.3% while 24.4% removal was reported for V6 (Liang et al., 2018) likely due to its comparatively high water solubility and low LogK_{OW}. Compared to the scarce amount of data in the published literature, *in silico* prediction (**Table 3-4**) of RDP is in agreement with the study in Beijing, however varies widely from the -101% removal efficiency reported following secondary treatment in a New York treatment plant (Kim et al., 2017). Further study of removal efficiency of novel OPEs in wastewater treatment could raise additional discrepancies in removal rates worldwide.

Persistence and accumulation of BPADP warrants further investigation given that all predicted or measured logK_{OW} values exceed the threshold of 5, denoting potential of bioaccumulation, and the estimated persistence in sediment (**Table 3-4**) exceeds 365 days/12 months as per CEPA 1999 Persistence and Bioaccumulation Regulations (Environment Canada, 2000). Predictions of half-life in air, water and soil compartments (**Table 3-4**) do not meet CEPA 1999 criteria of persistence. BCF indicates the total contaminant concentration per total wet weight of the organism relative to its environment therefore considering non-dietary uptake, while BAF represents contaminant concentration in the organism from all exposure routes including diet (US EPA, 2015). The modelled BCF and BAF (**Table 3-5**) are below the threshold for bioaccumulation ($\geq$ 5000) (Environment Canada, 2013), however these values are highly influenced by solubility and logK_{OW} values. **Table 3-4** also displays the predicted

removal efficiency, biological half-life, logBCF and logBAF of BPADP using conservative experimentally derived values (0.212 ppm water solubility and logK_{OW} of 8). This solubility value is several orders of magnitude higher than the modelled predictions, however it is the lower of the two available experimental values, while the logK_{OW} value of 8 is between the predicted value of 10.02 (**Table 3-2**) and the OECD experimental value recorded as ≥6. Taking this approach, the resulting predicted BAF and BCF values are far higher than if modelled estimates of solubility and logK_{OW} are used, demonstrating the uncertainty remaining in the prediction of properties with respect to poorly studied and newly produced OPEs.

As solubility in water and logK_{OW} are crucial to the calculation of BCF and BAF, more experimental data, particularly a specific experimental logK_{OW} is of importance in understanding the environmental fate of this understudied OPE. The lipophilicity of BPADP may be similar to or exceed that of previously studied contaminants including polychlorinated biphenyl (PCB) and PBDE congeners (**Table 3-5**). Such compounds with comparable logK_{OW} values and MW have demonstrated high bioconcentration and bioaccumulation potential, suggesting a similar environmental fate outcome is possible with respect to BPADP. The potential persistence and accumulation of BPADP warrants further investigation and would be highly relevant particularly if production and usage of BPADP increases in the future. For a few comparative and lipophilic substances, BCF and BAF values bolded in **Table 3-5** are > 5000 and therefore in exceedance of bioaccumulation criteria, indicating high bioaccumulation and bioconcentration potential.

Table 3-5. Octanol-water coefficient (logK_{OW}), molecular weight, bioconcentration and bioaccumulation factor values of bisphenol A bis(diphenyl phosphate) (BPADP) (based on a saturated water concentration of 0.212 ppm and logK_{ow} of 8) in comparison to PCB-153, tetraBDE and pentaBDE. Estimated values as predicted by EPI Suite™ are denoted via an asterisk (*).

Compound Name	**log*K*ow**	**Molecular Weight (amu)**	**Bioconcentration Factor (BCF) (L/kg wet weight)**	**Bioaccumulation Factor (BAF) (L/kg wet weight)**
BPADP	8	692.63	644.3*	1790*
PCB-153	6.72, 8.35	360.88	**1.8539e^4**	**2.1e^5**
tetraBDE (congeners present in commercial PeBDE, OBDE and DBDE)	6.81	485.79	**1.3e^6** ; **6.67e^4**	n/a
pentaBDE (2 congeners, specific nomenclature not disclosed)	6.64-6.97; 6.57	564.7	**2.74e^4** ; **1.77e^4** ; 1440	**1.4e^6**

Environment Canada, 2004, 2013; Gustafsson *et al.,* 1999; EU 2001; CDC ATSDR; Schlechtriem *et al.,* 2016

LogK_{OW} values and solubility are key values in the calculation of both BCF and BAF that need to be further studied experimentally, as current limited empirical data suggests the possibility of BPADP to be bioaccumulative. While a high degree of sorption to sediment is likely, one study of a lake food web in China detected BPADP in sediment, surface water and biota samples, with a BAF higher than those of monomeric OPEs (Zhao et al., 2019). Bioaccumulation varies between ecosystems and trophic levels, and experimental data concerning the environmental fate and persistence of BPADP remains preliminary. Further study of empirically generated physico-chemical property and fate values for BPADP are necessary to determine and understand the net persistence of the compound when considering sorption to sediment, bioavailability, water solubility and biotransformation rates.

BPADP toxicity remains poorly understood. In one study, at a water solubility saturation concentration of 0.212 ppm (BPADP, ≥ 80% purity) 25% immobility of *daphnia magnia* neonates was reported in a solution at pH 8.02 (Waaijers et al., 2013b). Waaijers *et al.* found that the acute (48 hour) half maximal effect concentration (EC_{50}) was not reached due to low solubility of BPADP. Due to the purity of the BPADP standard, it cannot be said whether the observed toxicity is from exposure to BPADP monomers or TPHP impurities. In the present study, for some predicted metabolites of BPADP the aquatic toxicities were estimated using EPI Suite™. Several predicted metabolites of BPADP include aromatic rings and can be considered phenolic compounds, including phenol, phenyl phosphate, catechol and hydroquinone (**Figure 3-1**). Toxicity of phenolic compounds to aquatic organisms has been reported at concentrations in the ppm range, including growth inhibition reported post exposure of *daphnia magnia* and *bacillus subtilis* to hydroquinone (Bahrs et al., 2013; Enguita & Leitao, 2013). In a study using a combined mixture of hydroquinone and catechol, growth inhibition of *bacillus subtilis* was reported as well as a synergistic effect of the mixture (Chen et al., 2010). Data is limited concerning chronic aquatic toxicity of phenol, though acute effects have been studied in multiple taxa, with toxicity ranging widely from slight to high ($10 < EC_{50} < 100$ and $0.1 < EC_{50} < 1$, respectively) (Duan et al., 2018). Developmental, behavioural and reproductive effects have been reported in several aquatic and avian species following exposure to BPA (Naveira et al., 2021; Wu & Seebacher, 2020; Cetin & Ozaydin, 2021) and zebrafish growth was found to be inhibited by exposure to DPHP (Zhang et al., 2020; Chen et al., 2021).

EPI Suite™ includes the ECOSAR model for the prediction of acute and chronic aquatic toxicity across several taxa. While ECOSAR could not be used for estimation of aquatic toxicity of BPADP due to its low solubility, the model was applied to predicted metabolites where experimental values were not available. *In vivo* metabolites two through six were assessed for aquatic toxicity in EPI Suite™, though again very low estimated solubility inhibited predictions of 48 hour and 96 hour half maximal lethal dose (LC_{50}) values.

3.2 In vitro Microsomal Metabolism of BPADP Using an RLM Assay

3.2.1 Preliminary Time-Dependent Metabolism Experiments for BPADP

At five dosing concentrations ranging between 0.514 and 2.57 μM, BPADP and DPHP concentrations were quantified at zero and five minute time points. DPHP formation at all concentrations and time points was too low to calculate V_{max} or K_m values using a Hanes-Wolf, Lineweaver-Burk or Eadie-Hofstee plot. **Figure 3-2** illustrates the depletion of BPADP in comparison to TPHP, a legacy and well-studied OPE known to be rapidly metabolized in similar Wistar-Han RLM assays, over a 60-minute incubation period and at comparable substrate concentrations considering the difference in MW between the compounds. While 17.89 ± 4.99% (n=3) BPADP depletion occurred over the total assay time, TPHP was 93.95 ± 8.09% (n=3) metabolized by the 20-minute time point.

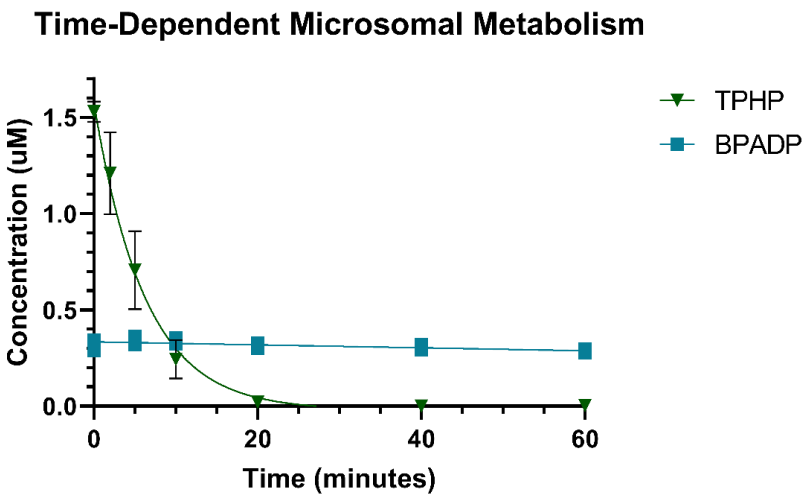

Figure 3-2. Comparison of the *in vitro* depletion of bisphenol A bis(diphenyl phosphate) (BPADP) and triphenyl phosphate (TPHP) over a 60-minute incubation period in a rat liver microsome based assay. Each data point is the average of triplicate samples (n =3).

TPHP has been previously demonstrated to undergo similarly rapid metabolism in polar bear liver microsomal assays with a 97% conversion to DPHP, however slower metabolism and 60% conversion to DPHP in ringed seal liver assays (Strobel et al., 2018a). In HLM assays a 41% depletion of TPHP was observed (Van den Eede, et al., 2013) and a 15% conversion rate of TPHP to DPHP was demonstrated in herring gull liver microsomal assays (Greaves et al., 2016). In the present study, positive controls using TPHP demonstrated a mean 45.89 ± 12.10% conversion to DPHP (n=3). The slow BPADP metabolism observed at all concentrations, including at above the two available experimental water solubility values, did not allow for the calculation of metabolism kinetics. This also informed the use of a 1780 ppb (2.57 µM) BPADP incubation concentration in all subsequent biotransformation assays to achieve zero-order kinetics as we have shown previously (Greaves et al., 2016; Strobel et al., 2018a).

3.2.2 Factors Considered for Optimization of the *In vitro* RLM Assay

Several steps were taken to optimize the *in vitro* biotransformation assay based on the properties of BPADP, including minimizing any analytical loss. Based on the

physico-chemical properties estimated previously (see **Tables 3-3** and **3-4**), BPADP has low solubility in aqueous solution and has the potential to be adsorptive on the glass of laboratory test tubes and other materials. It was presently found that the use of Teflon™ test tubes in the assay did not reduce BPADP adsorption, and therefore, use of glass test tubes was continued throughout all experiments. Ice bath assays did not increase t_0 concentrations compared to the known dose, therefore assays were continued at 37°C. Sonication of the BPADP buffer solution was conducted to minimize BPADP adsorption loss on glass, increasing availability within the aqueous incubation and resulting in t_0 concentrations more consistent with the known dose. While background concentrations of BPADP, target metabolites BPA and DPHP, and TPHP were consistently below 1.5 ppb (**Figure 3-3**), low metabolite recoveries, particularly of BPA, in initial assays interfered with the measurement of any metabolism quantification. BPADP depletion over a 60-minute incubation at the initial dose concentration of 356 ppb (0.514 µM) was observed to be slow (**Figure 3-4**), similar to the findings described in section 3.2.1 above.

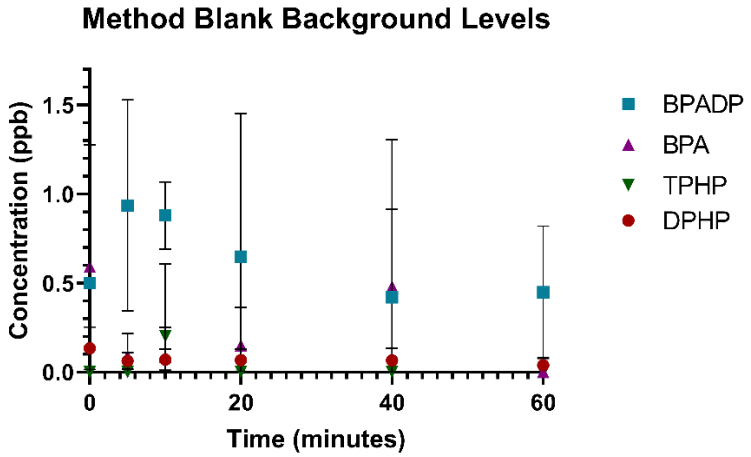

Figure 3-3. Concentrations of bis(diphenyl phosphate) (BPADP), diphenyl phosphate (DPHP), bisphenol A (BPA) and triphenyl phosphate (TPHP) in method blank samples, indicating background levels of each compound. Each data point is the mean of four same-day replicates (n=4). Standard deviation is represented for each mean by error bars.

Figure 3-4 illustrates the initial experiments to investigate the depletion of BPADP at an incubation concentration of 356 ppb, and the formation of DPHP. The enzyme deactivated control showed no time-dependent changes and thus not degradation appears to have occurred in the absence of active microsomes. DPHP was demonstrated as an *in vitro* metabolite in all active assay replicates, albeit it at low concentrations, however concentrations of the second hypothesized metabolite, BPA, did not exceed background levels (**Figure 3-3**) and displayed no time-dependent relationship.

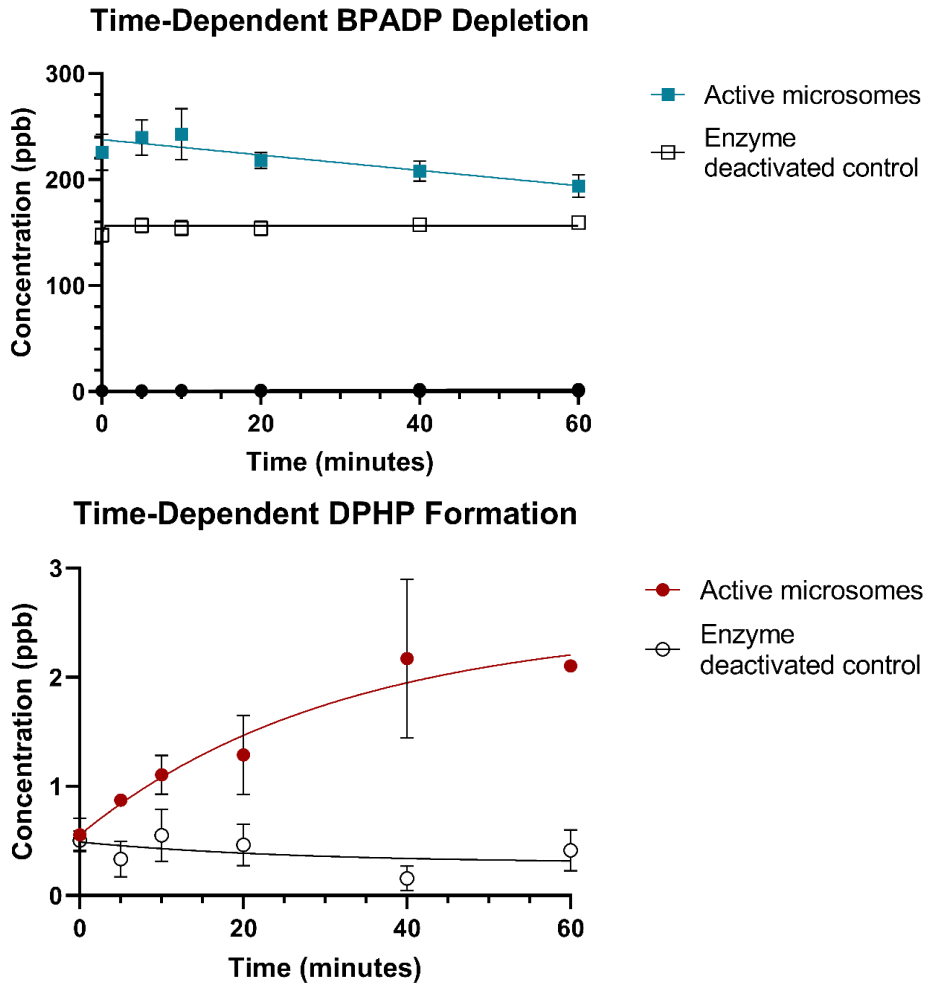

Figure 3-4. Bisphenol A bis(diphenyl phosphate) (BPADP) microsomal metabolism at an incubation concentration of 356 ppb and formation of the target metabolite diphenyl phosphate (DPHP), compared to enzyme deactivated negative controls. Each data point represents the mean of four same-day replicate samples (n = 4), with standard deviation represented by error bars.

Therefore, due to slow microsomal BPADP metabolism most notable at the 40 and 60- minute time points and BPA concentrations indistinguishable from the background, the initial 60-minute assays at 356 ppb incubations were changed to 120-minute assays at incubation concentrations of 1780 ppb, discussed in section 3.2.3 below.

3.2.3 Optimized *In Vitro* Quantification of BPADP and Target Metabolites

Using the fully optimized assay conditions and parameters as described in section 3.2.2 above, all further investigation of BPADP *in vitro* metabolism and metabolite formation as described in this subsection as well as subsection 3.2.4 and section 3.3 was conducted at the higher incubation concentration of 1780 ppb. In the active replicates, the mean percentage of BPADP measured at t_0 relative to the administered concentration of 1780 ppb was 69.85 ± 6.93% (n=9). In the NADPH-deficient and enzymatically deactivated controls the mean BPADP concentration at t_0 relative to the administered dose was 77.99 ± 9.98% (n=3) and 61.94 ± 18.14% (n=3), respectively. Slightly increased concentrations of BPADP were quantified at t_5 when compared to t_0 (**Figure 3-5**), potentially due to factors that are difficult to control such as adsorption and slow metabolism, which can limit the initial availability of BPADP within the aqueous incubation solution. Given that the administered concentration was in exceedance of experimental water solubility, BPADP may not have been homogenously distributed in the incubation at t_0 despite extensive sonication of the dosing solution. This may have led to the slightly increased concentrations measured in the t_5 aliquots.

In the present optimized assays, concentrations of BPADP and its target metabolites remained low and essentially negligible in all method blanks (BPADP <3

ppb; BPA, DPHP <1 ppb). Consistent, negligible target metabolite concentrations of <2ppb were found in enzymatically deactivated controls (**Figure 3-5**). This demonstrated that BPADP was subject to microsomal metabolism in the *in vitro* rat liver model. Specifically, in the enzymatically active 120 minute assay and relative to t_0 there was an average 44.38 ± 10.06% (n=9) depletion of BPADP and in assays deficient of NADPH the depletion of BPADP was on average 20.22 ± 6.95% (n=3).

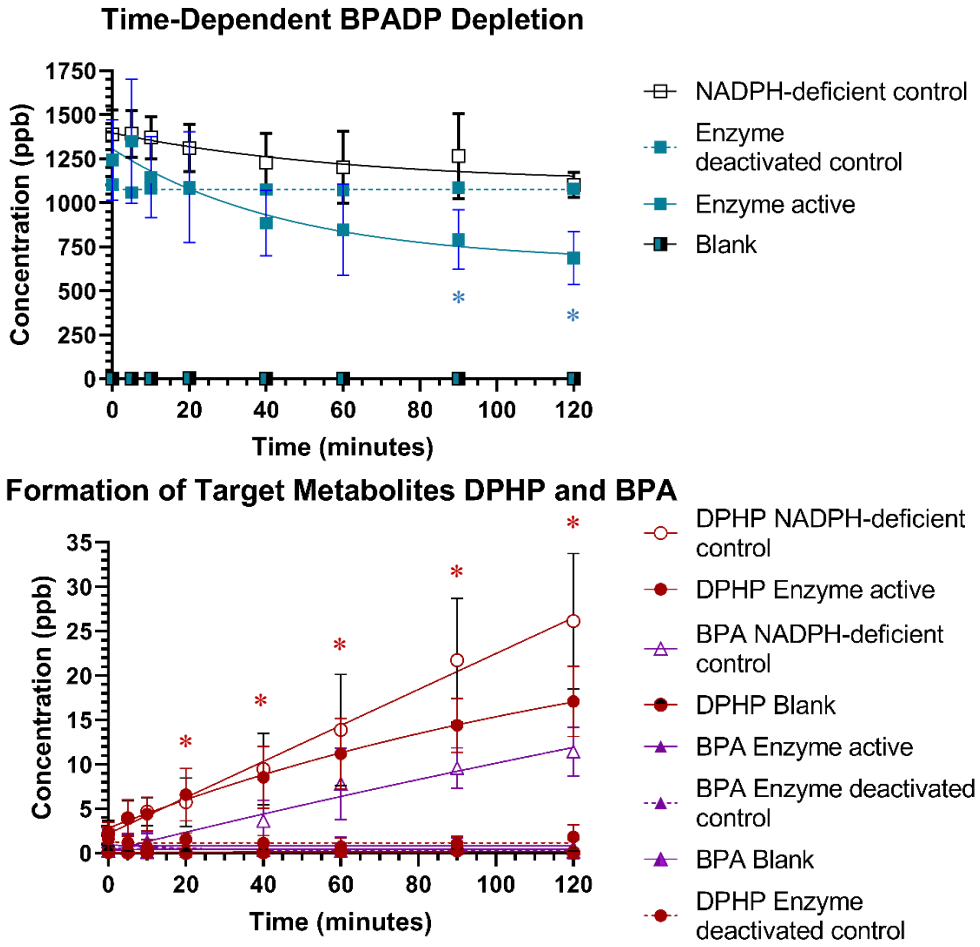

Figure 3-5. Bisphenol A bis(diphenyl phosphate) (BPADP) depletion and formation of the target metabolites diphenyl phosphate (DPHP) and bisphenol A (BPA) in assays of a 1780 ppb incubation concentration. Each method blank, NADPH-deficient and enzymatically deactivated control data point is the average of three inter-day replicates (n=3), each enzymatically active replicate data point is the average of three triplicate (n=3) assays conducted on three separate days (total n=9 replicates). Error bars represent the standard deviation of each mean, and an asterisk represents a time point where the active microsomal BPADP or metabolite concentration is significantly different ($p < 0.05$) from that of zero minutes.

In the active microsomal replicates, BPADP depletion at 90 and 120 minutes was found to be statistically significant compared to the time zero concentration ($p = 0.0060$ and 0.0007, respectively) (**Figure 3-5**). Despite less BPADP depletion, concentrations of both target metabolites were higher in the NADPH-deficient controls than in enzymatically active samples. For the target metabolite DPHP, formation was quantified in both enzymatically active and NADPH-deficient samples (**Figure 3-5**). In the active microsomal replicates, the DPHP concentration was significantly higher when compared to time zero at the 20, 40, 60, 90 and 120 min time points ($p = 0.0467$, 0.0103, 0.0028, < 0.0001, < 0.0001, respectively). Target BPA formation in the active triplicate and enzymatically deactivated samples was quantified at negligible concentrations (compared to the background; see **Figure 3-3**) at all incubation time points. In contrast, BPA concentration increased over time in the NADPH-deficient controls, displaying *in vitro* formation (**Figure 3-5**).

The present results indicate that BPA and DPHP are both *in vitro* microsomal metabolites of BPADP in a rat liver model, although may form via different degradation pathways. On average, DPHP only accounted for 1.27% and 1.87% of NADPH-dependent and –independent BPADP depletion, respectively, while BPA accounted for only 0.82% of NADPH-independent BPADP depletion. The *in vitro* microsomal metabolism of BPADP to DPHP appears to be linked to mediation by both CYP450 enzymes and NADPH-independent enzymes, and potentially PONs and/or aryl esterases. *In vitro* HLM metabolism of RDP demonstrated DPHP as a metabolite in the presence and absence of NADPH (Ballesteros-Gomez et al., 2015), similar to the present findings.

In the active microsomal samples, quantification of a time-dependent increase in BPA formation *in vitro* may be inhibited by the presence of CYP450 enzymes as the hydroxyl groups present on BPA allow for CYP-dependent metabolism, demonstrated in rat liver S9 fraction (Yoshihara et al., 2004; Ousji et al., 2020). However, a time-dependent increase in BPA concentration over the course of the incubation was quantified in NADPH-deficient samples where CYP450 enzymes, reliant on NADPH, are inactive. Several rat liver metabolites of BPA have been measured in the presence of NADPH, including compounds arising from oxidation and GSH conjugation (Ousji et al., 2020), supporting the findings of the present study where BPA formation was not observed in the presence of NADPH. The phenolic nature of BPA also renders Phase II conjugation, such as glucuronidation or sulphation to be feasible (Ramirez et al., 2021; Yoshihara et al., 2004; Thayer et al., 2015), which may minimize in the present BPADP study the quantification of a time-dependent increase in concentration in the presence or absence of NADPH. With respect to BPA, NADPH-deficient controls are crucial to an experimental design for the investigation of BPADP metabolism.

Mean DPHP formation appeared to be higher in the NADPH-deficient assays compared to the mean BPADP depletion in the absence of NADPH, though from standard deviation of the means (represented by error bars) the difference was not significant (**Figure 3-6**). These data suggest PONs/esterases may mediate rat liver microsomal metabolism of BPADP, which would agree with the limited literature data suggesting PONs predominantly mediate HLM metabolism of BPADP *in vitro* (Alves et al., 2018). Unlike Alves *et al*, the present study did not include a known PON-mediated substrate as a positive control, therefore this cannot be confirmed. The most studied

isoform, human PON1, has been found to have limited efficiency in catalysing the enzymatic hydrolysis of some organophosphate compounds however exhibits high efficiency in catalyzing the metabolism of the particular organophosphates diazoxon and chlorpyrifos oxon (Draganov & La Du, 2003). It is plausible that PON1 may mediate BPADP metabolism, however this contrasts much of the current understanding that CYP-mediated metabolism is an important pathway for many legacy OPEs (Van den Eede et al., 2013). An example of this are alkyl-TPHPs with aryl groups (e.g. isopropyl or *tert*-butyl functional groups), found to sterically hinder CYP450 monooxygenase-mediated metabolism as compared to TPHP alone (Strobel et al., 2018b). Further, several *in vitro* HLM metabolites of the novel OPE RDP were identified as CYP450 mediated (Ballesteros-Gomez et al., 2015), while preliminary investigation of the *in vitro* HLM metabolism of the novel OPE V6 suggests mediation primarily by CYP450 enzymes (Alves et al., 2018).

3.2.4 Investigation of NADPH-Independent Metabolism

Further investigations of BPADP microsomal metabolism and formation of target metabolites in NADPH-deficient assay was conducted via a same-day triplicate assay, displayed in **Figure 3-6**.

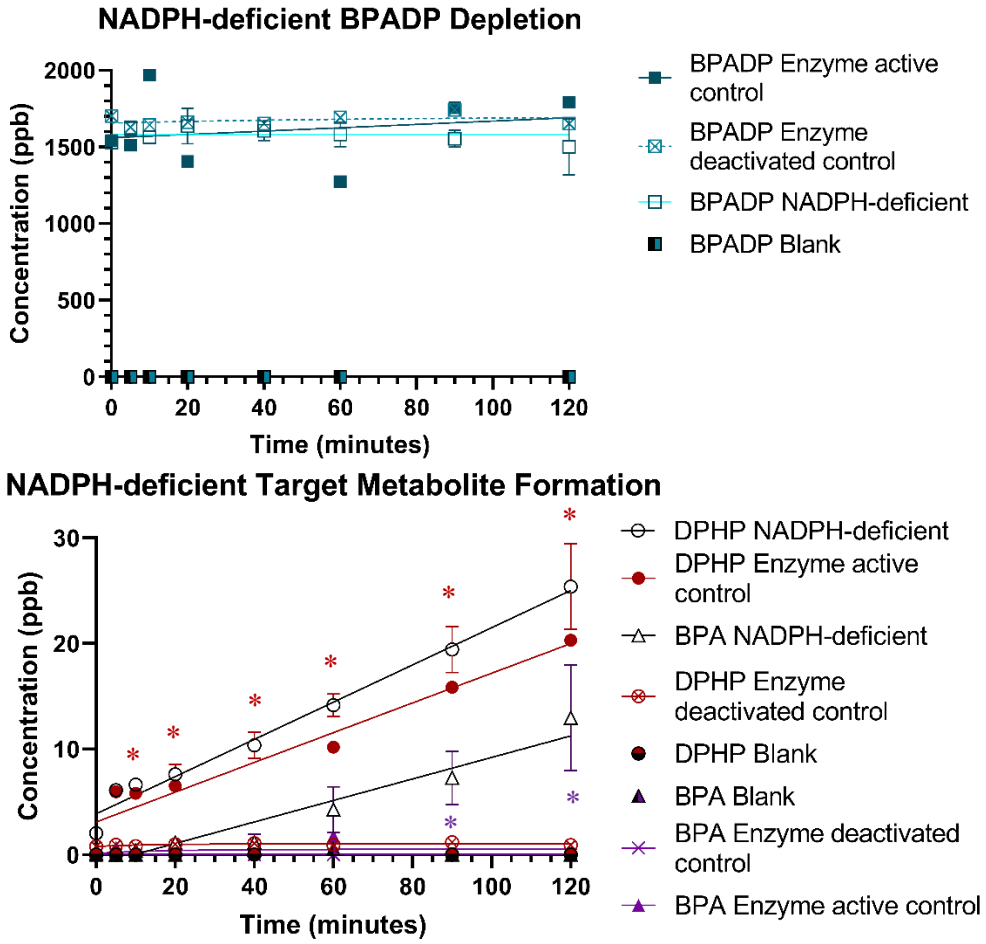

Figure 3-6. Time-dependent NADPH-deficient microsomal metabolism of bisphenol A bis(diphenyl phosphate) (BPADP) and formation of target metabolites bisphenol A (BPA) and diphenyl phosphate (DPHP). Each NADPH-deficient data point is the mean of same-day triplicate samples (n=3), each blank, enzyme active and enzyme deactivated control data point represents one sample (n=1). Error bars represent standard deviation of each mean, and an asterisk represents a time point where the NADPH-deficient metabolite concentration is significantly different ($p < 0.05$) from that of zero minutes.

BPADP assay depletion over time was limited and depletion was not found to be statistically significant at any time point relative to t0, and concentrations remained consistent over time in the enzymatically deactivated control. Lack of statistical significance may be attributed to the small sample size (n = 6) and does not confirm negligible BPADP depletion. A larger sample size is required to fully evaluate NADPH-deficient BPADP depletion. The additional same-day triplicate samples corroborate the results of section 3.2.3 in that BPA formation is negligible in the control sample

containing NADPH, however a consistent time-dependent increase in concentration is seen in the NADPH-deficient triplicate samples. Specifically, BPA formation at the 90 and 120 minute time points was statistically significant compared to time zero ($p = 0.0042$ and 0.0057, respectively).

As shown in **Figure 3-6**, increasing DPHP concentration was again quantified over time in both the NADPH-deficient triplicates and NADPH-containing controls, confirming it as an *in vitro* metabolite of BPADP not dependent on the presence of NADPH. This contrasts the findings of Alves *et al.* who reported detection of DPHP from HLM *in vitro* metabolism only in the presence of NADPH, not in NADPH-deficient controls. Given the limited depletion of BPADP in NADPH-deficient (**Figure 3-6**) controls when compared to active microsomal replicates (**Figure 3-5**), DPHP formation in the presence vs absence of NADPH was not tested for statistical significance, though error bars suggest a lack of significance (**Figure 3-6**). Formation of DPHP in NADPH-deficient replicates was significant in the 10, 20, 40, 60, 90 and 120 minute replicates, when compared to time zero ($p = 0.0199$, 0.0302, 0.0089, 0.0429, 0.0035 and 0.0020, respectively). The present results suggest *in vitro* RLM DPHP formation may not be exclusively mediated by CYP450 enzymes and may be somewhat inhibited by the presence of NADPH. A larger sample size is required to determine whether the presence of NADPH significantly reduces DPHP formation. The conversion of BPADP to either target metabolite remained minimal, in agreement with the results of section 3.2.3, meaning the mass balance of BPADP biotransformation cannot be fully explained by the formation of BPA and DPHP.

All *in vitro* assay samples were monitored over the full incubation duration to account for any TPHP impurities that may have been present and potentially interfere with accurate quantification of DPHP as a true metabolite of BPADP. TPHP concentrations remained negligible even in assays with 1780 ppb of BPADP. The highest TPHP concentrations quantified in any sample were 4.145, 14.33 and 10.03 ppb- recorded in a replicate, NADPH-deficient control, and enzyme deactivated control, respectively. Greater than three times the standard deviation, the latter two concentrations (14.33 and 10.03 ppb) were deemed to be outliers. Samples where TPHP concentrations exceeded those of method blanks but were not clear outliers may be explained by TPHP impurities in the BPADP standard (see Chapter 2, section 2.4.2).

Given that DPHP has been repeatedly demonstrated as a major metabolite of TPHP (Greaves et al., 2016, Strobel et al., 2018a, Van den Eede et al., 2013), it is possible that DPHP formation displayed in **Figures 3-5** and **3-6** can be attributed to both BPADP metabolism and degradation of TPHP impurities. TPHP concentrations in all active microsomal, enzyme deactivated, and NADPH-deficient samples were lower than that of DPHP, and DPHP formation was found to consistently increase with time beyond 20 minutes- the time point where near total TPHP depletion was consistently demonstrated in section 3.2.1 above. Monitored TPHP concentrations in each sample are compared to DPHP formation in **Appendix IV**. Given the 46.03 ± 12.10% conversion of TPHP to DPHP quantified in TPHP positive controls (subsection 3.2.1), it can be stated that DPHP formation is attributed at least in part to *in vitro* microsomal metabolism.

3.3 Additional BPADP Metabolite Assessment from *In Vitro* RLM Assays

Table 3-6 details the five additional metabolites of BPADP identified via re-analysis of *in vitro* time-dependent samples with a modified UHPLC-MS/MS analytical method as described in Chapter 2, sub-section 2.5.2. **Figure 3-7** displays the change in response over time of BPADP and additional metabolites detected by UHPLC-MS/MS analysis.

Table 3-6. Additional novel metabolites of bisphenol A bis(diphenyl phosphate) (BPADP) analyzed via UHPLC-MS/MS, including abbreviation, chemical formula and molecular weight.

Abbreviation	Identifier label	Chemical Formula	Molecular Weight (amu)
BPA – DPP	MM1	$C_{27}H_{25}O_5P$	460.4653
BPADP – BZ; SCHEMBL12670502	MM2; M4	$C_{33}H_{30}O_8P_2$	616.5427
BPADP + O	MM3	$C_{39}H_{34}O_9P_2$	708.6397
BPADP + 2O	MM4	$C_{39}H_{34}O_{10}P_2$	724.6391
BPADP + 2O + 2H	MM5	$C_{39}H_{36}O_{10}P_2$	726.6549

Structures of metabolites MM1 and MM2/M4 are presented in **Appendix VI**.

Qualitatively, four of the five analyzed additional metabolites displayed clear increasing peak area response over time, with results being semi-quantitative due to the lack of internal standards for the additional metabolites of interest. The exception is BPADP + 2O + 2H, which displayed similar concentrations over time and in all samples, including the method blank (**Figure 3-7**). Results are described by comparing the *m/*z response level (representing the mass chromatographic peak area) at all time points and to control samples. Despite limited depletion of BPADP in the active replicates when compared to enzymatically deactivated and NADPH-deficient controls, time-dependent microsomal metabolism is demonstrated. Identified oxidation metabolites demonstrated no increase in peak response over time in the NADPH-deficient control, indicating

NADPH as a requirement for formation of BPADP + O and BPADP + 2O, which would suggest CYP450-mediated metabolism.

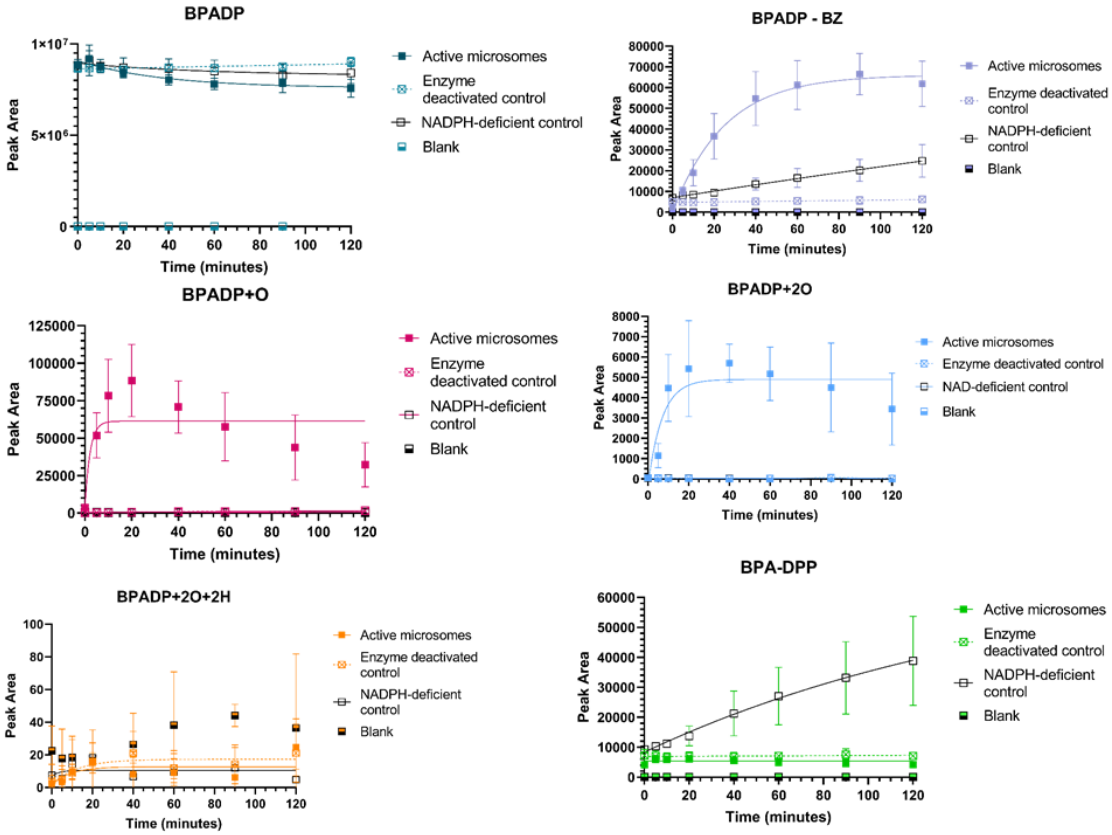

Figure 3-7. Response vs. time of bisphenol A bis(diphenyl phosphate) (BPADP) and all five additional metabolites analyzed: BPADP - DPP; BPADP – BZ; BPADP + O; BPADP + 2O; and BPADP + 2O + 2H. All data points are the mean of three replicates (n=3), error bars represent standard deviation.

Preliminary identification of BPADP metabolites suggests the involvement of human recombinant CYP450 (rCYP) enzymes in the mediation of DPHP formation, particularly rCYP3A4 and to a lesser extent rCYP1A2 and rCYP2B6 as reported by Alves *et al*. Involvement of the aforementioned three rCYPs as well as rCYP2C9 and rCYP2C19 was also confirmed by Alves *et al.* with respect to the *in vitro* HLM metabolism of V6. BPADP – BZ displayed a time-dependent increase in peak area in both the replicates (n = 3) and NADPH-independent control, suggesting its formation is

not dependent on the presence of NADPH, with the converse being demonstrated for BPADP – DPP which was only found to increase over time in the NADPH-deficient control. These data are in agreement with Alves *et al.* who identified BPADP – DPP via both enzymatic and non-enzymatic hydrolysis pathways.

While Phase I oxidation via CYP450 mediated metabolism has been demonstrated with many OPEs (Van den Eede et al., 2013; Ballesteros-Gomez et al., 2015; Hou et al., 2018), NADPH-deficient formation of BPADP – DPP and BPADP – BZ was demonstrated in the present study. This finding agrees with preliminary literature data suggesting PONs may play a major role in BPADP *in vitro* HLM metabolism, where six hydroxylated and O-dealkylated NADPH-independent metabolites of BPADP were identified (Alves et al., 2018). Perhaps BPADP – BZ formation may not depend on NADPH but is increased in the presence of this enzyme co-factor, though further study of this relationship with a larger sample size would be required to confirm this hypothesis. While abiotic hydrolysis of BPADP was not studied in the present thesis, the findings of Alves *et al.* also suggest BPADP – DPP may be formed by both enzymatic (likely PON-mediated) and abiotic/chemical hydrolysis. This indicates further investigation into the abiotic hydrolysis of BPADP is warranted particularly considering this thesis research quantified BPADP – DPP only in the absence of NADPH. SCHEMBL2290182 (M3) was only predicted *in silico,* however it was identified as a secondary *in vitro* HLM metabolite of BPADP resulting from loss of a phenyl group from BPADP – DPP (Alves et al., 2018). The same study identified one glucuronidated and one sulphated metabolite of BPADP – DPP, suggesting this compound as a primary HLM metabolite and important intermediate step in BPADP biotransformation.

While a time-dependent increase in the peak area of several BPADP metabolites was presently demonstrated in **Figure 3-7**, all results are semi-quantitative. These data do not allow for the calculation of a conversion rate between BPADP depletion and formation of any additional metabolites, however the information provides valuable insight regarding BPADP biotransformation and the mass balance of metabolites formed. When internal standards become available, time-dependent quantification of the concentrations of each additional metabolite formed would improve our understanding of the *in vitro* metabolism/degradation of BPADP. Depending on the concentrations quantified, it may be possible to define BPADP biotransformation kinetics using one or more novel additional metabolites (**Figure 3-7, Table 3-6**), rather than DPHP as described in section 3.2.1. While no agreement was found with *in silico* predictions, BPADP + O and BPADP + 2O were further confirmed via Q-E-Orbitrap NTA and detailed in section 3.5. This provides evidence from both *in vitro* and NTA approaches supporting the formation of two *in vitro* BPADP oxidation products in a RLM model.

3.4 Identified GSH Adduct

Phase II *in vitro* metabolism of BPADP was investigated to further understand its biotransformation, providing an idea of feasible conjugations and informing transformation pathways that may be highly relevant to organisms. Of the three Phase II GSH conjugates selected for identification in section 2.6.2 of Chapter 2, one could be confirmed via Q-E Orbitrap analysis. This adduct was detected at a t_{120}/t_0 ratio of infinity, with detection in three of four t_{120} samples and no detection in any of the non-GSH control samples. **Table 3-7** details the detection and potential structure of the identified adduct.

Table 3-7. Chemical formula, parent compound, transformations, composition change (from parent compound), Δ mass shift, molecular weight, retention time (RT) and replicated group areas of identified GSH adduct. A potential structure is posited.

Chemical Formula	**1: $C_{49}H_{49}N_3O_{16}P_2S$**	**Potential Chemical Structure**
Parent Compound	Bisphenol A bis(diphenyl phosphate)	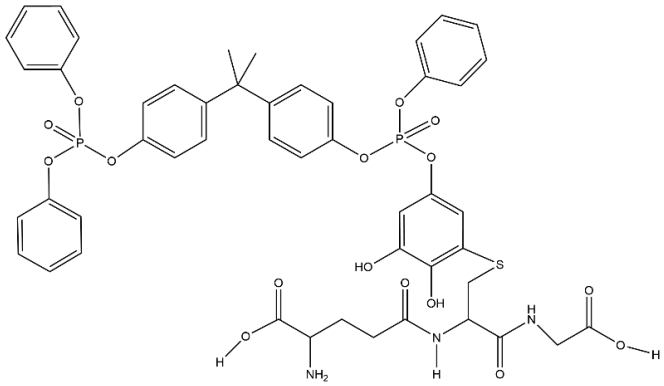
Transformations	Oxidation, Oxidation, GSH Conjugation 1	
Composition Change	$+C_{10}H_{15}N_3O_8S$	
Δ mass shift (ppm)	0.33	
Molecular Weight (amu)	1029.23122	
RT (min)	7.241	
Replicated Group Areas (t_{120})	Replicate 1: $1.3e^5$; Replicate 2: $3.95e^4$; Replicate 3: $0.0e^0$; Replicate 4: $4.99e^5$	

GSH Conjugation 1 refers to a specific composition change (+ $C_{10}H_{15}N_3O_6S$), while GSH Conjugation 2 results in the same change with two additional hydrogen atoms (+ $C_{10}H_{17}N_3O_6S$). Given the absence of ammonium ions in the buffer, and the low buffer pH due to the formic acid mobile phase, only hydrogen ions ($[M + H]^+$) were analyzed via mass spectra for the chromatographic peak at a retention time of 7.241 min (**Figure 3.8**), and confirmed GSH Conjugation 1 but not 2. The mass spectral peaks at 1031.2428 *m/z* and 1032.2439 *m/z* can be attributed to the natural isotopic ratios of relevant elements. The potential structure shown in **Table 3-7** is accurate as to the exact mass and molecular formula identified via Q-E Orbitrap analyses, however the specific structure remains unconfirmed as the exact location of the GSH adduct is unknown. This posited structure is based on recent study of TPHP-GSH adducts from an *o*-hydroquinone intermediate and reaction with *o*-benzoquinone (Chu & Letcher, 2019).

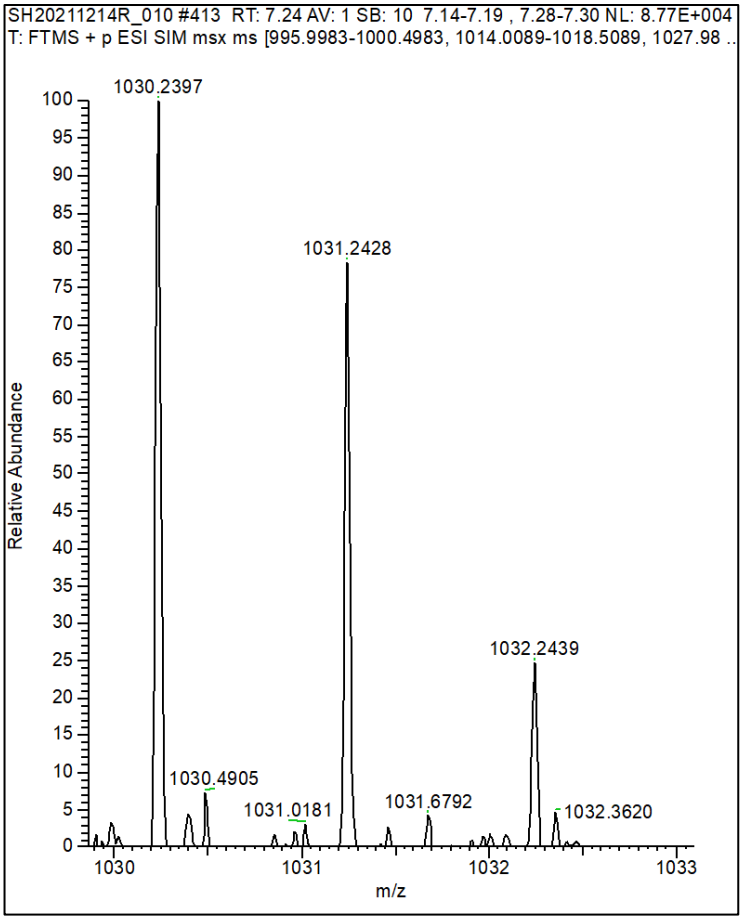

Figure 3-8. Molecular mass spectra of confirmed glutathione (GSH) Adduct, 'BPADP + GSH +2O -2H' ([M + H]) via GSH Conjugation 1 and oxidation.

Glucuronidation and sulphation of the BPADP metabolite BPADP – DPP have been identified previously in HLM S9 fraction incubated with BPADP (as described in section 3.3 above), with chemical formulas of $C_{33}H_{33}O_{11}P$ and $C_{27}H_{25}O_8PS$, respectively (Alves et al., 2018). The present results therefore demonstrate the first identification of this specific Phase II metabolite of BPADP, i.e. BPADP + GSH + 2O - 2H. Alves *et al.* also identified one sulphated Phase II metabolite of V6, with the chemical formula of $C_{13}H_{25}Cl_5O_{12}P_2S_2$. Phase II metabolites of RDP have been identified including several glucuronidated (GSH Conjugation 1 & 2) and several sulphated metabolites (Ballesteros-Gomez et al., 2015).

3.5 Non-Target Analysis (NTA) of *In Vitro* RLM Assay Incubates via UHPLC Q-Exactive-Orbitrap HRMS

Of the 80 compounds generated following the filtering of results by retention time, mass shift and t_{120}/t_0 response ratio (see Chapter 2, section 2.6.3), **Table 3-8** details the three metabolites confirmed and the additional compound considered tentatively confirmed via Q-E-Orbitrap NTA. Confirmed metabolites of BPADP include one compound (MM2) also predicted by the OECD Toolbox *in vitro* rat liver S9 simulation and in the *in vitro* results presented in section 3.3 above. Two confirmed metabolites (MM3, MM4) result from oxidation reactions and were confirmed in section 3.3, though not predicted *in silico*. Lastly, the tentatively confirmed metabolite (MM5) resulted from combined oxidation and hydration reactions and was not identified via *in silico* predictions nor confirmed *in vitro* in section 3.3 and is not likely to be a feasible biotransformation product of BPADP in the present *in vitro* RLM model.

Table 3-8. Detailed list of all confirmed and tentatively confirmed metabolites of BPADP identified via high mass resolution Q-E-Orbitrap NTA, including chemical formula, abbreviation, retention time (RT), molecular weight and confirmation status.

Chemical Formula	Identifier label	Abbreviation	RT (min)	Molecular Weight (amu)	Confirmation Status
$C_{33}H_{30}O_8P_2$	MM2; M4	SCHEMBL12670502; 'BPADP-BZ'	9.93	616.5427	Confirmed
$C_{39}H_{34}O_9P_2$	MM3	BPADP + O	11.385; 11.168; 11.534	708.6397	Confirmed
$C_{39}H_{34}O_{10}P_2$	MM4	BPADP + 2O	10.978	724.6391	Confirmed
$C_{39}H_{36}O_{10}P_2$	MM5	BPADP + 2O + 2H	11.048	726.6549	Tentative

Molecular mass spectra of all metabolites identified via NTA are presented in **Figure 3-9**. Mass spectra of isotopic simulations for metabolites are provided in **Appendix V**. Notably, neither target *in vitro* rat liver microsomal metabolite (BPA, DPHP) were confirmed experimentally via Q-E-Orbitrap NTA, likely due to the sensitivity of the analytical method. One patented industry compound (MM2/M4) was predicted *in silico* and confirmed experimentally as an *in vitro* metabolite via NTA, the first identification of this BPADP metabolite.

BPADP - DPP (M2/MM1) was identified in section 3.3 however not via NTA. This is very likely due to the fact that as a result of time constraints, NADPH-deficient samples were not included in the Q-E-Orbitrap analysis and the present thesis identified BPADP - DPP only in the absence of NADPH. BPADP – DPP was identified as an *in vitro* HLM metabolite by Alves *et al.,* therefore it is likely NTA of NAPDH-deficient samples would further corroborate the compound as a feasible *in vitro* RLM metabolite of BPADP. While NTA was not extended to an investigation into the metabolites of RDP, RDX or V6 at this time, a similar approach could be applied to these novel OPEs and others- particularly compounds such as RDX for which metabolism/biotransformation has not yet been studied experimentally.

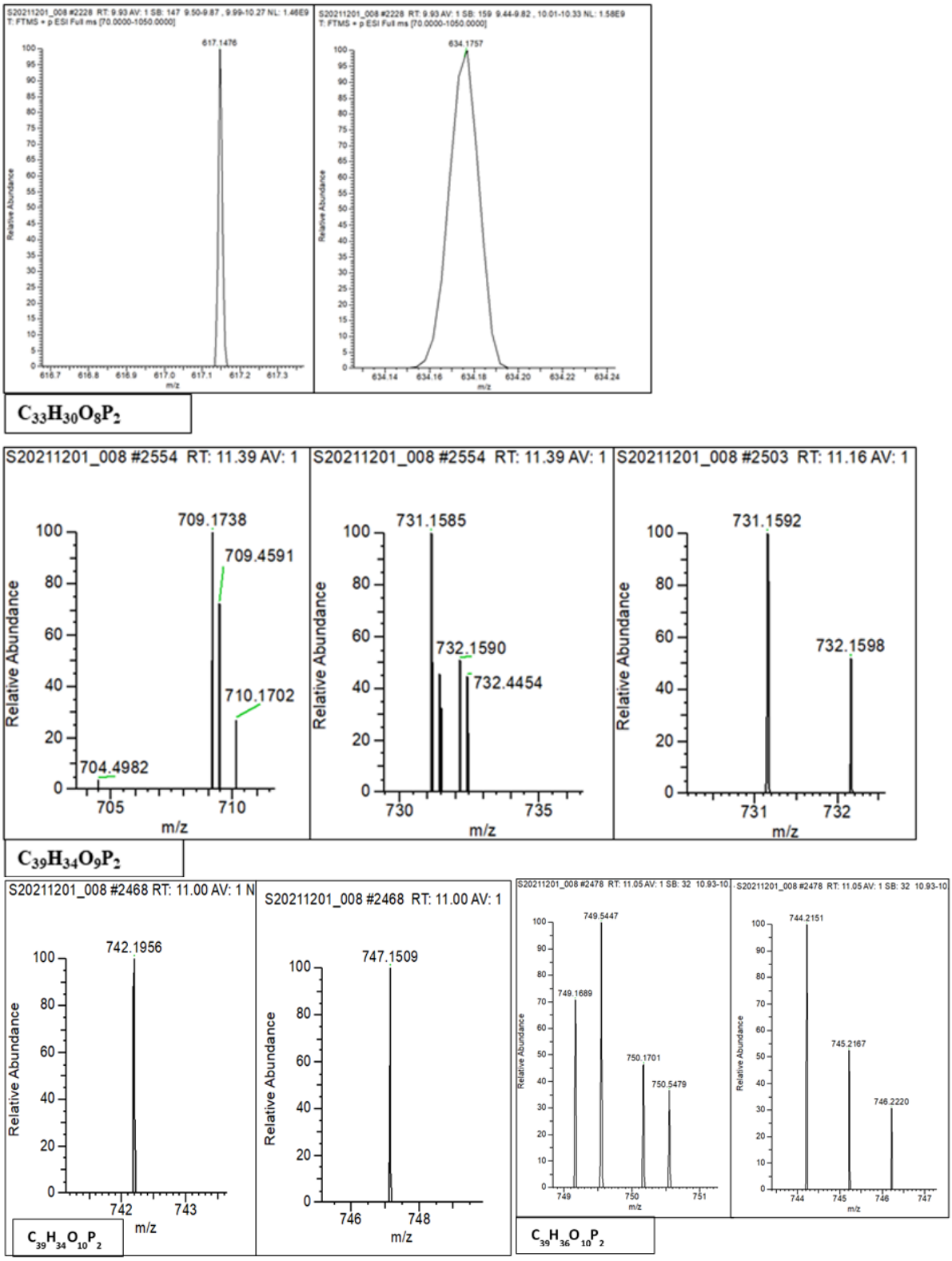

Figure 3-9. Molecular mass spectra of mass chromatographic peaks at specific retention times, of confirmed and tentatively confirmed metabolites of bisphenol A bis(diphenyl phosphate) (BPADP) identified via Q-E-Orbitrap Non-Target Analysis (NTA), investigated following the results of *in vitro* analysis of additional metabolites.

3.6 Value of a Lines of Evidence Approach

In silico modelling predicted three metabolites of BPADP that were confirmed via *in vitro* time dependent assays and/or Q-E-Orbitrap NTA (**Table 3-9**), demonstrating validity as a profiling tool for understanding the metabolism of novel OPEs. As detailed in section 3.1.1, some agreement can be seen between simulated *in vitro* rat metabolites of RDP & V6 and the limited available literature. While experimental data is always preferred, given the shorter time frame required for completing *in silico* modelling applications such as the OECD Toolbox could be useful in identifying novel OPEs for which metabolites may be of concern. This applies to all novel OPEs discussed in the present thesis and could be a powerful tool in highlighting *in vitro* and *in vivo* research priorities. While *in silico* modelling did not predict a phase II GSH conjugate or Phase I oxidation metabolites, these were confirmed via NTA- adding valuable insight as to feasible biotransformation products of BPADP.

BPA and DPHP have been demonstrated as *in vitro* metabolites of BPADP with confirmation across two of three applied lines of evidence (**Figure 3-10**), having been predicted *in silico* and with *in vitro* time-dependent formation quantified (**Table 3-9**). Further, agreement between two or more lines of evidence is demonstrated for several metabolites, indicating a higher degree of certainty regarding the feasibility of these *in vitro* transformations. BPADP - BZ (M4; MM2; SCHEMBL12670502) was confirmed by all three *in silico*, *in vitro* and NTA lines of evidence. Agreement can also be seen between the NTA and *in vitro* analysis of additional metabolites, with three confirmed metabolites identified in both lines of evidence. BPA was predicted only as an *in vivo* metabolite using *in silico* modelling and while no *in vivo* experiments were conducted in

the present thesis, while BPA was demonstrated to be an *in vitro* metabolite of BPADP in rat liver microsomal assays.

Table 3-9. Summary of all identified bisphenol A bis(diphenyl phosphate) (BPADP) metabolites and agreement (or lack thereof) between lines of evidence. Metabolites predicted only *in vivo* via the OECD Toolbox are denoted with an asterisk (*). The predicted unidentifiable metabolite (*in vivo*: 6; **Table 3-1**) is excluded as it is an isomer of M5. The tentatively confirmed metabolite MM5 (BPADP+2O+2H) is italicized and empty boxes indicate a metabolite not studied using the particular line of evidence.

Metabolite Chemical Formula	**Identifier label**	**Abbreviation**	***In silico***	***In vitro***	***In vitro* additional metabolites**	**Q-E-Orbitrap**	**Q-E-Orbitrap GSH**
$C_{27}H_{25}O_5P$	M2; MM1	SCHEMBL811002; BPADP - DPP	✓		✓	x	
$C_{33}H_{30}O_8P_2$	M4; MM2	SCHEMBL12670502; BPADP - BZ	✓		✓	✓	
$C_{12}H_{11}O_4P$	M7	diphenyl phosphate	✓	✓		x	
C_6H_6O	M10	phenol	✓				
$C_{15}H_{16}O_2$	M1	bisphenol A*	✓	✓		x	
$C_{21}H_{21}O_5P$	M3	SCHEMBL2290182*	✓				
$C_{27}H_{26}O_8P_2$	M5	SCHEMBL3693240*	✓				
$C_6H_7O_4P$	M8	monophenyl phosphate*	✓				
$C_6H_6O_2$	M9	hydroquinone*	✓				
$C_6H_6O_2$	M11	catechol*	✓				
$C_{39}H_{34}O_9P_2$	MM3	BPADP + O			✓	✓	
$C_{39}H_{34}O_{10}P_2$	MM4	BPADP + 2O			✓	✓	
$C_{39}H_{36}O_{10}P_2$	*MM5*	*BPADP + 2O + 2H*			x	✓	
$C_{49}H_{49}N_3O_{16}P_2S$	n/a	BPADP+GSH+2O-2H					✓

Monophenyl phosphate, hydroquinone and catechol were identified only via *in silico* predictions, each simulated only as *in vivo* rat metabolites and not confirmed in either *in vitro* or NTA approaches. While the OECD Toolbox predicts metabolites resulting from both Phase I and II transformations, no GSH adducts of BPADP were

predicted, nor did predicted metabolites of RDP and V6 align with demonstrated Phase II metabolites in the literature. Several *in silico* predicted metabolites were confirmed experimentally *in vitro*, however further experimental validation of predicted *in vivo* rat metabolites and *in vitro* Phase II transformations could be pursued. Considering the low concentrations of DPHP and BPA quantified (section 3.2.3, 3.2.4) relative to the dosed BPADP concentration, several *in silico* predicted metabolites may be feasible *in vitro* however not detectable as the Q-E-Orbitrap method is less sensitive, particularly in identification of compounds present at low concentrations, since it is based on a high mass resolution total ion scan. Low metabolite concentrations and NTA conducted only for samples containing NADPH likely contribute to the lack of *in silico – in vitro* or *in silico* – NTA corroboration and it should not be assumed from the present results that *in silico* predicted metabolites are not feasible.

The confirmation of BPADP metabolites demonstrated in the present thesis is vital to the hazard assessment of the compound, as biotransformation products are part of understanding overall environmental fate and their relevance is somewhat dependant on importance within the overall biotransformation mass balance. Past suggestion that BPADP may pose negligible toxicity and bioaccumulation risk- rendering it a suitable replacement of DecaBDE- may be questionable considering biotransformation products have not been considered. While estimated and experimental physico-chemical properties indicate BPADP may have limited mobility in soil, biotransformation is highly relevant given the toxicity risk posed by several metabolites (subsection 3.1.3). For example DPHP, if mobile in groundwater as suggested by Funk *et al.* 2019, demonstrates that biotransformation and degradation products can behave very differently in environmental

media compared to their parent compound. Broadly, these results underscore the need to quantify the BPADP biotransformation mass balance and on a larger scale to apply a similar lines of evidence approach to the hazard assessment of other novel OPEs. Closing knowledge gaps via *in silico* and NTA screening of novel OPEs must be combined with *in silico* estimation of accurate environmental fate parameters specific to identified metabolites in order to consider a more complete picture of OPE degradation, biotransformation and environmental fate.

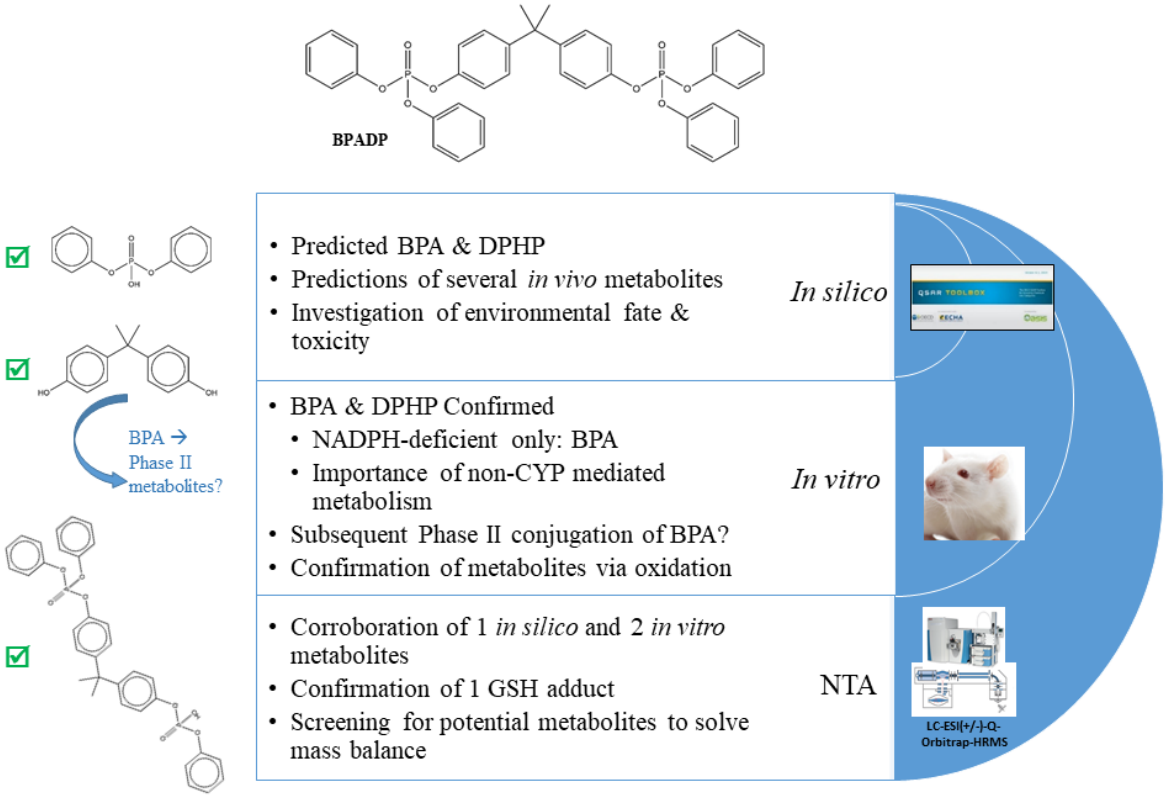

Figure 3-10. Understanding of bisphenol A bis(diphenyl phosphate) (BPADP) degradation and transformation as determined through a lines of evidence approach.

To conclude, NTA added valuable insight in the present study, both in verifying predicted *in silico* metabolites and to profile the array of potential *in vitro* metabolites. As found in Ye *et al.*, 2021 NTA methods applied to the screening of OPEs proves useful in identifying compounds not frequently sampled/quantified in the environment. It is a

method widely applicable to closing the knowledge gap surrounding the contaminant burden posed by novel OPEs versus legacy compounds. In agreement with the findings of Alves *et al.,* 2018, NADPH-deficient assays are a critical aspect of investigating the *in vitro* metabolism of BPADP, particularly in the identification and quantification of BPA as a metabolite.

Chapter 4: Conclusions and Directions of Future Research

4.1 Conclusions

Despite usage as a potentially suitable alternative to the phased-out DecaBDE (van der Veen & de Boer, 2012; Brandsma et al., 2013b), significant knowledge gaps remain concerning the persistence, bioaccumulation, fate, stability and hazard posed by BPADP (Liang et al., 2018; Zhang et al., 2019) and experimentally-derived physico-chemical properties are also lacking. The present research sought to address the biotransformation, physico-chemical properties and environmental fate of BPADP using three lines of evidence, with the goal of informing risk assessment and management of the compound. The developed and optimized method for quantification of BPADP in an *in vitro* Wistar-Han rat liver microsomal model will aid future study and analysis of the compound.

BPADP metabolism was demonstrated in this research to be very slow when compared to the legacy OPE TPHP, with metabolism kinetics non-quantifiable using a Wistar-Han RLM model under optimized *in vitro* assay parameters. In general, published literature concerning metabolism of novel OPEs is highly limited, however additional novel/oligomeric/complex OPEs such as BPADP may also be metabolized slowly compared to established/common OPEs. Specifically, RDP and RDX may exhibit a similar rate of metabolism as BPADP given both are also oligomeric OPEs, though the present results demonstrate only BPADP metabolism in a particular *in vitro* mammalian model and species-specific variations are possible.

In the first study of its kind, both DPHP and BPA were quantified and confirmed as *in vitro* metabolites of BPADP in a Wistar-Han RLM assay. While BPA was

quantified only in NADPH-deficient samples, suggesting non-CYP450 mediated metabolism, DPHP formation was quantified in both the presence and absence of NADPH. These findings are somewhat aligned with the only other study of BPADP metabolites, where DPHP and BPA were tentatively identified only in the presence and absence of NADPH, respectively (Alves et al., 2018). The lines of evidence approach applied in the present research further corroborated the metabolism of BPADP to both DPHP and BPA via *in silico* modelling, demonstrating validity of modelling tools in predicting and screening the biotransformation products of BPADP and other novel OPEs (e.g. RDP, RDX, and V6). NTA of BPADP metabolites corroborated one predicted *in silico* metabolite but crucially identified four additional metabolites- two of which were further confirmed via time-dependent quantification of peak area over time. In a targeted approach, one Phase II GSH adduct of a BPADP oxidation product was identified for the first time (BPADP + GSH + 2O – 2H) via Q-E-Orbitrap HRMS/MS.

This approach was highly applicable to the study of BPADP, and is likely relevant to additional novel compounds. Applying NTA identified all possible biotransformation products and allowed for efficient screening of feasible *in vitro* metabolites, providing valuable understanding of BPADP metabolism including for metabolites without suitable internal standards. These data are a crucial step in completing the total biotransformation mass balance- particularly as the development of reliable internal standards requires considerable time and limits quantifying the concentration of many feasible metabolites.

In silico prediction offers, in many cases, the only (estimated) metabolite profile or physico-chemical property when experimental data is unavailable as is often the case

in the context of novel OPEs. OECD Toolbox v4.4.1 predicted metabolites should be interpreted with caution if used in decision-making, particularly when considering the ranking of probability of occurrence. Given the structural complexity of novel OPEs, predicted metabolites, even if confirmed empirically, should not be assumed as metabolites of structurally similar parent compounds. Specific to EPI Suite™, estimated properties demonstrate considerable uncertainty when based solely on modelling and vary widely with every experimentally derived data point inputted into the model. Particularly relevant to novel OPEs where molecular structures are complex, logK_{OW} and logK_{OC} may be overestimated by the OECD Toolbox and corroboration via experimental data is suggested. These and water solubility are crucial values in the determination of environmental fate, persistence, bioaccumulation and bioconcentration therefore it is imperative that experimental values are used wherever possible in modelling the fate of novel OPEs.

In silico modelling was demonstrated as a valuable screening tool for prioritizing compounds of concern and provides a major advantage in time saved considering the number of novel compounds, continuous evolution of OPEs and approaching phase-out of animal testing. The present results suggest high lipophilicity and adsorption, as well as low water solubility and low volatility for BPADP, RDP and RDX and to a comparably lesser degree, V6. Environmental persistence may be of high concern for these novel compounds, though bioaccumulation, bioconcentration and biological half-life remain dependent on physico-chemical properties largely unverified experimentally.

Confirmation of the well-established xenoestrogen (Yoshishara et al., 2004; Rubin et al., 2011) and acute aquatic toxicant (Wu & Seebacher, 2020; Naveira et al.,

2021) BPA as a metabolite of BPADP should be considered in hazard and risk assessment. Further study as to the feasibility and practicality of this metabolite would better quantify the risk posed to biota from biotransformation of BPADP to BPA. The present results suggest novel and oligomeric OPEs may be highly stable and potentially bioaccumulative in environmental media and biota, however species-specific differences in metabolism could lead to increased metabolite concentrations formed in some exposed species. Should this be the case, biotransformation of BPADP to BPA may be a relevant toxicity consideration. The structural complexity of novel OPEs allows for varied and complex degradation products, which may pose additional persistence or toxicity concerns and may vary between species. Addressing these knowledge gaps can elucidate whether exposure of novel OPEs to biota may add to the burden of PBT contaminants in the environment in a similar fashion as the PBDEs OPEs were developed to replace.

4.2 Directions of Future Research

1) Investigation of BPADP Degradation and Species-Specific Variation in Metabolism:

- The current understanding of BPADP biotic degradation is based on *in vitro* metabolism studies using only mammalian models (HLM, S9, serum; RLM) and indirect study of abiotic/chemical hydrolysis.
    i. Abiotic/chemical (non-enzymatic) hydrolysis of BPADP warrants further investigation, as Alves *et al.* identified a metabolite resulting from both enzymatic and chemical hydrolysis that was further confirmed (only in NADPH-deficient samples) in the present thesis (MM1 / M2 / BPADP – DPP). Further, abiotic hydrolysis of OPEs has been found to be pH-dependent (Su et al., 2016) therefore degradation products of BPADP and/or its rate of hydrolysis may vary

at different environmentally relevant pH values. Studies conducted using living cell lines and/or hepatocytes from different species would allow for the robust study of cell metabolism and enzyme mediation, including Phase I & II metabolism.

ii. The metabolism kinetics of several legacy OPEs have been demonstrated as species-specific (Greaves et al., 2016; Strobel et al., 2018a,b), a pattern that may also hold true with BPADP and other novel OPEs. Investigation of BPADP metabolism in herring gulls, which have demonstrated faster metabolism of legacy OPEs than ringed seals (Greaves et al., 2016) may allow for the calculation of BPADP biotransformation kinetics or may further corroborate the slow metabolism quantified in the present thesis. Additionally, as a freshwater feeding avian species the use of herring gulls as a model species would further elucidate the persistence and fate of this novel OPE in aquatic environments, adding ecological relevance. The use of fish models could also achieve this goal.

2) Investigation of Specific, Relevant Enzymes Mediating BPADP Metabolism:

- Rather than CYP450s, the present thesis results are more aligned with the one available study of BPADP metabolites in that NADPH-independent enzymes mediate the formation of BPA and various other additional metabolites.

  i. Alves *et al.* studied exclusively human metabolism, though similar findings with RLM metabolism were demonstrated in this thesis. Further investigation may confirm whether NADPH-independent enzymes (e.g. PONs) are primarily responsible for mediating BPADP *in vitro* metabolism, and the degree to which

such enzymes mediate metabolism could be compared between species (e.g. mammalian and aquatic).

ii. Specific, relevant CYP450 and PON enzyme isoforms should be identified, and their involvement in the mediation of individual BPADP metabolites detailed. This would allow for comparison with legacy OPEs for which more studies have been conducted focussing on relevant enzymes and therefore addressing the knowledge gap concerning how the metabolism of novel OPEs differs from our established understanding of legacy OPEs.

3) Addressing Knowledge Gaps Concerning BPADP and Additional Novel OPEs:

- This project has highlighted the applicability of a lines of evidence approach in understanding novel OPE biotransformation, physico-chemical properties and environmental fate. This efficient method could be applied to several compounds for which data is lacking.

  i. Building on the present results, NTA could be applied for the other novel OPEs (RDP, RDX, V6) following the development of tailored and optimized *in vitro* and/or *in vivo* assay and analytical methods. This could include identification of both Phase I & II metabolism pathways if the incubates of hepatocyte and cell line assays are studied via NTA.

  ii. The development of pure standards (rather than technical mixtures), sensitive ILODs & ILOQs and suitable internal standards are important in the further study of novel OPEs. This allows for clear demonstration and quantification of metabolites of the parent compound rather than of an impurity as demonstrated with the monitoring of TPHP impurities in the present thesis. Additionally,

mixture studies could be conducted to assess the array of relevant degradation products resulting from the application of commercial OPE mixtures in products.

4) Prioritizing Experimental Designs that Inform Risk Assessment & Management:

- Overall, scientific understanding of how the persistence, fate and degradation/biotransformation products of novel OPEs may differ from their legacy counterparts is severely limited. These knowledge gaps coupled with projections of increased OPE consumption and continual innovation within the flame retardant industry underscore a need for efficient study of these compounds.
  i. NTA of *in vitro* metabolism and biotransformation studies in connection with *in silico* metabolite predication screening should be applied in a lines of evidence approach to prioritize OPEs of immediate research priority (i.e. higher PBT potential, slower metabolism, more hazardous biotransformation products) to avoid regrettable substitution.
  ii. Accurate data are needed for the physico-chemical properties of novel OPEs including BPADP (especially logK_{OW}, logK_{OC} and water solubility) (Zhang et al., 2016), which will subsequently allow for more accurate determination of environmental fate. New *in silico* models are being developed for the prediction of environmental fate specific to aquatic species (ARC Arnot Research & Consulting, 2020) though some require biotransformation rate constants, suggesting the importance of improving the understanding of novel OPE metabolism in ecologically relevant species.

Organophosphates are a major class of pesticides, with some usage dating back to the 19th century and toxic effects including neurotoxicity, neurodegenerative diseases and

carcinogenicity to non-target organisms including humans (Costa et al., 2018). Several OPE insecticides gradually saw usage as FRs in examples of regrettable substitution following the phase-out of legacy FRs. These legacy compounds included BFRs such as PBDEs where the Penta-BDE and Octa-BDE formulations were internationally regulated under Annex A (Elimination) of the United Nations Stockholm Convention in 2009 (Blum et al., 2019), with hexabromocyclododecane and deca-BDE also listed in 2013 and 2017, respectively (Strobel et al., 2018a).

Various iterations or 'generations' of FRs have been used for decades, and amidst continuous demand a logical and efficient approach is required when assessing replacements. Using compounds only after effective hazard assessment has been conducted and limiting production and usage to essential purposes requires robust methods of identifying OPEs of concern- ideally before widespread usage- as was a goal of this thesis research project. Indeed the present results have been disseminated to an industry consortia working towards green chemistry within the FR industry (GreenScreen Chemicals, 2022), where these data will inform hazard assessment as to whether BPADP should become a high production FR compound. Similar proactive approaches should ideally be applied to future proposed replacement FRs, such that adequate biotransformation and persistence data is available for effective hazard assessment prior to potential widespread production.

References

Allan, I.J., Garmo, Ø.A., Rundberget, J.T., Terentjev, P., Christensen, G., Kashulin, N.A., 2018. Detection of tris(2,3-dibromopropyl) phosphate and other organophosphorous compounds in Arctic rivers. Environmental Science and Pollution Research 25(28), 28730–28737. doi: 10.1007/s11356-018-2947-5

Alves, A., Erratico, C., Lucattini, L., Cuykx, M., Ballesteros-Gómez, A., Leonards, P.E.G., Voorspoels, S., Covaci, A., 2018. Mass spectrometric identification of *in vitro*-generated metabolites of two emerging organophosphate flame retardants: V6 and BDP. Chemosphere 212, 1047–1057. doi: 10.1016/j.chemosphere.2018.08.142

Andresen, J.A., Grundmann, A., Bester, K., 2004. Organophosphorus flame retardants and plasticisers in surface waters. Science of The Total Environment 332(1), 155–166. doi: 10.1016/j.scitotenv.2004.04.021

ARC Arnot Research & Consulting, 2020. Eas-E-Suite. Toronto, Canada. Available at: https://arnotresearch.com/eas-e-suite/

Bährs, H., Putschew, A., Steinberg, C.E.W., 2013. Toxicity of hydroquinone to different freshwater phototrophs is influenced by time of exposure and pH. Environmental Science and Pollution Research 20(1), 146–154. doi: 10.1007/s11356-012-1132-5

Ballesteros-Gómez, A., Brandsma, S., Boer, J.D., Leonards, P., 2014. Analysis of two alternative organophosphorus flame retardants in electronic and plastic consumer products: Resorcinol bis-(diphenylphosphate) (PBDPP) and bisphenol A bis (diphenylphosphate) (BPA-BDPP). Chemosphere 116:10–14. doi: 10.1016/j.chemosphere.2013.12.099

Ballesteros-Gómez, A., Van den Eede, N., Covaci, A., 2015. *In Vitro* Human Metabolism of the Flame Retardant Resorcinol Bis(diphenylphosphate) (RDP). Environmental Science & Technology 49(6), 3897–3904. doi: 10.1021/es505857e

Bekele, T.G., Zhao, H., Wang, Q., 2021. Tissue distribution and bioaccumulation of organophosphate esters in wild marine fish from Laizhou Bay, North China: Implications of human exposure via fish consumption. Journal of Hazardous Materials 401:123410. doi: 10.1016/j.jhazmat.2020.123410

Bergh, C., Torgrip, R., Emenius, G., Östman, C., 2011. Organophosphate and phthalate esters in air and settled dust - a multi-location indoor study. Indoor Air 21(1): 67–76. doi: 10.1111/j.1600-0668.2010.00684.x

Bergman, Å., Rydén, A., Law, R.J., de Boer, J., Covaci, A., Alaee, M., Birnbaum, L., Petreas, M., Rose, M., Sakai, S., van den Eede, N., van der Veen, I., 2012. A novel abbreviation standard for organobromine, organochlorine and organophosphorus flame retardants and some characteristics of the chemicals. Environment International 49:57–82. doi: 10.1016/j.envint.2012.08.003

Blum, A., Behl, M., Birnbaum, L.S., Diamond, M.L., Phillips, A., Singla, V., Sipes, N.S., Stapleton, H.M., Venier, M., 2019. Organophosphate Ester Flame Retardants: Are They a Regrettable Substitution for Polybrominated Diphenyl Ethers? Environmental Science & Technology Letters 6(11), 638–649. doi: 10.1021/acs.estlett.9b00582

Brandsma, S.H., de Boer, J., Leonards, P.E.G., Cofino, W.P., Covaci, A., Leonards, P.E.G., 2013a. Organophosphorus flame-retardant and plasticizer analysis, including recommendations from the first worldwide interlaboratory study. Trends in Analytical Chemistry 43, 217–228. doi: 10.1016/j.trac.2012.12.004

Brandsma, S.H., Leonards, P.E.G., Leslie, H.A., de Boer, J., 2015. Tracing organophosphorus and brominated flame retardants and plasticizers in an estuarine food web. Science of the Total Environment 505, 22–31. doi: 10.1016/j.scitotenv.2014.08.072

Brandsma, S.H., Sellström, U., de Wit, C.A., de Boer, J., Leonards, P.E.G., 2013b. Dust Measurement of Two Organophosphorus Flame Retardants, Resorcinol Bis(diphenylphosphate) (RBDPP) and Bisphenol A Bis(diphenylphosphate) (BPA-BDPP), Used as Alternatives for BDE-209. Environmental Science and Technology 47(24), 14434–14441. doi: 10.1021/es404123q

Brits, M., Brandsma, S.H., Rohwer, E.R., De Vos, J., Weiss, J.M., de Boer, J., 2019. Brominated and organophosphorus flame retardants in South African indoor dust and cat hair. Environmental Pollution 253, 120–129. doi: 10.1016/j.envpol.2019.06.121

Cao, D., Guo, J., Wang, Y., Li, Z., Liang, K., Corcoran, M.B., Hosseini, S., Bonina, S.M.C., Rockne, K.J., Sturchio, N.C., Giesy, J.P., Liu, J., Li, A., Jiang, G., 2017. Organophosphate Esters in Sediment of the Great Lakes. Environmental Science & Technology 51:1441–1449. doi: 10.1021/acs.est.6b05484

Cao, D., Lv, K., Gao, W., Fu, J., Wu, J., Fu, J., Wang, Y., Jiang, G., 2019. Presence and human exposure assessment of organophosphate flame retardants (OPEs) in indoor dust and air in Beijing, China. Ecotoxicology and Environmental Safety 169, 383–391. doi: 10.1016/j.ecoenv.2018.11.038

CBC News, 2010. BPA declared toxic by Canada. Available at: https://www.cbc.ca/news/science/bpa-declared-toxic-by-canada-1.873250

Center for Disease Control Agency for Toxic Substances and Disease Registry. Unknown date. PCBs – Chemical and Physical Information. Washington, DC, USA. Available at: https://www.atsdr.cdc.gov/toxprofiles/tp17-c4.pdf

Çetin, S., Özaydın, T., 2021. The effects of bisphenol A given in ovo on bursa of Fabricius development and percentage of acid phosphatase positive lymphocyte in chicken. Environmental Science and Pollution Research 28(31), 41688–41697. doi: 10.1007/s11356-021-13640-z

Chemical Book Chemical Information Search, nd. Bisphenol A CAS#: 80-05-7. Available at: https://www.chemicalbook.com/ProductChemicalPropertiesCB5854419_EN.htm.

Chemical Book Chemical Information Search, nd. Diphenyl Phosphate CAS#: 838-85-7. Available at: https://www.chemicalbook.com/ProductChemicalPropertiesCB4297385_EN.htm.

Chemical book Chemical Information Search, n.d. Triphenyl phosphate. Available at: https://www.chemicalbook.com/ProductList_En.aspx?kwd=triphenyl phosphate.

Chen, Q., Lian, X., An, J., Geng, N., Zhang, H., Challis, J. K., Luo, Y., Liu, Y., Su, G., Xie, Y., Li, Y., Liu, Z., Shen, Y., Giesy, J.P., Gong, Y., 2021. Life Cycle Exposure to Environmentally Relevant Concentrations of Diphenyl Phosphate (DPhP) Inhibits Growth and Energy Metabolism of Zebrafish in a Sex-Specific Manner. Environmental Science & Technology 55, 19, 13122–13131. doi: 10.1021/acs.est.1c03948

Chen, H., Yao, J., Wang, F., Zhou, Y., Chen, K., Zhuang, R., Choi, M.M.F., Zaray, G., 2010. Toxicity of three phenolic compounds and their mixtures on the gram-positive bacteria Bacillus subtilis in the aquatic environment. Science of the Total Environment 408(5), 1043–1049. doi: 10.1016/j.scitotenv.2009.11.051

Chmiel, T., Mieszkowska, A., Kempińska-Kupczyk, D., Kot-Wasik, A., Namieśnik, J., Mazerska, Z., 2019. The impact of lipophilicity on environmental processes, drug delivery and bioavailability of food components. Microchemical Journal 146: 393-406. doi: 10.1016/j.microc.2019.01.030

Choi, Y., Jeon, J., Choi, Y., Kim, S.D., 2020. Characterizing biotransformation products and pathways of the flame retardant triphenyl phosphate in Daphnia magna using non-target screening. Science of the Total Environment 708, 135106. doi: 10.1016/j.scitotenv.2019.135106

Chokwe, T.B., Abafe, O.A., Mbelu, S.P., Okonkwo, J.O., & Sibali, L.L. 2020. A review of sources, fate, levels, toxicity, exposure and transformations of organophosphorus flame-retardants and plasticizers in the environment. *Emerging Contaminants*, 6, 345–366. doi: 10.1016/j.emcon.2020.08.004

Chu, S., Chen, D., Letcher, R.J., 2011. Dicationic ion-pairing of phosphoric acid diesters post-liquid chromatography and subsequent determination by electrospray positive ionization-tandem mass spectrometry. Journal of Chromatography A 1218(44), 8083–8088. doi: 10.1016/j.chroma.2011.09.011

Chu, S., Letcher, R.J., 2015. Determination of organophosphate flame retardants and plasticizers in lipid-rich matrices using dispersive solid-phase extraction as a sample cleanup step and ultra-high performance liquid chromatography with atmospheric pressure chemical ionization mass spectrometry. Analytica Chimica Acta 885, 183–190. doi: 10.1016/j.aca.2015.05.024

Chu, S., Letcher, R.J., 2018. A mixed-mode chromatographic separation method for the analysis of dialkyl phosphates. Journal of Chromatography A 1535, 63–71. doi: 10.1016/j.chroma.2017.12.069

Chu, S., Letcher, R.J., 2019. *In vitro* metabolic activation of triphenyl phosphate leading to the formation of glutathione conjugates by rat liver microsomes. Chemosphere 237, 124474. doi: 10.1016/j.chemosphere.2019.124474

Chupeau, Z., Bonvallot, N., Mercier, F., Le Bot, B., Chevrier, C., Glorennec, P., 2020. Organophosphorus Flame Retardants: A Global Review of Indoor Contamination and Human Exposure in Europe and Epidemiological Evidence. International Journal of Environmental Research and Public Health 17, 6713. doi: 10.3390/ijerph17186713

Compound Dictionary, nd. Bisphenol A Bis(diphenyl phosphate) 5945-33-5 Price, CAS No., Alias. Available at: http://www.molbase.com/en/overview_5945-33-5-moldata-67758.html.

Costa, L.G., Giordano, G., Cole, T.B., Marsillach, J., Furlong, C.E., 2013. Paraoxonase 1 (PON1) as a Genetic Determinant of Susceptibility to Organophosphate Toxicity. Toxicology 307, 115–122. doi: 10.1016/j.tox.2012.07.011

de Boer, J., Ballesteros-Gómez, A., Leslie, H.A., Brandsma, S.H., Leonards, P.E.G., 2016. Flame retardants: Dust – And not food – Might be the risk. Chemosphere 150, 461–464. doi: 10.1016/j.chemosphere.2015.12.124

Ding J, Xu Z, Huang W, Feng L, Yang F., 2016. Organophosphate ester flame retardants and plasticizers in human placenta in Eastern China. Science of the Total Environment 554-555:211–217. doi: 10.1016/j.scitotenv.2016.02.171

Draganov, D.I., La Du, B.N., 2004. Pharmacogenetics of paraoxonases: A brief review. Naunyn-Schmiedeberg's Archives of Pharmacology 369(1), 78–88. doi: 10.1007/s00210-003-0833-1

Duan, W., Meng, F., Cui, H., Lin, Y., Wang, G., Wu, J., 2018. Ecotoxicity of phenol and cresols to aquatic organisms: A review. Ecotoxicology and Environmental Safety 157, 441–456. doi: 10.1016/j.ecoenv.2018.03.089

Enguita, F.J., Leitão, A.L., 2013. Hydroquinone: Environmental Pollution, Toxicity, and Microbial Answers. BioMed Research International Article ID 542168. doi: 10.1155/2013/542168

Environment Canada, 2004. Canadian Environmental Protection Act, 1999 Environmental Screening Assessment Report on Polybrominated Diphenyl Ethers (PBDEs) – Draft for Public Comments. Available at: https://www.ec.gc.ca/lcpe-cepa/documents/substances/pbde/pbde_draft-eng.pdf

Environment Canada, 2013. ARCHIVED- Environmental Screening Assessment Report on Polybrominated Diphenyl Ethers (PBDEs) – Draft for Public Comments. Available at:

https://www.ec.gc.ca/lcpe-cepa/default.asp?lang=En&n=DF7DE982-1&offset=3&toc=hide

European Chemicals Agency (ECHA), 2011. (1-methylethylidene)di-4,1-phenylenetetraphenyl diphosphate- Registration Dossier; Physical & Chemical Properties. Helsinki, Finland. Available at: https://echa.europa.eu/registration-dossier/-/registered-dossier/6592/4/8/?documentUUID=dae1147a-fc9c-4818-905c-78b84a7265a1

European Commission Joint Research Centre, 2001. Diphenyl Ether, Pentabromo Derivative (Pentabromodiphenyl Ether). Belgium. Available at: https://echa.europa.eu/documents/10162/781ee1e9-6c90-467e-998b-8910ca2793e5

Frederiksen, M., Stapleton, H.M., Vorkamp, K., Webster, T.F., Jensen, N.M., Sørensen, J.A., Nielsen, F., Knudsen, L.E., Sørensen, L.S., Clausen, P.A., Nielsen, J.B., 2018. Dermal uptake and percutaneous penetration of organophosphate esters in a human skin ex vivo model. Chemosphere 197, 185–192. doi: 10.1016/j.chemosphere.2018.01.032

Funk, S.P., Duffin, L., He, Y., McMullen, C., Sun, C., Utting, N., Martin, J.W., Goss, G.G., Alessi, D.S., 2019. Assessment of impacts of diphenyl phosphate on groundwater and near-surface environments: Sorption and toxicity. Journal of Contaminant Hydrology 221, 50–57. doi: 10.1016/j.jconhyd.2019.01.002

Glazer, L., Hawkey, A.B., Wells, C.N., Drastal, M., Odamah, K.-A., Behl, M., Levin, E.D., 2018. Developmental Exposure to Low Concentrations of Organophosphate Flame Retardants Causes Life-Long Behavioral Alterations in Zebrafish. Toxicological Sciences 165 (2), 487–498. doi: 10.1093/toxsci/kfy173

Gobas, F.A.P.C., Kelly, B.C., Arnot, J.A., 2003. Quantitative Structure Activity Relationships for Predicting the Bioaccumulation of POPs in Terrestrial Food-Webs. QSAR & Combinatorial Science 22(3), 329–336. doi: 10.1002/qsar.200390022

Government of Canada, 2019. Flame Retardants. Available from https://www.canada.ca/en/health-canada/services/chemicals-product-safety/flame-retardants.html.

Government of Canada, 2021, November 13. Canada Gazette, Part 1, Volume 155, Number 46: Government of Canada, Public Works and Government Services Canada, Integrated Services Branch, Canada Gazette. Available at: https://gazette.gc.ca/rp-pr/p1/2021/2021-11-13/html/notice-avis-eng.html#na2

Greaves, A.K., Letcher, R.J., 2014. Comparative Body Compartment Composition and In Ovo Transfer of Organophosphate Flame Retardants in North American Great Lakes Herring Gulls. Environmental Science & Technology 48(14): 7942–7950. doi: 10.1021/es501334w

Greaves, A.K., Su, G., Letcher, R.J., 2016. Environmentally relevant organophosphate triesters in herring gulls: *In vitro* biotransformation and kinetics and diester metabolite

formation using a hepatic microsomal assay. Toxicology and Applied Pharmacology 308, 59–65. doi: 10.1016/j.taap.2016.08.007

GreenScreen, 2022. All About GreenScreen. Available at: https://www.greenscreenchemicals.org/learn

Gustafsson, K., Björk, M., Burreau, S., Gilek, M., 1999. Bioaccumulation kinetics of brominated flame retardants (polybrominated diphenyl ethers) in blue mussels (Mytilus edulis). Environmental Toxicology and Chemistry 18(6), 1218–1224. doi: 10.1002/etc.5620180621

Gustavsson, J., Wiberg, K., Ribeli, E., Nguyen, M.A., Josefsson, S., Ahrens, L., 2018. Screening of organic flame retardants in Swedish river water. Science of the Total Environment 625, 1046–1055. doi: 10.1016/j.scitotenv.2017.12.281

Hallanger, I.G., Sagerup, K., Evenset, A., Kovacs, K.M., Leonards, P., Fuglei, E., Routti, H., Aars, J., Strøm, H., Lydersen, C., Gabrielsen, G.W., 2015. Organophosphorous flame retardants in biota from Svalbard, Norway. Marine Pollution Bulletin 101(1), 442–447. doi: 10.1016/j.marpolbul.2015.09.049

Hanas, A.K., Guigueno, M.F., Fernie, K.J., Letcher, R.J., Ste-Marie Chamberland, F., Head, J.A., 2020. Assessment of the effects of early life exposure to triphenyl phosphate on fear, boldness, aggression, and activity in Japanese quail (Coturnix japonica) chicks. Environmental Pollution 258, 113695. doi : 10.1016/j.envpol.2019.113695

Harnett, K.G., Chin, A., Schuh, S.M., 2021. BPA and BPA alternatives BPS, BPAF, and TMBPF, induce cytotoxicity and apoptosis in rat and human stem cells. Ecotoxicology and Environmental Safety 216, 112210. doi: 10.1016/j.ecoenv.2021.112210

Hou, R., Huang, C., Rao, K., Xu, Y., Wang, Z., 2018. Characterized *in Vitro* Metabolism Kinetics of Alkyl Organophosphate Esters in Fish Liver and Intestinal Microsomes. Environmental Science & Technology 52(5), 3202–3210. doi: 10.1021/acs.est.7b05825

Jurgens, S.S., Helmus, R., Waaijers, S.L., Uittenbogaard, D., Dunnebier, D., Vleugel, M., Kraak, M.H., Voogt, P.D., Parsons, J.R., 2014. Mineralisation and primary biodegradation of aromatic organophosphorus flame retardants in activated sludge. Chemosphere 111:238–242. doi: 10.1016/j.chemosphere.2014.04.016

Kim, U.-J., Oh, J.K., Kannan, K., 2017. Occurrence, Removal, and Environmental Emission of Organophosphate Flame Retardants/Plasticizers in a Wastewater Treatment Plant in New York State. Environmental Science & Technology 51(14), 7872–7880. doi: 10.1021/acs.est.7b02035

Li, W., Wang, Y., Kannan, K., 2019a. Occurrence, Distribution and Human Exposure to 20 Organophosphate Esters in Air, Soil, Pine Needles, River Water, and Dust Samples

Collected around an Airport in New York State, United States. Environment International 131, 105054. doi: 10.1016/j.envint.2019.105054

Li, J., Zhao, L., Letcher, R.J., Zhang, Y., Jian, K., Zhang, J., Su, G., 2019b. A review on organophosphate Ester (OPE) flame retardants and plasticizers in foodstuffs: Levels, distribution, human dietary exposure, and future directions. Environment International 127:35–51. doi: 10.1016/j.envint.2019.03.009

Li, X., Zhao, N., Fu, J., Liu, Y., Zhang, W., Dong, S., Wang, P., Su, X., Fu, J., 2020. Organophosphate Diesters (Di-OPEs) Play a Critical Role in Understanding Global Organophosphate Esters (OPEs) in Fishmeal. Environmental Science & Technology 54(19), 12130–12141. doi: 10.1021/acs.est.0c03274

Liang, K., Shi, F., Liu, J., 2018. Occurrence and distribution of oligomeric organophosphorus flame retardants in different treatment stages of a sewage treatment plant. Environmental Pollution 232, 229–235. doi: 10.1016/j.envpol.2017.09.036

Liu, Y., Luo, X., Guan, K., Huang, C., Zhu, C., Qi, X., Zeng, Y., Mai, B., 2020. Legacy and Emerging Organophosphorus Flame Retardants and Plasticizers in Frogs: Sex Difference and Parental Transfer. Environmental Pollution 266, 115336. doi: 10.1016/j.envpol.2020.115336

Ma, Y., Jin, J., Li, P., Xu, M., Sun, Y., Wang, Y., Yuan, H., 2017. Organophosphate ester flame retardant concentrations and distributions in serum from inhabitants of Shandong, China, and changes between 2011 and 2015. Environmental Toxicology and Chemistry 36(2), 414–421. doi: 10.1002/etc.3554

Ma, Y., Xie, Z., Lohmann, R., Mi, W., Gao, G., 2017. Organophosphate Ester Flame Retardants and Plasticizers in Ocean Sediments from the North Pacific to the Arctic Ocean. Environmental Science & Technology 51(7), 3809–3815. doi: 10.1021/acs.est.7b00755

Maine Department of Environmental Protection, Maine Center for Disease Control & Prevention, 2007. Brominated Flame Retardants: Third Annual Report to the Maine Legislature. Augusta, Maine, USA.

Marteinson, S., Guigueno, M.F., Fernie, K.J., Head, J.A., Chu, S., Letcher, R.J., 2020. Uptake, Deposition, and Metabolism of Triphenyl Phosphate in Embryonated Eggs and Chicks of Japanese Quail (Coturnix japonica). Environmental Toxicology and Chemistry 39(3), 565–573. doi: 10.1002/etc.4637

Matsukami, H., Suzuki, G., Takigami, H., 2015a. Compositional Analysis of Commercial Oligomeric Organophosphorus Flame Retardants Used as Alternatives for PBDEs: Concentrations and Potential Environmental Emissions of Oligomers and Impurities. Environmental Science & Technology 49, 21, 12913–12921. doi: 10.1021/acs.est.5b03447

Matsukami, H., Tue, N.M., Suzuki, G., Someya, M., Tuyen, L.H., Viet, P.H., Takahashi, S., Tanabe, S., Takigami, H., 2015b. Flame Retardant Emission from E-Waste Recycling Operation in Northern Vietnam: Environmental Occurrence of Emerging Organophosphorus Esters Used as Alternatives for PBDEs. Science of The Total Environment 514, 492–499. doi: 10.1016/j.scitotenv.2015.02.008

Mesnage, R., Phedonos, A., Arno, M., Balu, S., Corton, J.C., Antoniou, M.N., 2017. Editor's Highlight: Transcriptome Profiling Reveals Bisphenol A Alternatives Activate Estrogen Receptor Alpha in Human Breast Cancer Cells. Toxicological Sciences 158(2), 431–443. doi: 10.1093/toxsci/kfx101

Meyer, J., Bester, K., 2004. Organophosphate flame retardants and plasticisers in wastewater treatment plants. Journal of Environmental Monitoring 6: 599-605. doi: 10.1039/b403206c

Möller, A., Xie, Z., Caba, A., Sturm, R., Ebinghaus, R., 2011. Organophosphorus flame retardants and plasticizers in the atmosphere of the North Sea. Environmental Pollution 159(12), 3660–3665. doi: 10.1016/j.envpol.2011.07.022

National Institute of Environmental Health Sciences, 2018. Flame Retardants. North Carolina, USA. Available at: https://www.niehs.nih.gov/health/topics/agents/flame_retardants/index.cfm.

Naujokaitytė, G., 2021. Parliament votes through demand for faster phase out of animal testing in research. Science Business Publishing International SRL, Brussels, Belgium. Available at: https://sciencebusiness.net/news/parliament-votes-through-demand-faster-phase-out-animal-testing-research

Naveira, C. Rodrigues, N., Santos, F.S., Santos, L.N., Neves, R.A.F., 2021. Acute toxicity of Bisphenol-A (BPA) to tropical marine and estuarine species from different trophic groups. Environmental Pollution 268, 115911. doi: 10.1016/j.envpol.2020.115911

Ousji, O., Ohlund, L., Sleno, L., 2020. Comprehensive *In Vitro* Metabolism Study of Bisphenol A Using Liquid Chromatography-High Resolution Tandem Mass Spectrometry. Chemical Research in Toxicology 33, 6, 1468-1477. doi: 10.1021/acs.chemrestox.0c00042

Pagé-Larivière, F., Chiu, S., Jones, S.P., Farhat, A., Crump, D., O'Brien, J.M., 2018. Prioritization of 10 organic flame retardants using an avian hepatocyte toxicogenomic assay. Environmental Toxicology and Chemistry 37(12): 3134–3144. doi: 10.1002/etc.4260

Pakalin, S., Cole, T., Steinkellner, J., Nicolas, R., Tissier, C., Munn, S., Eisenreich, S., 2007. Review on Production Processes of Decabromodiphenyl Ether (DecaBDE) Used in Polymeric Applications in Electrical and Electronic Equipment, and Assessment of the Availability of Potential Alternatives to DecaBDE. European Chemicals Bureau, Institute of Health and Consumer Protection, European Report EUR 22693 EN, Brussel, Belgium.

Pawlowski, K.H. Schartel, B., 2007. Flame retardancy mechanisms of triphenyl phosphate, resorcinol bis(diphenyl phosphate) and bisphenol A bis(diphenyl phosphate) in polycarbonate/acrylonitrile–butadiene–styrene blends. Polymer International 56: 1404–1414. doi: 10.1002/pi.2290

Poopal, R.-K., He, Y., Zhao, R., Li, B., Ramesh, M., Ren, Z., 2021. Organophosphorus-based chemical additives induced behavioral changes in zebrafish (Danio rerio): Swimming activity is a sensitive stress indicator. Neurotoxicology and Teratology 83, 106945. doi: 10.1016/j.ntt.2020.106945

Ramírez, V., Gálvez-Ontiveros, Y., Porras-Quesada, P., Martinez-Gonzalez, L. J., Rivas, A., Álvarez-Cubero, M.J., 2021. Metabolic pathways, alterations in miRNAs expression and effects of genetic polymorphisms of bisphenol a analogues: A systematic review. Environmental Research 197, 111062. doi: 10.1016/j.envres.2021.111062

Reemtsma, T., Quintana, J.B., Rodil, R., Garcı´a-López, M., Rodrıguez, I., 2008. Organophosphorus flame retardants and plasticizers in water and air- Occurrence and fate. Trends in Analytical Chemistry 27(9), 727–737. doi: 10.1016/j.trac.2008.07.002

Riddell, N., van Bavel, B., Ericson Jogsten, I., McCrindle, R., McAlees, A., Chittim, B., 2017. Examination of technical mixtures of halogen-free phosphorus based flame retardants using multiple analytical techniques. Chemosphere 176, 333–341. doi : 10.1016/j.chemosphere.2017.02.129

Rodriguez, I., Calvo, F., Quintana, J., Rubi, E., Rodil, R., Cela, R., 2006. Suitability of solid-phase microextraction for the determination of organophosphate flame retardants and plasticizers in water samples. Journal of Chromatography A 1108, 158–165. doi: 10.1016/j.chroma.2006.01.008

Rosenmai, A.K., Dybdahl, M., Pedersen, M., Vugt-Lussenburg, B.M.A.V., Wedebye, E.B., Taxvig, C., Vinggaard, A.M., 2014. Are Structural Analogues to Bisphenol A Safe Alternatives? Toxicological Sciences 139: 35–47. doi: 10.1093/toxsci/kfu030

Rossi, M., Heine, L., 2007. The Green Screen for Safer Chemicals: Evaluating Flame Retardant for TV Enclosures. Somerville, MA, USA. Available at: https://www.bizngo.org/static/ee_images/uploads/resources/EvaluatingFlameRetardants_GreenScreenSaferChemicals_2007.pdf.

Rubin, B.S., 2011. Bisphenol A: An endocrine disruptor with widespread exposure and multiple effects. The Journal of Steroid Biochemistry and Molecular Biology 127:27–34. doi: 10.1016/j.jsbmb.2011.05.002

Sala, B., Giménez, J., de Stephanis, R., Barceló, D., Eljarrat, E., 2019. First Determination of High Levels of Organophosphorus Flame Retardants and Plasticizers in Dolphins from Southern European Waters. Environmental Research 172, 289–295. doi: 10.1016/j.envres.2019.02.027

Santin, G., Eljarrat, E., Barceló, D., 2016. Simultaneous determination of 16 organophosphorus flame retardants and plasticizers in fish by liquid chromatography-tandem mass spectrometry. Journal of Chromatography A 1441: 34-43. doi: 10.1016/j.chroma.2016.02.058

Schlechtriem, C., Böhm, L., Bebon, R., Bruckert, H.-J., Düring, R.-A., 2017. Fish bioconcentration studies with column-generated analyte concentrations of highly hydrophobic organic chemicals. Environmental Toxicology and Chemistry 36(4), 906–916. doi: 10.1002/etc.3635

Shen, J., Zhang, Y., Yu, N., Crump, D., Li, J., Su, H., Letcher, R.J., Su, G., 2019. Organophosphate Ester, 2-Ethylhexyl Diphenyl Phosphate (EHDPP), Elicits Cytotoxic and Transcriptomic Effects in Chicken Embryonic Hepatocytes and Its Biotransformation Profile Compared to Humans. Environmental Science & Technology 53(4), 2151–2160. doi: 10.1021/acs.est.8b06246

Strobel, A., Willmore, W.G., Sonne, C., Dietz, R., Letcher, R.J., 2018a. Organophosphate esters in East Greenland polar bears and ringed seals: Adipose tissue concentrations and *in vitro* depletion and metabolite formation. Chemosphere 196: 240–250. doi: 10.1016/j.chemosphere.2017.12.181

Strobel, A., Letcher, R.J., Willmore, W.G., Sonne, C., Dietz, R., 2018b. Structure-Dependent *in Vitro* Metabolism of Alkyl-Substituted Analogues of Triphenyl Phosphate in East Greenland Polar Bears and Ringed Seals. Environmental Science & Technology Letters 5(4), 214–219. doi: 10.1021/acs.estlett.8b00064

Su, G., Letcher, R.J., Crump, D., Gooden, D.M., Stapleton, H.M., 2015a. *In Vitro* Metabolism of the Flame Retardant Triphenyl Phosphate in Chicken Embryonic Hepatocytes and the Importance of the Hydroxylation Pathway. Environmental Science & Technology Letters 2, 100−104. doi: 10.1021/acs.estlett.5b00041

Su, G., Letcher, R.J., Yu, H., 2015b. Determination of organophosphate diesters in urine samples by a high-sensitivity method based on ultra high pressure liquid chromatography-triple quadrupole-mass spectrometry. Journal of Chromatography A 1426, 154–160. doi: 10.1016/j.chroma.2015.11.018

Su, G., Letcher, R J., Yu, H., 2016. Organophosphate Flame Retardants and Plasticizers in Aqueous Solution: PH-Dependent Hydrolysis, Kinetics, and Pathways. Environmental Science & Technology 50(15), 8103–8111. doi: 10.1021/acs.est.6b02187

Sühring, R., Scheringer, M., Rodgers, T.F.M., Jantunen, L.M., & Diamond, M.L., 2020. Evaluation of the OECD P_{OV} and LRTP Screening Tool for Estimating the Long-Range Transport of Organophosphate Esters. Environmental Science: Processes & Impacts 22 (1), 207–216. doi: 10.1039/C9EM00410F

Sun, Y., De Silva, A.O., St Pierre, K.A., Muir, D.C.G., Spencer, C., Lehnherr, I., MacInnis, J.J., 2020. Glacial Melt Inputs of Organophosphate Ester Flame Retardants to the Largest

High Arctic Lake. Environmental Science & Technology 54(5), 2734–2743. doi: 10.1021/acs.est.9b06333

Thayer, K.A., Doerge, D.R., Hunt, D., Schurman, S.H., Twaddle, N.C., Churchwell, M.I., Garantziotis, S., Kissling, G.E., Easterling, M.R., Bucher, J.R., Birnbaum, L.S., 2015. Pharmacokinetics of bisphenol A in humans following a single oral administration. Environment International 83, 107–115. doi: 10.1016/j.envint.2015.06.008

Toronto Research Chemicals, n.d. B519530 Product Detail. Available at: https://www.trc-canada.com/product-detail/?B519530.

United Nations Environment Programme, 2019. Stockholm Convention Polybromodiphenyl ethers—Overview. Chatelaine, Switzerland. Available at: http://chm.pops.int/Implementation/IndustrialPOPs/BDEs/Overview/tabid/5371/Default.aspx

United States Environmental Protection Agency, 2012. Estimation Programs Interface Suite™ for Microsoft® Windows, v 4.11. Washington, DC, USA

United States Environmental Protection Agency, 2014. An Alternatives Assessment for the Flame Retardant Decabromodiphenylether (DecaBDE) Final Report. Washington, DC, USA. Available at: http://www.epa.gov/dfe/pubs/projects/decaBDE/deca-report-complete.pdf; p 4-149.

United States Environmental Protection Agency, 2015. KABAM Version 1.0 User's Guide and Technical Documentation—Appendix F -Description of Equations Used to Calculate the BCF, BAF, BMF, and BSAF Values [Data and Tools]. Washington, DC, USA. Available at: https://www.epa.gov/pesticide-science-and-assessing-pesticide-risks/kabam-version-10-users-guide-and-technical-3

United States Environmental Protection Agency, 2017. Technical Fact Sheet – Polybrominated Diphenyl Ethers (PBDEs). Washington, DC, USA. Available at: https://www.epa.gov/sites/default/files/2014-03/documents/ffrrofactsheet_contaminant_perchlorate_january2014_final_0.pdf

United States Environmental Protection Agency, 2020. EPA Announces Guidance to Waive Toxicity Tests on Animal Skin. Washington, DC, USA. Available at: https://www.epa.gov/newsreleases/epa-announces-guidance-waive-toxicity-tests-animal-skin

United States Patent and Trademark Office (USPTO), 2009. Patent Public Search. Alexandria, VA, USA. Available at: https://ppubs.uspto.gov/pubwebapp/

United States Patent and Trademark Office (USPTO), 2022. Patent Public Search. Alexandria, VA, USA. Available at: https://ppubs.uspto.gov/pubwebapp/static/pages/landing.html

Van den Eede, N., Maho, W., Erratico, C., Neels, H., Covaci, A., 2013. First insights in the metabolism of phosphate flame retardants and plasticizers using human liver fractions. Toxicology Letters 223:9–15. doi: 10.1016/j.toxlet.2013.08.012

van der Veen, I., de Boer, J., 2012. Phosphorus flame retardants: Properties, production, environmental occurrence, toxicity and analysis. Chemosphere 88(10), 1119–1153. doi : 10.1016/j.chemosphere.2012.03.067

Velencoso, M.M., Battig, A., Markwart, J.C., Schartel, B., Wurm, F.R., 2018. Molecular Firefighting—How Modern Phosphorus Chemistry Can Help Solve the Challenge of Flame Retardancy. Angewandte Chemie International Edition 57(33), 10450–10467. doi: 10.1002/anie.201711735

Waaijers, S.L., Kong, D., Hendriks, H.S., de Wit, C.A., Cousins, I.T., Westerink, R.H.S., Leonards, P.E.G., Kraak, M.H.S., Admiraal, W., de Voogt, P., Parsons, J.R., 2013a. Persistence, Bioaccumulation, and Toxicity of Halogen-Free Flame Retardants. In: Whitacre D. (eds) Reviews of Environmental Contamination and Toxicology (Continuation of Residue Reviews) vol 222, p.1-71. Springer, New York, NY. doi: 10.1007/978-1-4614-4717-7_1

Waaijers, S.L., Hartmann, J., Soeter, A.M., Helmus, R., Kools, S.A.E., de Voogt, P., Admiraal, W., Parsons, J.R., Kraak, M.H.S., 2013b. Toxicity of new generation flame retardants to Daphnia magna. Science of the Total Environment 463–464, 1042–1048. doi: 10.1016/j.scitotenv.2013.06.110

Wang, G., Chen, H., Du, Z., Li, J., Wang, Z., Gao, S., 2017. *In Vivo* Metabolism of Organophosphate Flame Retardants and Distribution of Their Main Metabolites in Adult Zebrafish. Science of the Total Environment 590–591, 50–59. doi: 10.1016/j.scitotenv.2017.03.038

Wang, X., Zhong, W., Xiao, B., Liu, Q., Yang, L., Covaci, A., Zhu, L., 2019. Bioavailability and biomagnification of organophosphate esters in the food web of Taihu Lake, China: Impacts of chemical properties and metabolism. Environment International 125, 25–32. doi: 10.1016/j.envint.2019.01.018

WIPO, 2021. Patentscope. World Intellectual Property Organization, Geneva, Switzerland. Available at: https://www.wipo.int/patentscope/en/

Wu, N., Seebacher, F., 2020. Effect of the plastic pollutant bisphenol-A on the biology of aquatic organisms: A meta-analysis. Global Change Biology 26: 3821–3833. doi: 10.1111/gcb.15127

Yao, C., Yang, H., Li, Y., 2021. A review on organophosphate flame retardants in the environment: Occurrence, accumulation, metabolism and toxicity. Science of the Total Environment 795, 148837. doi: 10.1016/j.scitotenv.2021.148837

Ye, L., Meng, W., Huang, J., Li, J., Su, G., 2021. Establishment of a Target, Suspect, and Functional Group-Dependent Screening Strategy for Organophosphate Esters (OPEs):

"Into the Unknown" of OPEs in the Sediment of Taihu Lake, China. Environmental Science & Technology 55, 9, 5836−5847. doi: 10.1021/acs.est.0c07825

Yoshihara, S., Mizutare, T., Makishima, M., Suzuki, N., Fujimoto, N., Igarashi, K., Ohta, S., 2004. Potent Estrogenic Metabolites of Bisphenol A and Bisphenol B Formed by Rat Liver S9 Fraction: Their Structures and Estrogenic Potency. Toxicological Sciences 78(1), 50–59. doi: 10.1093/toxsci/kfh047

Zhang, Q., Ji, S., Chai, L., Yang, F., Zhao, M., Liu, W., Schüürmann, G., Ji, L., 2018. Metabolic Mechanism of Aryl Phosphorus Flame Retardants by Cytochromes P450: A Combined Experimental and Computational Study on Triphenyl Phosphate. Environmental Science & Technology 52, 24: 14411–14421. doi: 10.1021/acs.est.8b03965

Zhang, Q., Yu, C., Fu, L., Gu, S., Wang, C., 2020. New insights in the endocrine disrupting effects of three primary metabolites of organophosphate flame retardants. Environmental Science & Technology 54 (7), 4465−4474. doi: 10.1021/acs.est.9b07874

Zhang, X., Sühring, R., Serodio, D., Bonnell, M., Sundin, N., Diamond, M.L., 2016. Novel Flame Retardants: Estimating the Physical–Chemical Properties and Environmental Fate of 94 Halogenated and Organophosphate PBDE Replacements. Chemosphere 144, 2401–2407. doi: 10.1016/j.chemosphere.2015.11.017

Zhao, H., Liu, L., Li, Y., Zhao, F., Zhang, S., Mu, D., Liu, J., An, L., Wan, Y., Hu, J., 2019. Occurrence, Bioaccumulation, and Trophic Transfer of Oligomeric Organophosphorus Flame Retardants in an Aquatic Environment. Environmental Science & Technology Letters 6(6), 323–328. doi: 10.1021/acs.estlett.9b00262

Zhong, W., Cui, Y., Li, R., Yang, R., Li, Y., Zhu, L., 2021. Distribution and sources of ordinary monomeric and emerging oligomeric organophosphorus flame retardants in Haihe Basin, China. Science of the Total Environment 785, 147274. doi: 10.1016/j.scitotenv.2021.147274

Appendices

Appendix I: Complete list of chemical reagents and compounds referenced, identified by CAS RN and including molecular weight and purity.

Chemical Reagents

Compound Name	Molecular Weight (amu)	CAS #	Abbreviation	Supplier	Purity
$^{13}C_{12}$-Bisphenol A	240.20	263261-65-0	$^{13}C_{12}$-BPA	Sigma-Aldrich	>98%
Bisphenol A	228.29	80-05-7	BPA	Sigma-Aldrich	99+%
Bisphenol A bis(diphenyl phosphate)	692.64	5945-33-5	BPADP	Toronto Research Chemicals	98%
d_{10}-Diphenyl phosphate	260.25	1477494-97-5	d_{10}-DPHP	Toronto Research Chemicals	95%
d_{15}-triphenyl phosphate	341.38	1173020-30-8	d_{15}-TPHP	Wellington Labs	>98%
Diphenyl phosphate	250.19	838-85-7	DPHP	Sigma-Aldrich	99%
Trans-1,4-cyclohexanediol-bis(diphenyl phosphate)	580.516	No CAS#	T-CH-BDP	Sigma-Aldrich	>97%
Triphenyl phosphate	326.28	115-86-6	TPHP	Sigma-Aldrich	99+%
L-Glutathione reduced	307.32	70-18-8	GSH	Sigma-Aldrich	≥98 %

Other Studied Compounds

Compound Name	**CAS #**	**Abbreviation**	**Molecular Weight (amu)**
Phenol	108-95-2	n/a	94.11
Tetrakis(2,6-dimethylphenyl)-m-phenylene biphosphate	139189-30-3	RDX; PBDMPP	686
resorcinol bis (diphenylphosphate)	57583-54-7	RDP; PBDPP	574.4
Tetrakis(2-chloroethyl)dichloroisopentyldiphosphate	38051-10-4	V6; BCMP-BCEP	583

Appendix II: SMILES codes of all *in silico* OECD Toolbox v4.4.1 predicted metabolites and corresponding CAS RN.

Predicted Metabolites of BPADP

M1: CC(C)(c1ccc(O)cc1)c1ccc(O)cc1

CAS #80-05-7; bisphenol-A; IUPAC Name: 4-[2-(4-hydroxyphenyl)propan-2-yl]phenol

M2: CC(C)(c1ccc(O)cc1)c1ccc(OP(=O)(Oc2ccccc2)Oc2ccccc2)cc1

No CAS# registered; Supplier Synonym: SCHEMBL811002; IUPAC Name: [4-[2-(4-hydroxyphenyl)propan-2-yl]phenyl] diphenyl phosphate

M3: CC(C)(c1ccc(O)cc1)c1ccc(OP(O)(=O)Oc2ccccc2)cc1

No CAS# registered; Supplier Synonym: SCHEMBL2290182; IUPAC Name: [4-[2-(4-hydroxyphenyl)propan-2-yl]phenyl] phenyl hydrogen phosphate

M4: CC(C)(c1ccc(OP(O)(=O)Oc2ccccc2)cc1)c1ccc(OP(=O)(Oc2ccccc2)Oc2ccccc2)cc1

No CAS# registered; Supplier Synonym: SCHEMBL12670502; IUPAC Name: [4-[2-[4-[Hydroxy(phenoxy)phosphoryl]oxyphenyl]propan-2-yl]phenyl] diphenyl phosphate

M5: CC(C)(c1ccc(OP(O)(=O)Oc2ccccc2)cc1)c1ccc(OP(O)(=O)Oc2ccccc2)cc1

No CAS# registered; Supplier Synonym: SCHEMBL3693240; IUPAC Name: [4-[2-[4-[Hydroxy(phenoxy)phosphoryl]oxyphenyl]propan-2-yl]phenyl] phenyl hydrogen phosphate

M6: CC(C)(c1ccc(OP(O)(O)=O)cc1)c1ccc(OP(=O)(Oc2ccccc2)Oc2ccccc2)cc1

No CAS# registered; unidentifiable

M7: OP(=O)(Oc1ccccc1)Oc1ccccc1

CAS#838-85-7; diphenyl phosphate (DPHP); IUPAC Name: diphenyl hydrogen phosphate

M8: OP(O)(=O)Oc1ccccc1

CAS#701-64-4; monophenyl phosphate; IUPAC Name: phenyl dihydrogen phosphate

M9: Oc1ccc(O)cc1

CAS#123-31-9; hydroquinone; IUPAC Name: benzene-1,4-diol

M10: Oc1ccccc1

CAS#108-95-2; IUPAC Name: phenol

M11: Oc1ccccc1O

CAS#120-80-9; catechol; IUPAC Name: 1,2-dihydroxybenzene

Predicted Metabolites of RDP

M_a1: OP(=O)(Oc1ccccc1)Oc1cccc(OP(=O)(Oc2ccccc2)Oc2ccccc2)c1

No CAS# Registered; IUPAC Name: [3-[hydroxy(phenoxy)phosphoryl]oxyphenyl] diphenyl phosphate

M_a2: OP(=O)(Oc1ccccc1)Oc1cccc(OP(O)(=O)Oc2ccccc2)c1

No CAS# Registered; Supplier Synonym: SCHEMBL15910518; IUPAC Name: [3-[hydroxy(phenoxy)phosphoryl]oxyphenyl] phenyl hydrogen phosphate

M_a3: OP(=O)(Oc1ccccc1)Oc1ccccc1

CAS#838-85-7; diphenyl phosphate (DPHP); IUPAC Name: diphenyl hydrogen phosphate

M_a4: OP(O)(=O)Oc1cccc(OP(=O)(Oc2ccccc2)Oc2ccccc2)c1

Unidentifiable

M_a5: OP(O)(=O)Oc1ccccc1

CAS# 701-64-4; phenyl phosphate; IUPAC Name: phenyl dihydrogen phosphate

M_a6: Oc1ccc(O)c(OP(=O)(Oc2ccccc2)Oc2ccccc2)c1

No CAS# Registered; Supplier Synonym: SCHEMBL3158378; IUPAC Name: (2,5-dihydroxyphenyl) diphenyl phosphate

M_a7: Oc1ccc(O)cc1

CAS# 123-31-9; hydroquinone; IUPAC Name: benzene-1,4-diol

M_a8: Oc1cccc(O)c1

CAS# 108-46-3; resorcinol; IUPAC Name: benzene-1,3-diol

M_a9: Oc1cccc(OP(=O)(Oc2ccccc2)Oc2ccccc2)c1

CAS# 105937-68-6; resorcinol diphenyl phosphate 'SCHEMBL1025837'

M_a10: Oc1cccc(OP(O)(=O)Oc2ccccc2)c1

No CAS# Registered; Supplier Synonym: SCHEMBL5222942; IUPAC Name: (3-hydroxyphenyl) phenyl hydrogen phosphate

M_a11: Oc1ccccc1

CAS# 108-95-2; IUPAC Name: phenol

M_a12: Oc1ccccc1O

CAS# 120-80-9; catechol; IUPAC Name: benzene-1,2-diol

Predicted Metabolites of RDX

M_b1: Cc1cc(O)cc(C)c1O

CAS# 654-42-2 ; IUPAC Name: 2,6-dimethylhydroquinone

M_b2: Cc1cccc(C)c1O

CAS# 576-26-1 ; IUPAC Name: 2,6-dimethylphenol

M_b3: Cc1cccc(C)c1OP(=O)(Oc1cc(O)ccc1O)Oc1c(C)cccc1C

No CAS# Registered; IUPAC Name: (2,5-dihydroxyphenyl) bis(2,6-dimethylphenyl) phosphate

M_b4: Cc1cccc(C)c1OP(=O)(Oc1cccc(O)c1)Oc1c(C)cccc1C

CAS # 154162-69-3; IUPAC Name: resorcinol bis(2,6-dimethylphenyl) phosphate; 'SCHEMBL1013059'

M_b5: Cc1cccc(C)c1OP(=O)(Oc1cccc(O)c1)Oc1c(C)cccc1CO

No CAS# Registered; Unidentifiable

M_b6: Cc1cccc(C)c1OP(=O)(Oc1cccc(OP(=O)(Oc2c(C)cccc2C)Oc2c(C)cccc2C(O)=O)c1)Oc1c(C)cccc1C

No CAS# Registered; Unidentifiable

M_b7: Cc1cccc(C)c1OP(=O)(Oc1cccc(OP(=O)(Oc2c(C)cccc2C)Oc2c(C)cccc2C=O)c1)Oc1c(C)cccc1C

No CAS# Registered; Unidentifiable

M_b8: Cc1cccc(C)c1OP(=O)(Oc1cccc(OP(=O)(Oc2c(C)cccc2C)Oc2c(C)cccc2CO)c1)Oc1c(C)cccc1C

No CAS# Registered; Unidentifiable

M_b9: Cc1cccc(C)c1OP(=O)(Oc1cccc(OP(O)(O)=O)c1)Oc1c(C)cccc1C

No CAS# Registered; Unidentifiable

M_b10: Cc1cccc(C)c1OP(O)(=O)Oc1c(C)cccc1C

CAS# 18350-99-7; IUPAC Name: Bis(2,6-dimethylphenyl)phosphate; 'SCHEMBL272850'

M_b11: Cc1cccc(C)c1OP(O)(=O)Oc1cccc(O)c1

No CAS# Registered; Supplier Synonym: SCHEMBL1609938; IUPAC Name: (2,6-dimethylphenyl) (3-hydroxyphenyl) hydrogen phosphate

M_b12: Cc1cccc(C)c1OP(O)(=O)Oc1cccc(OP(=O)(Oc2c(C)cccc2C)Oc2c(C)cccc2C)c1

No CAS# Registered; Unidentifiable

M_b13: Cc1cccc(C)c1OP(O)(=O)Oc1cccc(OP(O)(=O)Oc2c(C)cccc2C)c1

No CAS# Registered; Supplier Synonym: SCHEMBL76820; IUPAC Name: [3-[(2,6-dimethylphenoxy)-hydroxyphosphoryl]oxyphenyl] (2,6-dimethylphenyl) hydrogen phosphate

M_b14: Cc1cccc(C)c1OP(O)(O)=O

No CAS# Registered; Supplier Synonym: SCHEMBL2220467; IUPAC Name: (2,6-dimethylphenyl) dihydrogen phosphate

M_b15: Cc1cccc(CO)c1O

No CAS# Registered; Supplier Synonym: SCHEMBL1901144; IUPAC Name: 2-(hydroxymethyl)-6-methylphenol

M_b16: Oc1cccc(O)c1

CAS# 108-46-3; resorcinol; IUPAC Name: benzene-1,3-diol

M_b17:
Cc1cccc(C)c1OP(=O)(Oc1cccc(OP(=O)(Oc2c(C)cccc2C)Oc2c(C)ccc(O)c2C)c1)Oc1c(C)cccc1C

No CAS# Registered; Unidentifiable

Predicted Metabolites of V6

M_c1: ClCC=O

CAS# 107-20-0; IUPAC Name: 2-chloroacetaldehyde

M_c2: ClCCOP(=O)(OCCCl)OCC(CCl)(CCl)C=O

No CAS# Registered; unidentifiable

M_c3: ClCCOP(=O)(OCCCl)OCC(CCl)(CCl)COP(=O)(OCCCl)OCC=O

No CAS# Registered; unidentifiable

M_c4: OC(=O)C(CCl)(CCl)COP(=O)(OCCCl)OCCCl

No CAS# Registered; unidentifiable

M_c5: OC(=O)CCl

CAS# 79-11-8; IUPAC Name: 2-chloracetic acid

M_c6: OC(=O)COP(=O)(OCCCl)OCC(CCl)(CCl)COP(=O)(OCCCl)OCCCl

No CAS# Registered; unidentifiable

M_c7: OCC(CCl)(CCl)COP(=O)(OCCCl)OCCCl

No CAS# Registered; unidentifiable

M_c8: OCC(CCl)(CCl)COP(O)(=O)OCCCl

No CAS# Registered; unidentifiable

M_c9: OCCCl

CAS#107-07-3 ; IUPAC Name: 2-chloroethanol

M_c10: OCCOP(=O)(OCCCl)OCC(CCl)(CCl)COP(=O)(OCCCl)OCCCl

No CAS# Registered; unidentifiable

M_c11: OP(=O)(OCCCl)OCC(CCl)(CCl)COP(=O)(OCCCl)OCCCl

No CAS# Registered; unidentifiable

M_c12: OP(=O)(OCCCl)OCC(CCl)(CCl)COP(O)(=O)OCCCl

No CAS# Registered; unidentifiable

M_c13: OP(=O)(OCCCl)OCCCl

CAS# 3040-56-0; IUPAC Name: bis(2-chloroethyl) hydrogen phosphate

M_c14: OP(O)(=O)OCC(CCl)(CCl)COP(=O)(OCCCl)OCCCl

No CAS# Registered; unidentifiable

M_c15: OP(O)(=O)OCCCl

No CAS# registered; Supplier Synonym: SCHEMBL991756; IUPAC Name: 2-chloroethyl dihydrogen phosphate

Appendix III: Chemical structure and identifier of all predicted metabolites of RDP, RDX and V6.

RDP *in silico* rat liver S9 fraction and rat liver *in vivo* simulated metabolites, predicted by the OECD Toolbox v4.4.1 (The phenyl hydrogen atoms have been omitted for structural clarity):

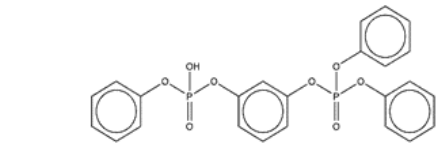

M_a1

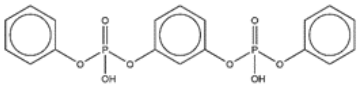

M_a2

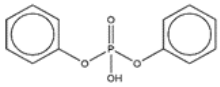

M_a3

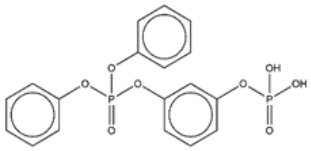

M_a4

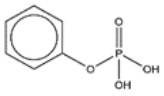

M_a5

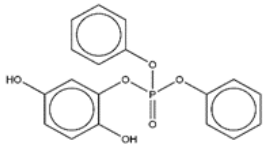

M_a6

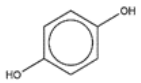

M_a7

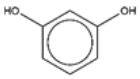

M_a8

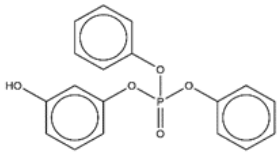

M_a9

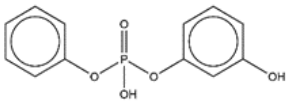

M_a10

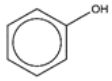

M_a11

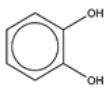

M_a12

RDX *in silico* rat liver S9 fraction and rat liver *in vivo* simulated metabolites, predicted by the OECD Toolbox v4.4.1 (The phenyl hydrogen atoms have been omitted for structural clarity):

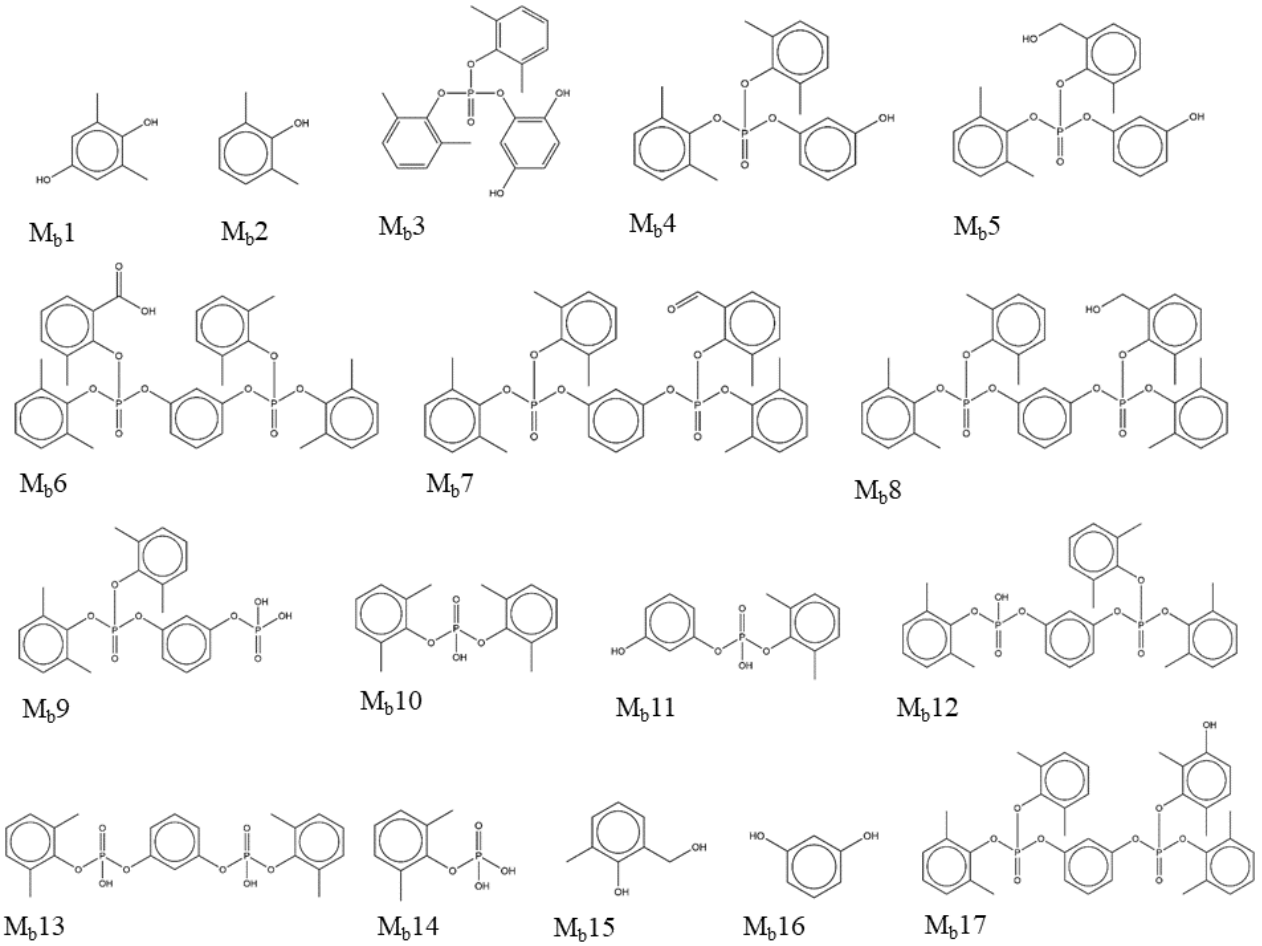

V6 *in silico* rat liver S9 fraction and rat liver *in vivo* simulated metabolites, predicted by the OECD Toolbox v4.4.1 (The phenyl hydrogen atoms have been omitted for structural clarity):

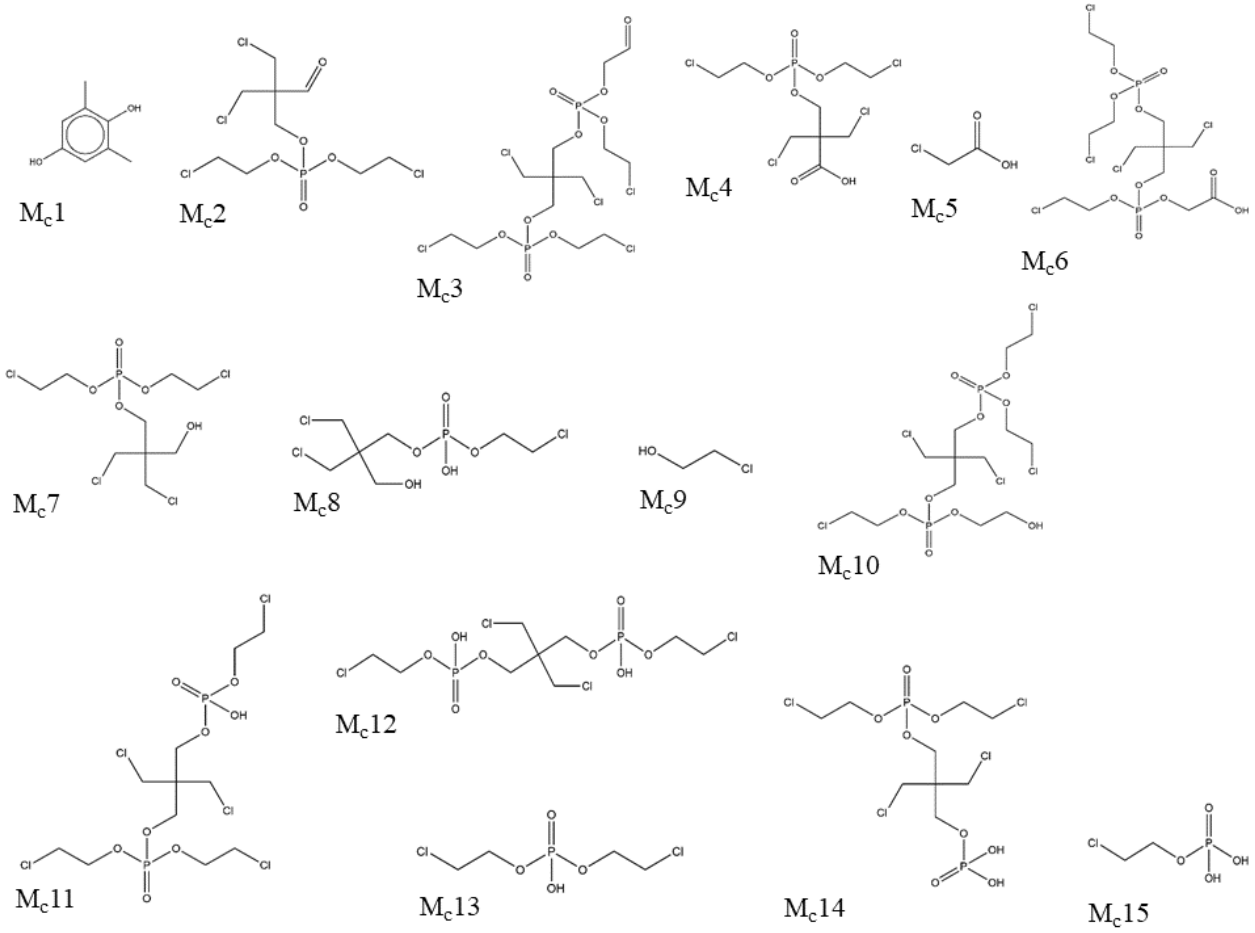

Appendix IV: Monitored TPHP concentrations and DPHP formation in each sample from all 1780 ppb BPADP incubation assays.

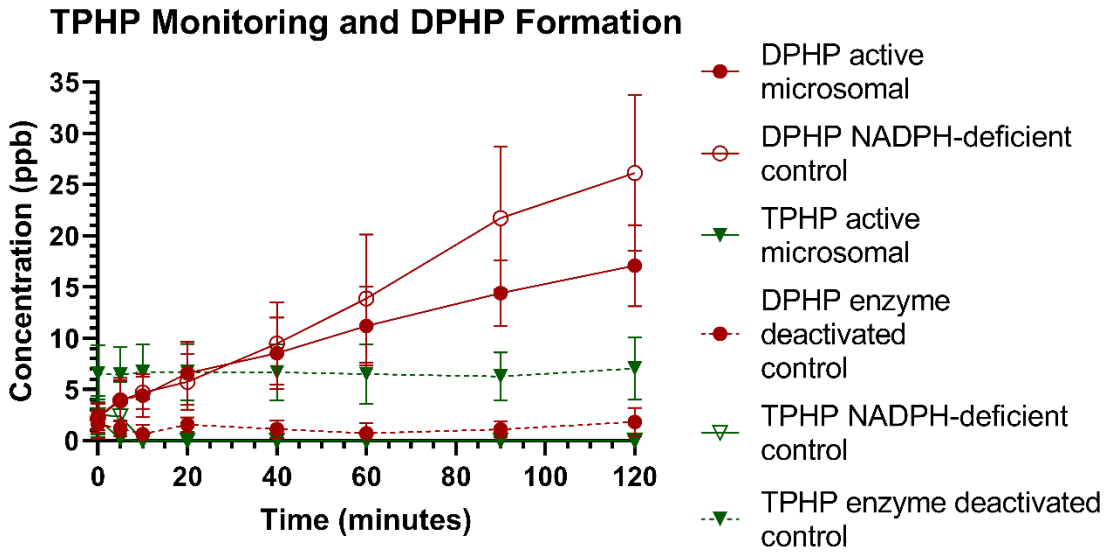

Mean TPHP and DPHP concentrations in each active replicate sample, NADPH-deficient control and enzyme deactivated control of the assays conducted at a 1780 ppb BPADP incubation concentration as presented in section 3.2.3, **Figure 3-5**. Each active microsomal data point is the mean of three triplicate samples (n=9), each control data point is the mean of triplicate samples (n=3).

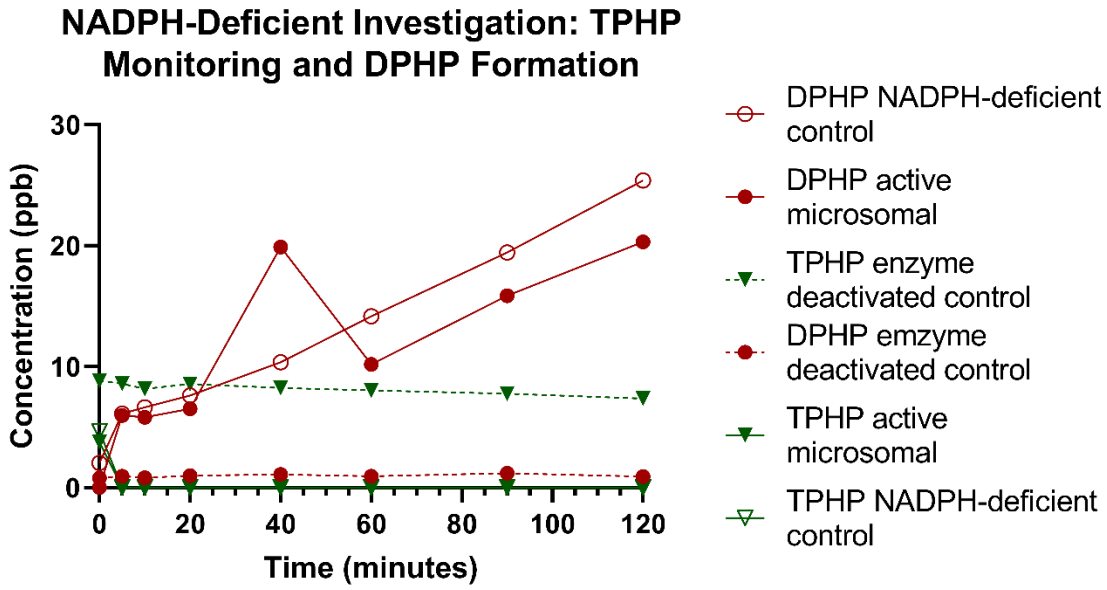

Mean TPHP and DPHP concentrations in each NADPH-deficient replicate sample, active microsomal control and enzyme deactivated control of the assays conducted at a 1780 ppb BPADP incubation concentration as presented in section 3.2.4, **Figure 3-6**. Each NADPH-deficient data point is the mean of triplicate samples (n=3), each control data point is the mean of one sample (n=1).

Appendix V: Isotopic simulation of additional metabolites identified via Q-E-Orbitrap Non-Target Analysis.

$C_{33}H_{30}O_8P_2$

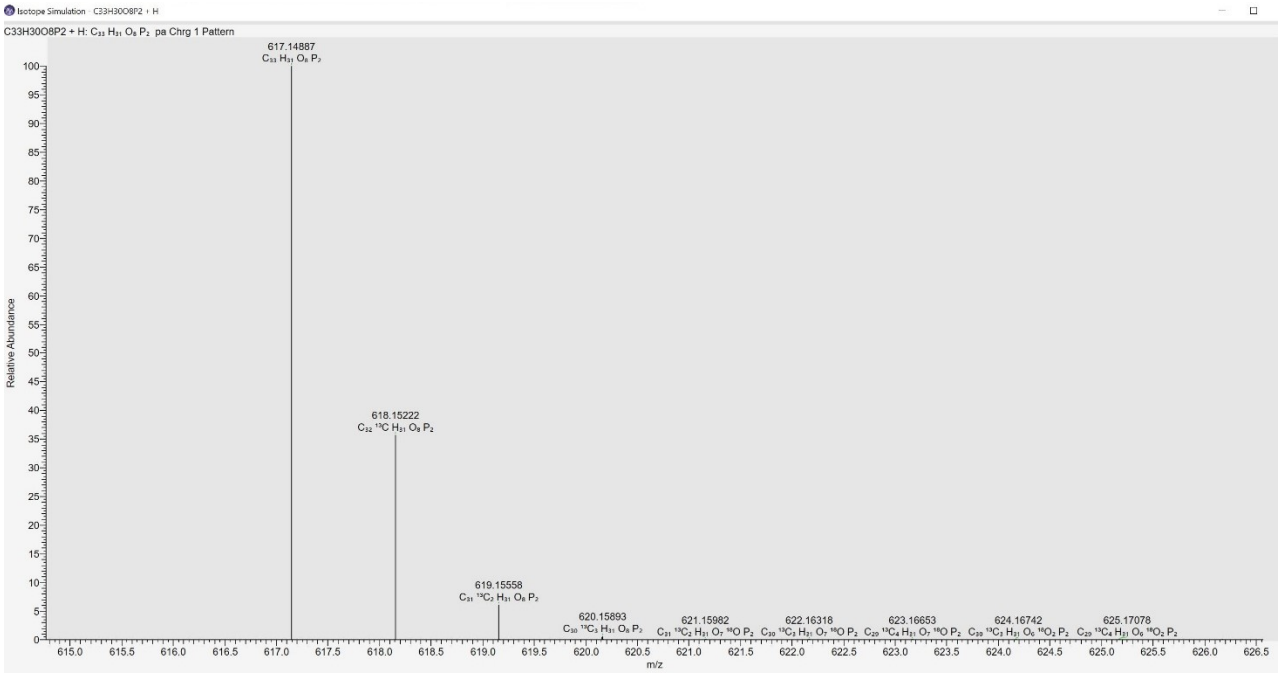

$C_{39}H_{34}O_{10}P_2$

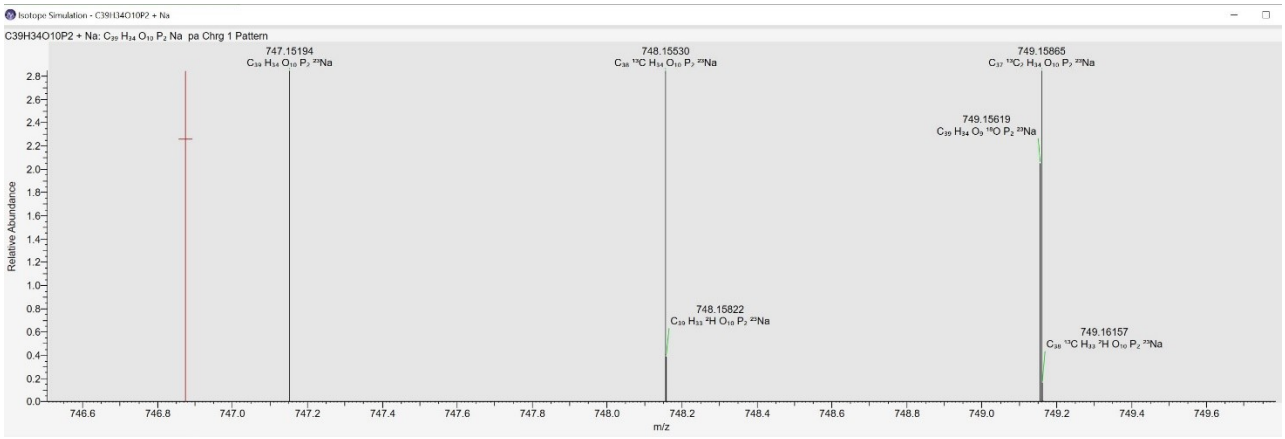

$C_{39}H_{34}O_9P_2$

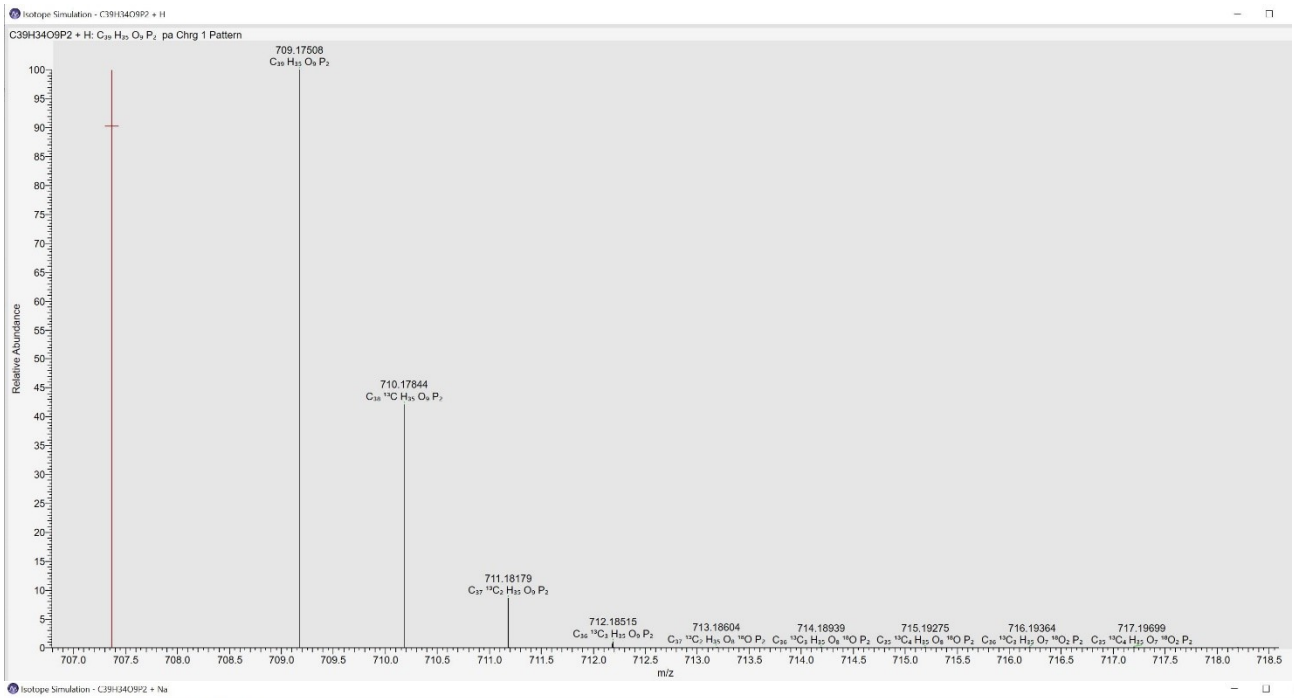
Isotope Simulation - C39H34O9P2 + H
C39H34O9P2 + H: C39 H35 O9 P2 pa Chrg 1 Pattern
709.17508
C39 H35 O9 P2
710.17844
C38 13C H35 O9 P2
711.18179
C37 13C2 H35 O9 P2
712.18515
C36 13C3 H35 O9 P2
713.18604
C37 13C2 H35 O8 18O P2
714.18939
C36 13C3 H35 O8 18O P2
715.19275
C35 13C4 H35 O8 18O P2
716.19364
C36 13C3 H35 O7 18O2 P2
717.19699
C35 13C4 H35 O7 18O2 P2
Relative Abundance
m/z

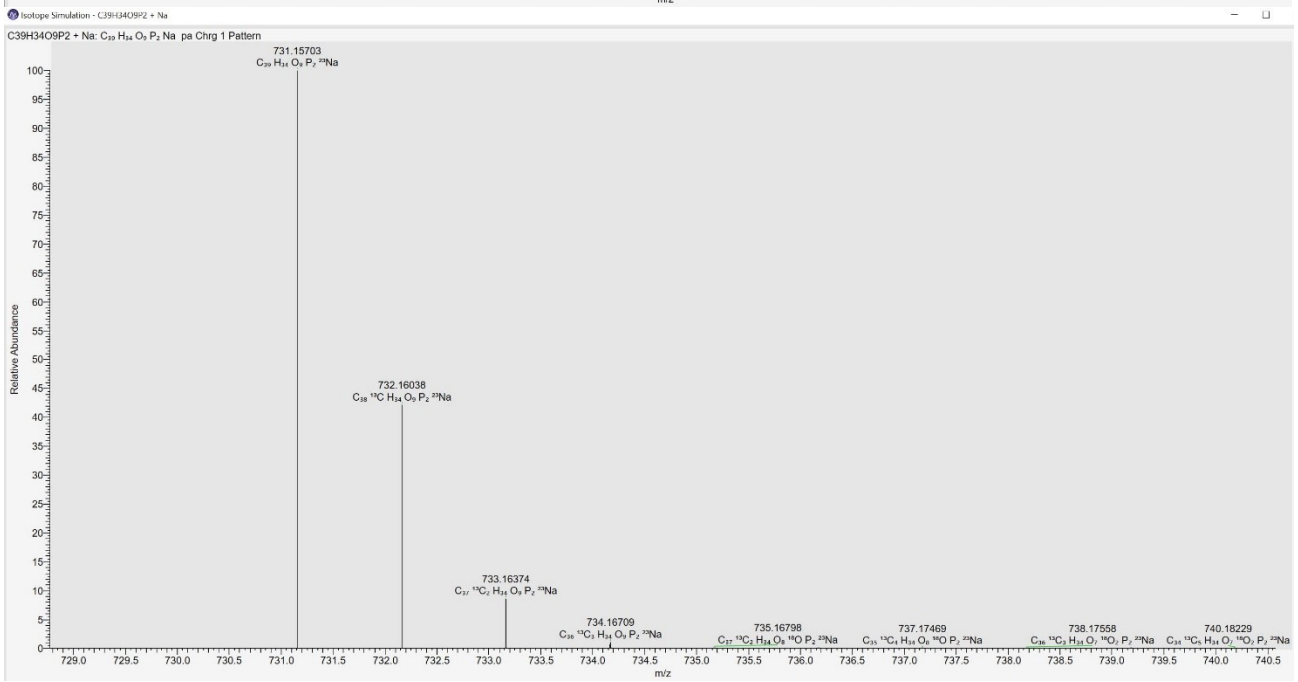
Isotope Simulation - C39H34O9P2 + Na
C39H34O9P2 + Na: C39 H34 O9 P2 Na pa Chrg 1 Pattern
731.15703
C39 H34 O9 P2 23Na
732.16038
C38 13C H34 O9 P2 23Na
733.16374
C37 13C2 H34 O9 P2 23Na
734.16709
C36 13C3 H34 O9 P2 23Na
735.16798
C37 13C2 H34 O8 18O P2 23Na
737.17469
C35 13C4 H34 O8 18O P2 23Na
738.17558
C36 13C3 H34 O7 18O P2 23Na
740.18229
C35 13C4 H34 O7 18O P2 23Na
Relative Abundance
m/z

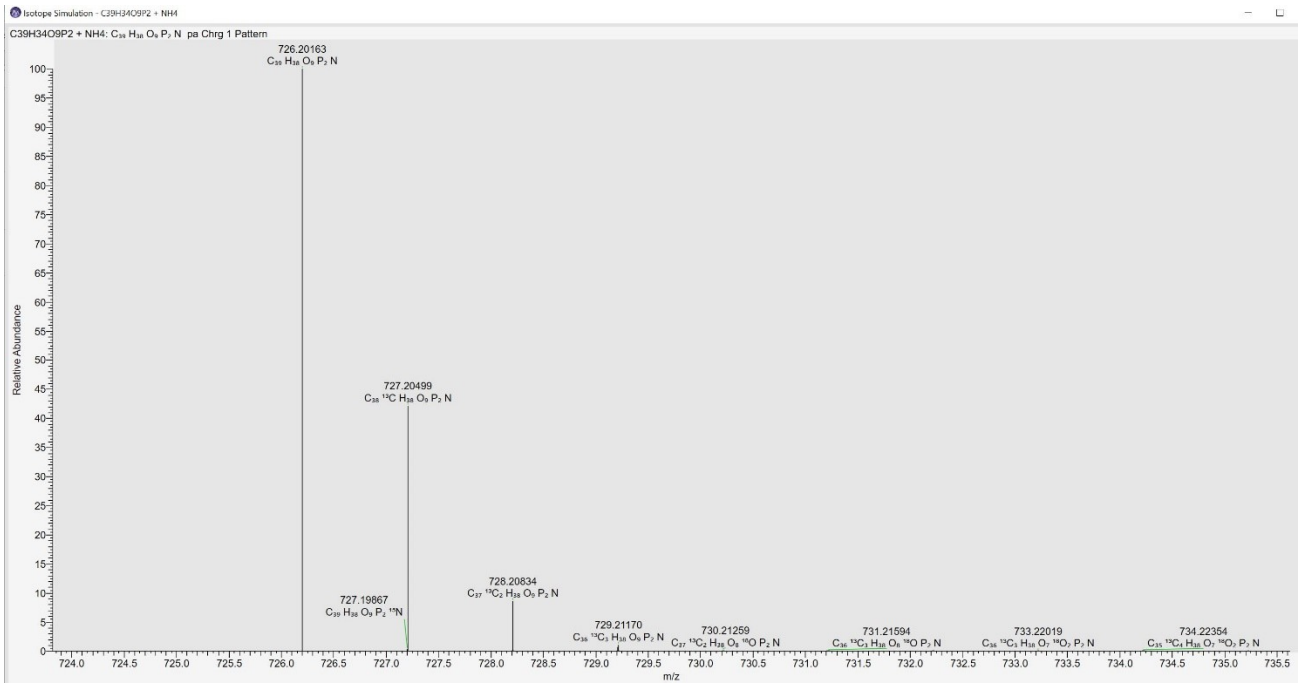
Isotope Simulation - C39H34O9P2 + NH4
C39H34O9P2 + NH4: C39 H38 O9 P2 N pa Chrg 1 Pattern
726.20163
C39 H38 O9 P2 N
727.20499
C38 13C H38 O9 P2 N
727.19867
C39 H38 O9 P2 15N
728.20834
C37 13C2 H38 O9 P2 N
729.21170
C36 13C3 H38 O9 P2 N
730.21259
C37 13C2 H38 O8 18O P2 N
731.21594
C36 13C3 H38 O8 18O P2 N
733.22019
C36 13C3 H38 O7 18O2 P2 N
734.22354
C35 13C4 H38 O7 18O2 P2 N
Relative Abundance
m/z

Appendix VI: 2D chemical structures of BPADP metabolites MM1 (BPADP – DPP) and MM2/M4 (BPADP – BZ).

MM1, BPADP – DPP

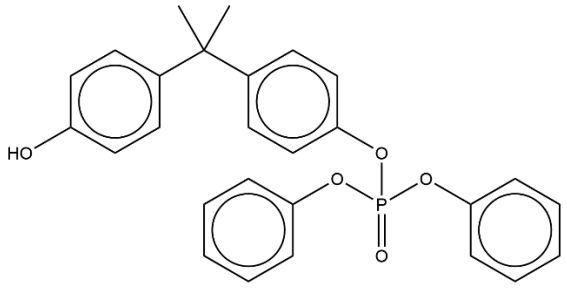

MM2/M4, BPADP – BZ